University of Southern Queensland

Faculty of Engineering and Surveying

A TWO-DIMENSIONAL ANALYSIS OF THE BEARING CAPACITY OF FOOTINGS NEAR SLOPES

A dissertation submitted by

Matthew David Arnold

in fulfilment of the requirements of

Courses ENG 4111 and 4112 Research Project

towards the degree of

Bachelor of Civil Engineering

Submitted: November, 2008

Abstract

The problem of a footing near slope is encountered regularly in engineering practice, with some noteworthy examples being bridge abutments and the basement construction of high-rise buildings. This study demonstrates the use of a computer model to analyse the interaction between the slope and the footing. FLAC (Fast Lagrangian Analysis of Continua) is a program which uses explicit finite difference techniques to solve the footing near slope problem and its effectiveness will be demonstrated in this study. Design charts will be presented using non-dimensional parameters to highlight what effect material and geometrical properties have on the normalised bearing capacity of a footing near slope. The paramaters comprehensively analysed in this study include dimensionless strength ratio, soil friction angle, slope angle, slope height ratio and footing distance ratio. Initial studies into further footing near slope conditions will also be presented in this paper. This includes dimensionless surcharge loading and dilation angle. These parameters will be investigated using a two-dimensional model within the FLAC program.

University of Southern Queensland

Faculty of Engineering and Surveying

ENG4111 Research Project Part 1 & ENG4112 Research Project Part 2

Limitations of Use

The Council of the University of Southern Queensland, its Faculty of Engineering and Surveying, and the staff of the University of Southern Queensland, do not accept any responsibility for the truth, accuracy or completeness of material contained within or associated with this dissertation.

Persons using all or any part of this material do so at their own risk, and not at the risk of the Council of the University of Southern Queensland, its Faculty of Engineering and Surveying or the staff of the University of Southern Queensland.

This dissertation reports an educational exercise and has no purpose or validity beyond this exercise. The sole purpose of the course pair entitled "Research Project" is to contribute to the overall education within the student's chosen degree program. This document, the associated hardware, software, drawings, and other material set out in the associated appendices should not be used for any other purpose: if they are so used, it is entirely at the risk of the user.

Prof Frank Bullen
Dean
Faculty of Engineering and Surveying

Certification

I certify that the ideas, designs and experimental work, results, analyses and conclusions set out in this dissertation are entirely my own effort, except where otherwise indicated and acknowledged.

I further certify that the work is original and has not been previously submitted for assessment in any other course or institution, except where specifically stated.

Matthew David Arnold
Student Number: 0050040825

_____
Signature

_____
Date

Acknowledgements

This research was carried out under the principal supervision of Dr. Jim Shiau. I would like to thank Dr. Jim Shiau for the on-going support and guidance while undertaking this project.

Appreciation is also due to friends and family, without their support this project would not have been as fulfilling.

Table of Contents

List of Figures

List of Tables

Notation

The principal symbols used are presented in the following list.

B	width of footing.
β	slope angle.
c	soil cohesion.
$\frac{c}{\gamma B}$	dimensionless strength ratio.
D	footing distance from edge of slope.
$\frac{D}{B}$	footing distance ratio.
D_f	depth of footing embedment.
$F_{cc},\ F_{\gamma c},\ F_{qc}$	cavity factors.
$F_{cd},\ F_{\gamma d},\ F_{qd}$	depth factors.
$F_{ci},\ F_{\gamma i},\ F_{qi}$	inclination factors.
$F_{cs},\ F_{\gamma s},\ F_{qs}$	shape factors.
γ	unit weight of soil.
H	slope height.
$\frac{H}{B}$	slope height ratio.
$N_c,\ N_\gamma,\ N_q$	bearing capacity factors.
$N_{cq},\ N_{\gamma q}$	bearing capacity factors for footing near slope.
N_s	slope stability factor.

p	average pressure beneath the footing.
$\frac{p}{\gamma B}$	normalised bearing capacity.
ϕ	friction angle of soil.
ψ	dilation angle of soil.
q	surcharge load.
$\frac{q}{\gamma B}$	dimensionless surcharge load.
q_u	ultimate bearing capacity.

Introduction

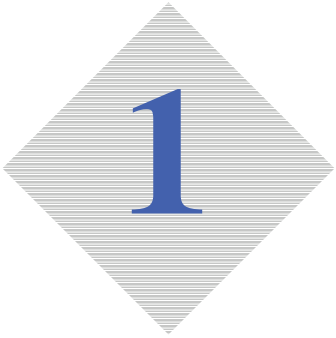

1.1 Problem Statement

The problem of a footing near slope is encountered regularly in engineering practice, with some noteworthy examples being bridge abutments and the basement construction of high-rise buildings. Such engineering structures emphasise a strong importance of the footing near slope problem. These examples highlight the fact that the footing near slope scenario can be broken into two categories, being the construction of a footing near a slope or the excavation adjacent to an existing structure. This study focuses on the ultimate bearing capacity of the slope and the fact that slope failure can be caused by foundation bearing capacity failure or slope stability failure. The combination of these two failure modes is what makes the problem difficult to solve.

1.1.1 Shallow Foundations

A structure supported by the earth can be broken into two main components, the upper section is known as the superstructure and the lower section adjacent to the earth's surface as the foundation. A shallow foundation transfers the load of the superstructure to the immediate underlying material. In the event of the underlying material being too weak the loads may be transferred through a deep foundation or pile foundation. A shallow foundation known as a footing supports a single structure and is often simply an enlargement of the base. A mat or raft foundation can be used to support a number of columns or walls. The general classification of a shallow foundation is that the depth be $D_f/B \leq 1$. The purpose of this paper is to investigate shallow footings and their influence when located near a slope.

1.1.2 Ultimate Bearing Capacity

The bearing capacity of a material is the ability to safely carry the load applied by a structure. The ultimate bearing capacity refers to the pressure per unit area applied which will cause shear failure with accompanying settlements. Excessive settlements can result in minor damages in buildings such as sticking doors and windows, cracking and rutting

may result in road construction and realignment may cause excessive wear in machinery operations. If no remedial action is taken situations could worsen in to building collapse, motor vehicle accidents or equipment failure. The most common form of bearing capacity failure is general shear failure. This type of failure is characterised by a well-defined slip surface and bulging of the ground surface either side of the footing. There are however, other failure modes such as local and punching shear failure.

1.1.3 General Shear Failure

General shear failure causes little compression of the soil below the foundation, instead large zones of plastic equilibrium with slip surfaces develop. The slip surfaces will extend to the ground surface resulting in significant heave affects as shown in figure 1-1. Failure occurs at a certain point when the load per unit area equals the ultimate bearing capacity. The failure mechanism usually occurs on one side of the foundation causing the structure to tilt. This type of failure is typical of dense or stiff soils. Figure 1-1 also displays a typical load-displacement curve for general shear failure.

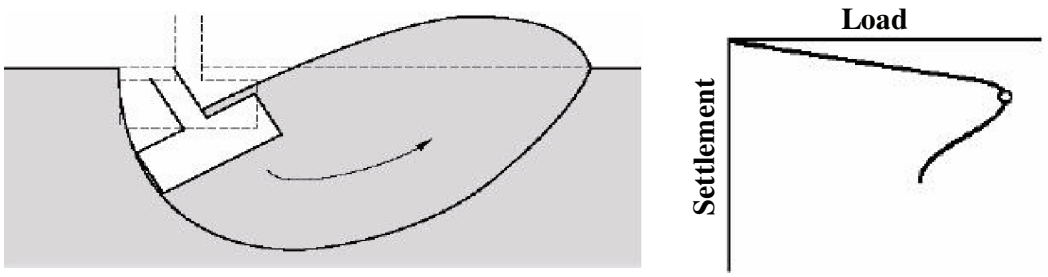

Figure 1-1. General Shear Failure

1.1.4 Local Shear Failure

Local shear failure exhibits more compression of the soil below the foundation with less plastic zones of equilibrium. Slip surfaces do not reach ground level and there is little heave. In most cases the foundation would not be expected to tilt but only settle. This type of failure is typical of compressible soils. No peak ultimate bearing capacity value exists for this type of failure. Figure 1-2 shows the mode of failure and load-displacement curve for local shear.

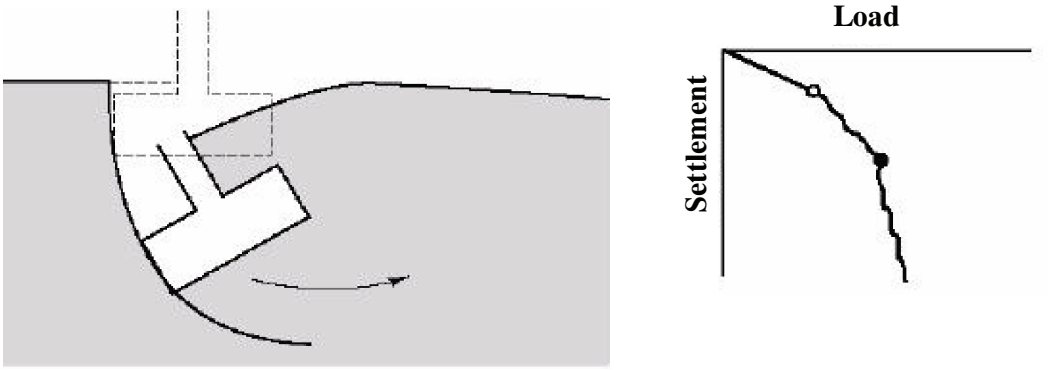

Figure 1-2. Local Shear Failure

1.1.5 Punching Shear Failure

For a punching shear failure the foundation settles extensively as it punches into soft compressible soil. There is virtually no development of plastic zones and settlement is through shear and compression of the supporting soil below the foundation. Figure 4-3 shows the failure mode and load-displacement curve for punching shear.

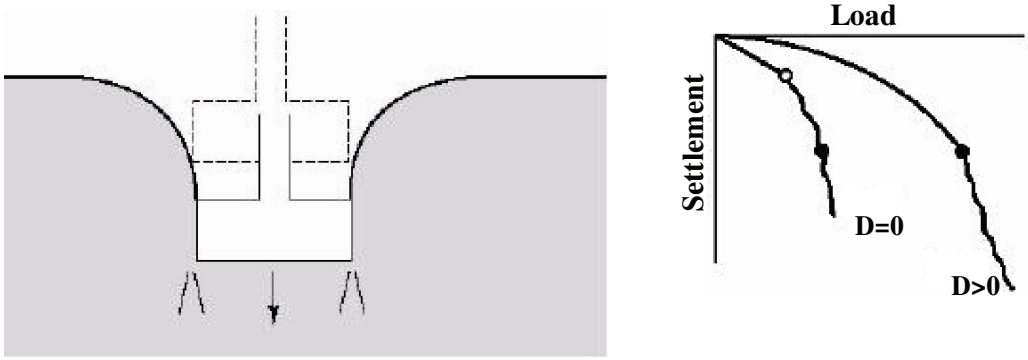

Figure 1-3. Punching Shear Failure

1.1.6 Slope Stability

Slope stability refers to the stability of earth masses against sliding or gravity effects. Such occurances are commonly experienced in cut or fill situations as in roads, railways, dams or naturally occurring in mountainous areas. Failure occurs when an outer section of the slope slides downward and outward in relation to the remainder of the slope. Field observations indicate that the failure surface is generally curved unless a definite weaker plane exists and becomes a boundary condition.

The bearing capacity of a footing near slope scenario is illustrated in Figure 1-1. This project aims to analyse the affects on the ultimate bearing capacity of a slope which is influenced by the following parameters:

- Cohesion (c)
- Friction angle (ϕ)
- Soil unit weight (γ)
- Slope angle (β)
- Slope height (H)
- Distance from edge of slope (D)
- Width of footing (B)
- Surcharge loading (q)

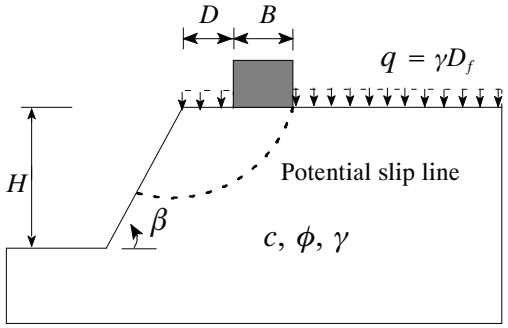

Figure 1-4. Footing Near Slope Problem Definition

This study seeks to investigate what effects each of the above mentioned parameters has on the bearing capacity of a footing near a slope. The problem can therefore be defined as

$$\frac{P}{\gamma B} = f\left(\beta, \phi, \frac{D}{B}, \frac{c}{\gamma B}, \frac{q}{\gamma B}, \frac{H}{B}\right) \tag{1.1}$$

P is the average limit pressure under the footing. As defined in equation 1.1 this study will use the dimensionless quantities:

- Normalised bearing capacity ($\frac{p}{\gamma B}$)
- Friction angle (ϕ)
- Slope angle (β)
- Slope height ratio ($\frac{H}{B}$)
- Footing distance ratio ($\frac{D}{B}$)
- Dimensionless surcharge loading ($\frac{q}{\gamma B}$)

- Dimensionless strength ratio ($\frac{c}{\gamma B}$)

The simplicity of well structured design charts using non-dimensional analysis will be advantageous to design engineers who often require a quick check during initial design stages. This method produces very clear trends in data and is a practical method for which reasonable confidence in design can be achieved. For design purposes, charts using dimensionless quantities have the ability to represent a far greater range of possible real-world situations.

The primary focus of this study is to investigate the behaviour of cohesive-granular, $c - \phi$, materials. The governing characteristics of such a material is that both friction angle and cohesion are positive.

1.2 Literature Review

The problem of bearing capacity on level ground and slope stability has been extensively studied in the past. The bearing capacity of soils can be determined analytically using Terzaghi's (1943), Hansen's (1970), Mayerhof's (1951), or Balla's (1961) methods, all of which require the parameters of cohesion and friction angle.

A comparison of values by Milovic (1965) shows that Hansen's equations appear best for cohesive soils and that Balla's method is best for soils with little or no cohesion.

The complexity of the footing near slope problem makes it difficult to solve and is the reason why limited research has been carried out. Some methods include the slip-line methods (such as Meyerhof's solution and Hansen & Vesic's solution), limit equilibrium methods and lower bound-upper bound solutions. The limit equilibrium methods are less rigorous but more flexible than the slip-line methods. This makes them a preferred method for engineers. The lower bound-upper bound methods have become more common since the development of the finite element and linear/non-linear programming methods.

1.2.1 Terzaghi's Level Ground Bearing Capacity Theory

Terzaghi was the first to present a detailed study on the ultimate bearing capacity of shallow foundations. In this study a shallow foundation was considered to be one where the embedment depth, D_f, was less than or equal to the footing width, B. Terzaghi's analysis was based on a strip foundation, a foundation where the width-to-length ratio approaches zero. Terzaghi made the assumption that the soil above the bottom of the foundation was equal to a uniform load, known as surcharge, $q = \gamma D_f$. Figure 1-5 shows how Terzaghi analysed the failure in three separate zones.

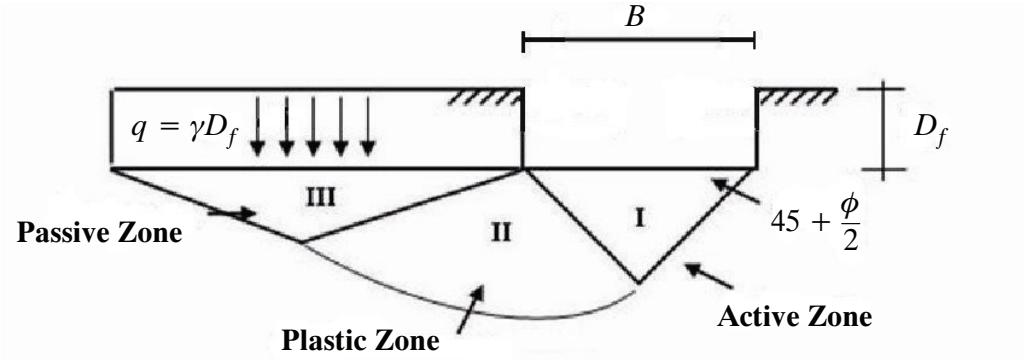

Figure 1-5. Terzaghi's Failure Zones

Another assumption made was that the base of the footing is rough to prevent any shear displacement. Terzaghi's study resulted in a solution for the ultimate bearing capacity of a soil based on the soil's cohesion, friction and weight giving:

$$q_u = cN_c + qN_q + \frac{1}{2}\gamma BN_\gamma \tag{1.2}$$

where N_c, N_q and N_γ are non-dimensional bearing capacity factors tabulated by Terzaghi as functions of friction angle.

Figure 1-5 represents general shear failure for the case of a highly compacted material. Terzaghi also presented results for the ultimate bearing capacity of local shear failure.

1.2.2 Mayerhof's Level Ground Bearing Capacity Theory

Mayerhof (1957) aimed to improve the bearing capacity theory proposed by Terzaghi . A superposition method was used to determine the contribution made by cohesion, friction angle and soil unit weight on the ultimate bearing capacity. This was achieved with the use of Mohr's circle. Similar to Terzaghi, values for N_c, N_q and N_γ were obtained. A comparison for these factors is shown in Table 1-1. Mayerhof also added shape, depth and inclination correction factors which produced a less conservative and far more complex equation in the form of:

$$q_u = cN_c F_{cs} F_{cd} F_{ci} + qN_q F_{qs} F_{qd} F_{qi} + \frac{1}{2}\gamma BN_\gamma F_{\gamma s} F_{\gamma d} F_{\gamma i} \tag{1.3}$$

Table 1-1. Comparison of Terzaghi's and Meyerhof's bearing capacity factors

	Terzaghi's Factors			Meyerhof's Factors		
ϕ	N_c	N_q	N_γ	N_c	N_q	N_γ
0	5.70	1.00	0.00	5.14	1.00	0.00
10	9.60	2.69	0.56	8.34	2.47	0.367
20	17.69	7.44	3.64	14.83	6.40	2.871
30	37.16	22.46	19.13	30.14	18.40	15.668
40	95.66	81.27	115.31	75.31	64.20	93.691

Numerous modifications have been made to the bearing capacity equation by such researches as Balla and Hansen. Compressibility factors were added to the equation by Vesic (1973) to account for the change of failure mode due to a soils compressibility. The factors F_{cc} , F_{qc} and $F_{\gamma c}$ were derived by analogy to the expansion of cavities using a rigidity index. The effect of water table can also be modelled within the mentioned bearing capacity equations.

1.2.3 Slope Stability

There are many ways in which a slope failure can occur, either due to a sudden, triggering event or possibly from an unstable slope creeping over a large time period. Triggered events can be from such causes as slope modification, either by humans or naturally, heavy rainfall or groundwater change, shocks such as earthquakes and structural construction alongside a slope.

The basic approach to solving a slope stability problem is by using limit equilibrium techniques where the failure surface is assumed to occur along a defined slip surface. A defined circular slip surface is shown in Figure 1-6.

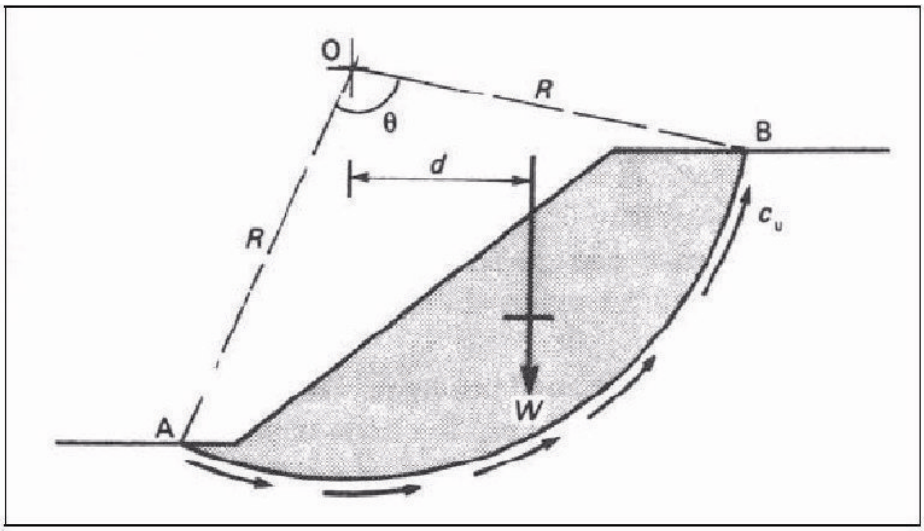

Figure 1-6. Circular Slip Surface for Slope Stability Problem

There are a variety of available limit equilibrium methods used for solving slope stability problems. These include:

- Swedish Method of Slices
- Bishop's Simplified Method of Slices
- Culmann's Wedge Analysis
- Infinite Slope Analysis
- Taylor's Charts
- Bishop-Morgenstern & Barnes Tables

Each of the method's are generally favourable for various situations. For example the Wedge method can be used for non-circular slips surfaces and the Swedish Method of Slices can be used with simple hand calculations.

Now, in addition to general, local and punching shear failure there is also the concept of footing near slope shear failure as shown in Figure 1-7. The research undertaken in this paper attempts to define this shear failure mode for various footing on slope parameters.

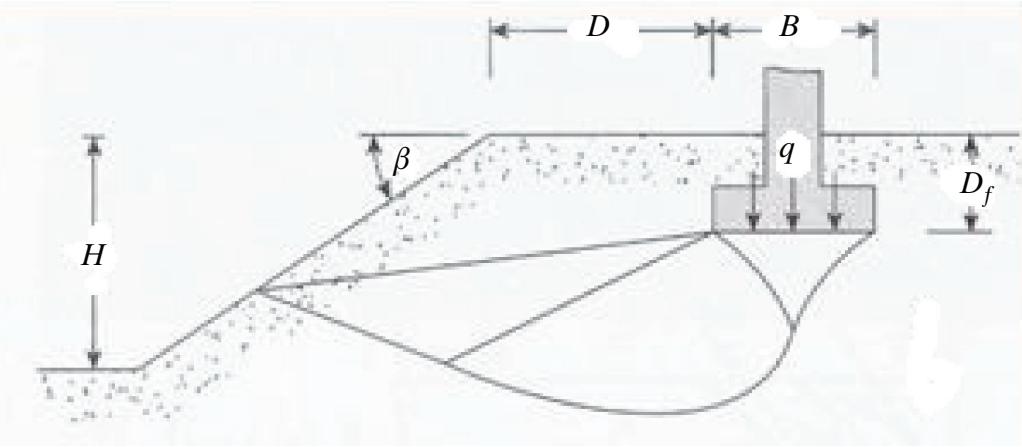

Figure 1-7. Footing Near Slope Shear Failure

1.2.4 Meyerhof's Footing Near Slope Bearing Capacity Theory

Meyerhof (1957) also proposed the following theoretical relation for the ultimate bearing capacity of foundations located near slopes:

$$q_u = cN_{cq} + \frac{1}{2}\gamma B N_{\gamma q} \tag{1.4}$$

This theory only considered purely granular, c = 0, and purely cohesive, $\phi = 0^\circ$, soils. Charts are used to obtain values for the facotrs N_{cq} and $N_{\gamma q}$. A slope stability factor, $N_s = \frac{\gamma H}{c}$, is also used to account for slope height.

1.2.5 Graham, et. al. Footing Near Slope Bearing Capacity Theory

Graham et. al. (1988) proposed revised values to Mayerhof's (1957) ultimate bearing capacity factor $N_{\gamma q}$ for purely granular materials. The revised factors were made using the basis of a stress characteristics method and the values were plotted in various charts.

1.2.6 Research Project by Catherine Smith (2006)

Catherine Smith used FLAC, a geotechnical modelling program, to validate it as a reliable tool against previous known methods such as the theory by Terzaghi (1943), the theory by Mayerhof (1957) and the theory of upper and lower bounds by Davis and Booker (1973) and Shiau et. al. (2006). This study was primarily of FLAC and the problem of a footing near a slope was only a component of the study. However, the conclusions made of FLAC being a reliable tool will be the basis for this research.

The study involved verifying a weightless slope of a purely granular material, c = 0, against Meyerhof's N_c factor as well as against Upper-Bound Lower-Bound methods. The two UB-LB methods were Davis & Booker (1973) and Shiau et. al. (2006). A wider range of parameters were investigated with a purely cohesive material, $\phi = 0$, to study the effect of

dimensionless strength ratio, slope angle and footing distance ratio on the bearing capacity of a slope. Purely granular material for a non-weightless slope was not investigated. A cohesive-granular study was undertaken for the effect of dimensionless strength ratio and footing distance ratio for a ninety degree slope.

An important conclusion which came from this study was that a coarse mesh produces a higher normalised bearing capacity. An overestimated solution for a coarse mesh which is regarded as stable would in fact be unstable when using a fine mesh. Figure 1-8 shows how the FLAC solution approaches the true solution as the mesh becomes finer. However, an increased number of elements to produce a fine mesh results in an increased program run-time which can be quite substantial, up to 2 or more hours for particular cases. Therefore a balance between mesh size and degree of accuracy is required.

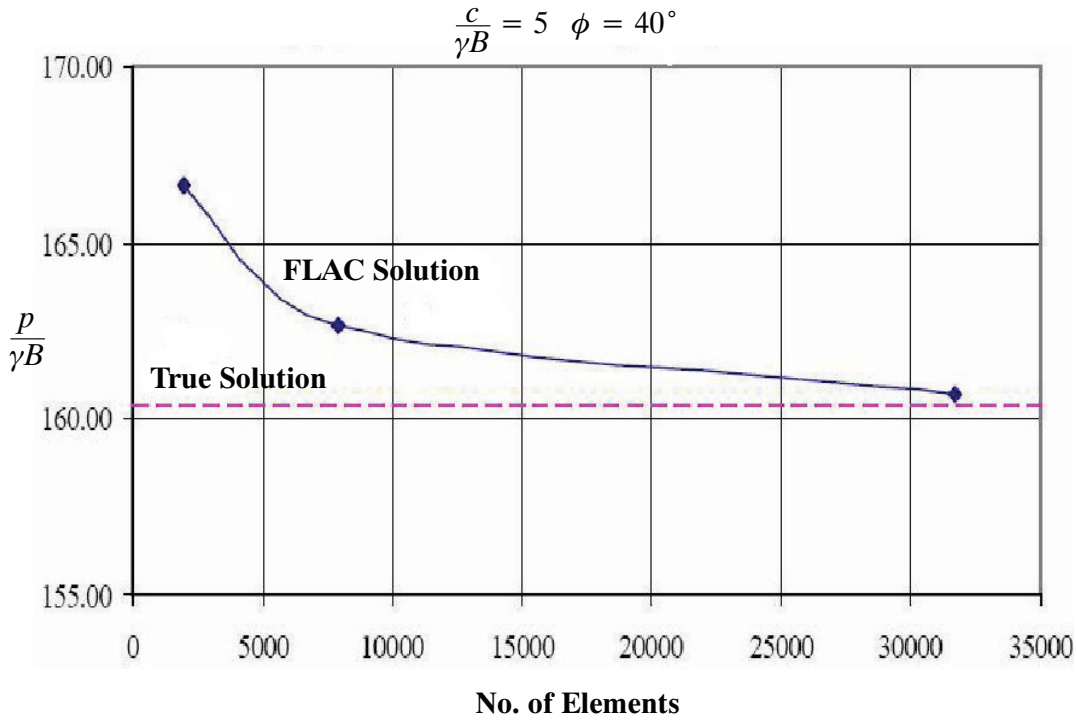

Figure 1-8. Variation in Normalised Bearing Capacity with Mesh Fineness

An example of a mesh for a 30˚slope is shown in Figure 1-9. This mesh contains 13680 elements, therefore looking at Figure 1-8 the results will be slightly overestimated.

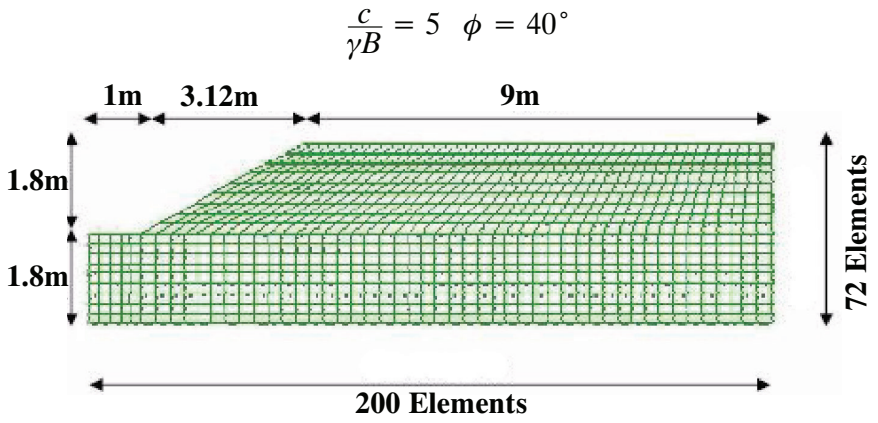

Figure 1-9. 30˚ Slope Mesh

1.2.7 Research Project by Joshua Watson (2008)

This study was undertaken to continue on from the work presented by Catherine Smith. Joshua Watson focused on the problem of a footing located near a slope. A greater range of dimensionless strength ratio's were studied along with varying the slope height ratio.

A number of improvements were made for further accuracy of results. A re-design of the FLAC slope mesh, shown in Figure 1-10, was necessary for this increased accuracy.

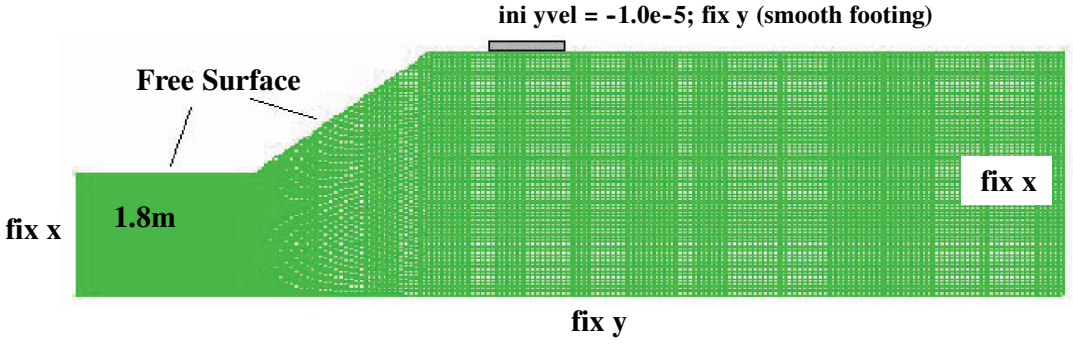

Figure 1-10. Revised Slope Mesh

Figure 1-10 shows how the mesh was changed so that only the zone beneath the slope is inclined which results in a more accurate solution.

After initial two-dimensional investigations Joshua Watson's Research Thesis is concentrated on a three-dimensional analysis of the footing near slope problem.

1.3 Project Resources

1.3.1 FLAC - Fast Lagrangian Analysis of Continua

FLAC uses explicit finite differencing methods to solve geotechnical engineering problems. FLAC simulates the behaviour of structures built of soil, rock or other materials that may undergo plastic flow when their yield limits are reached. With a defined set of parameters and a slope mesh FLAC determines the slope to be stable or unstable.

Other computational software such as limit equilibrium programs are based on a number of assumptions and only give an approximate answer. FLAC is useful in that it can solve highly non-linear situations. The program uses a time marching sceme to solve the governing equations which leads to the disadvantage of the long run times experienced by the program.

FLAC is also a very useful tool as it is possible to produce a number of plots such as material velocities, displacements and deformed shapes. Other data including program run times can be obtained which prove very useful for such a large study.

1.3.2 Surfer

Surfer is a grid-based graphics program which is capable of plotting x, y, z data, therefore is ideal for producing the required design charts for this study. The benefit of this project is that it will produce design charts which will include a number of parameters in each chart. Such a program is therefore a key tool for this study. Design charts created by Surfer will be analysed in a later chapter.

Footing on Level Ground and Footing Near Slope Bearing Capacities

2.1 Introduction

The objective of this research is to investigate the complex problem of the footing near slope scenario. To properly understand this problem, an understanding of the behaviour of a footing located on a level ground is essential.

Early in the study unpredicted results were being obtained where the shear failure zone was much larger than expected and hence the boundary conditions were interfering with the solution. A level ground study was undertaken with the hope that in later parametric studies cases could be better predicted.

2.2 Boundary Interference

This research started out investigating a 45 degree slope and because such a slope and such conditions had not been studied before it was hard to predict results. In previous studies only cohesive, $\phi = 0^{\circ}$, and cohesionless, c = 0, soils were investigated. The bahaviour of cohesive-granular materials was uncertain. Another initial factor was trying to keep programming run times to a minimum. With large mesh sizes and strong material cases the run time to obtain a solution is quite large, greater than 2 hours in some cases. As shown in Figure 2-1, if the mesh size is too small boundary interference occurs.

$\beta = 45^\circ \quad \frac{D}{B} = 0 \quad \phi = 40^\circ \quad \frac{c}{\gamma B} = 30$

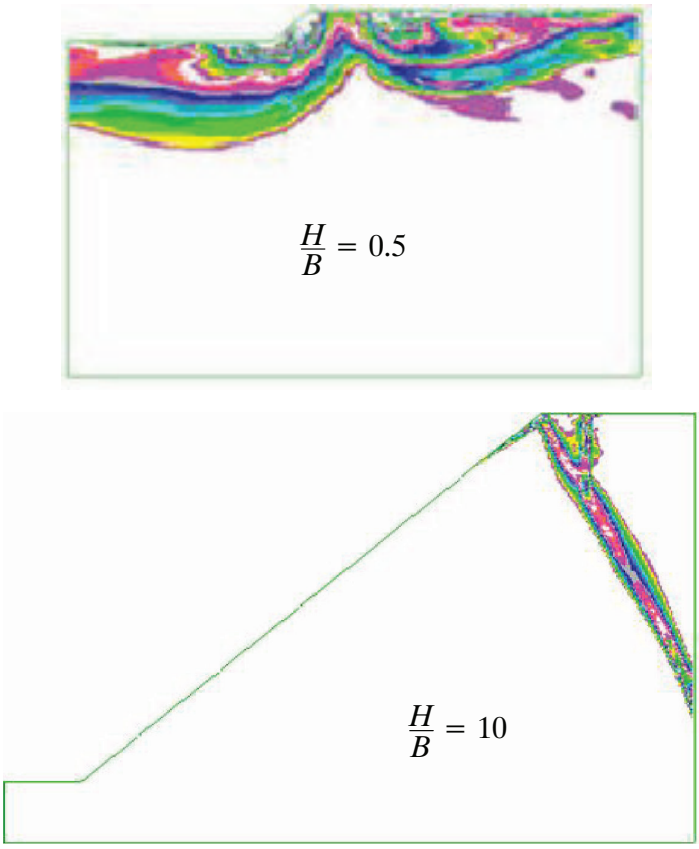

Figure 2-1. Contour plots of boundary interference

This error in solution lead to a level ground study to investigate the variation in the failure zone for various material parameters.

2.3 Footing on level Ground Investigation

The first observation which came from this study was that a symmetrical failure zone was confirmed for a footing on level ground. This observation is shown in Figure 2-2.

Figure 2-2. Symmetrical failure zone

With this conclusion it was possible to model only half of the scenario while still obtaining accurate results. An example of a halsf mesh solution is shown as Figure 2-2. The ability to only model half the mesh basically reduced programming time by half also.

Figure 2-3. Half mesh contour plot

For these results to be useful in a later parametric study the size of the failure zones were plotted with the hope that these plots would aid in deciding mesh sizes for future slope models. Figure 2-4 to Figure 2-7 show the variation in failure zone for sand, clay and cohesive-granular material.

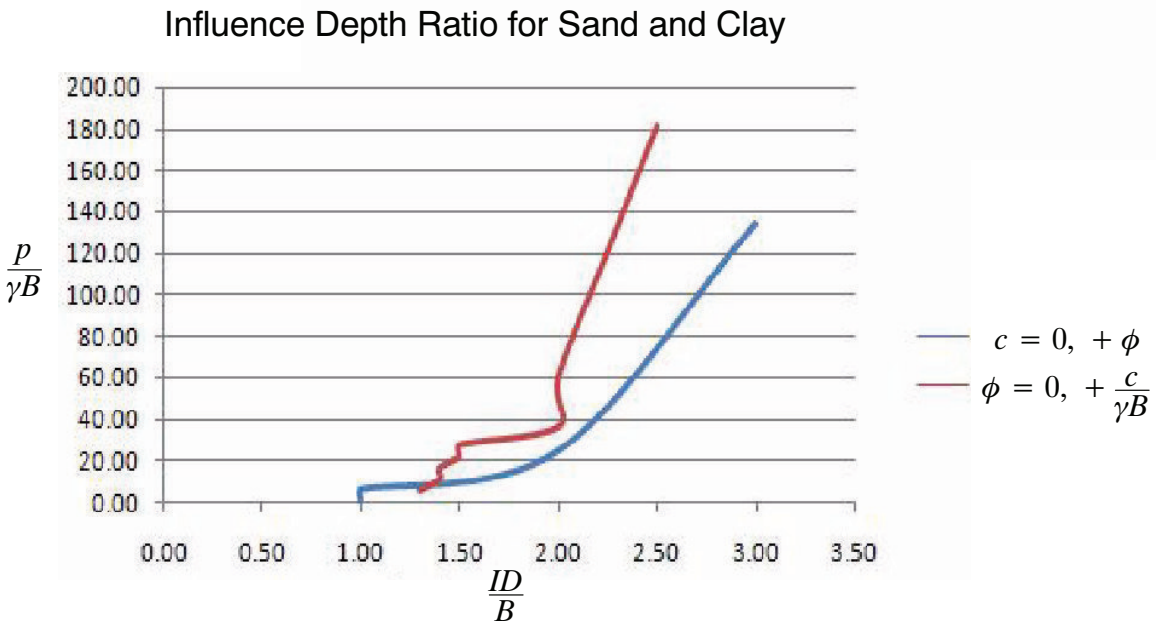

Figure 2-4. Influence depth ratio for sand and clay

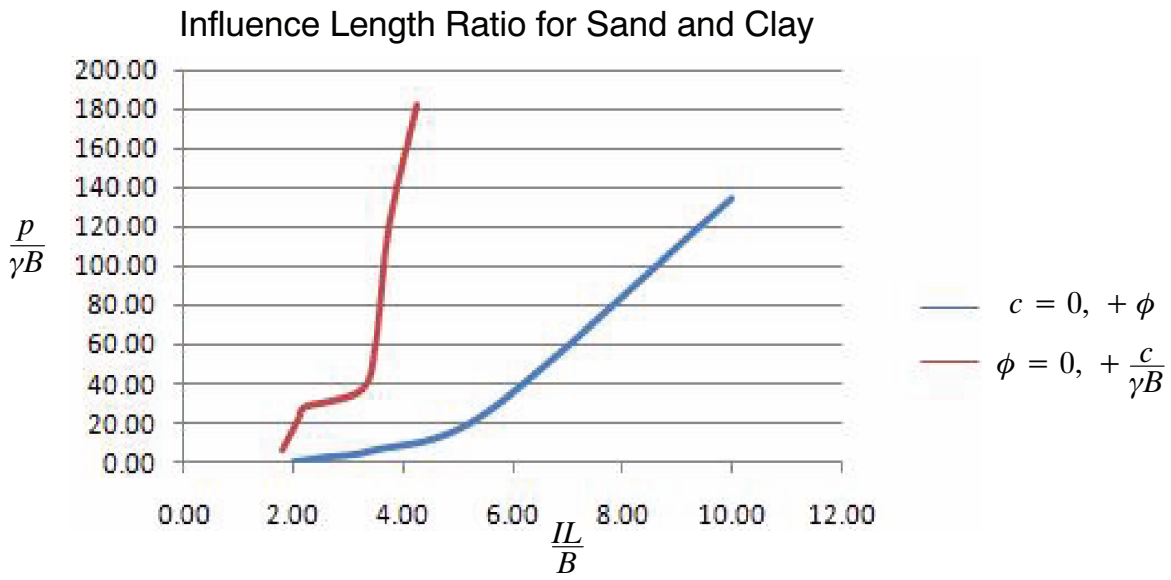

Figure 2-5. Influence length ratio for sand and clay

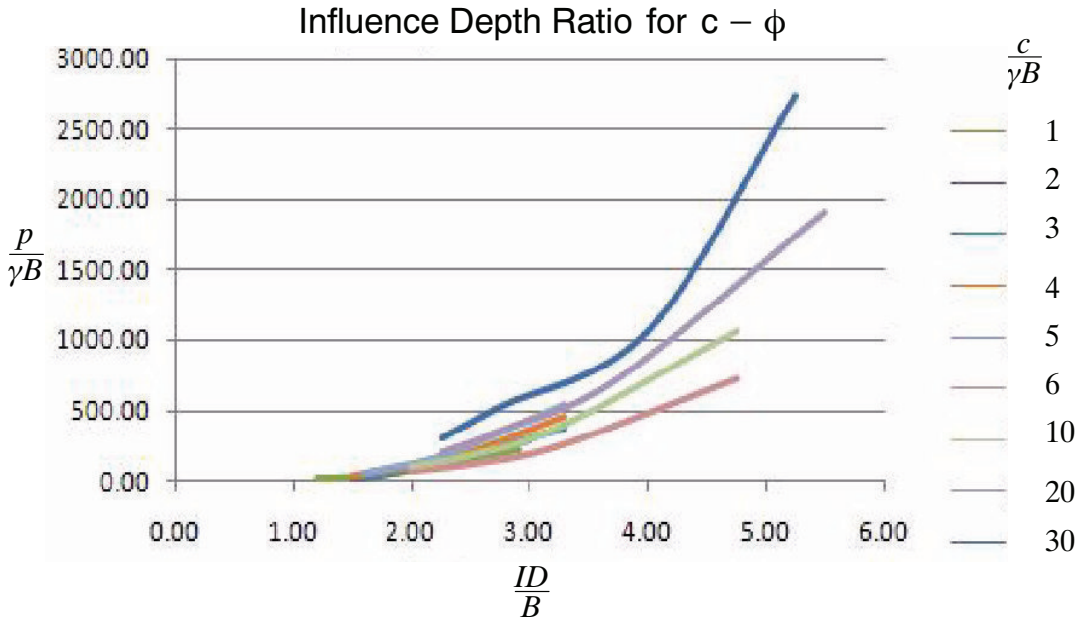

Figure 2-6. Influence depth ratio for cohesive granular material

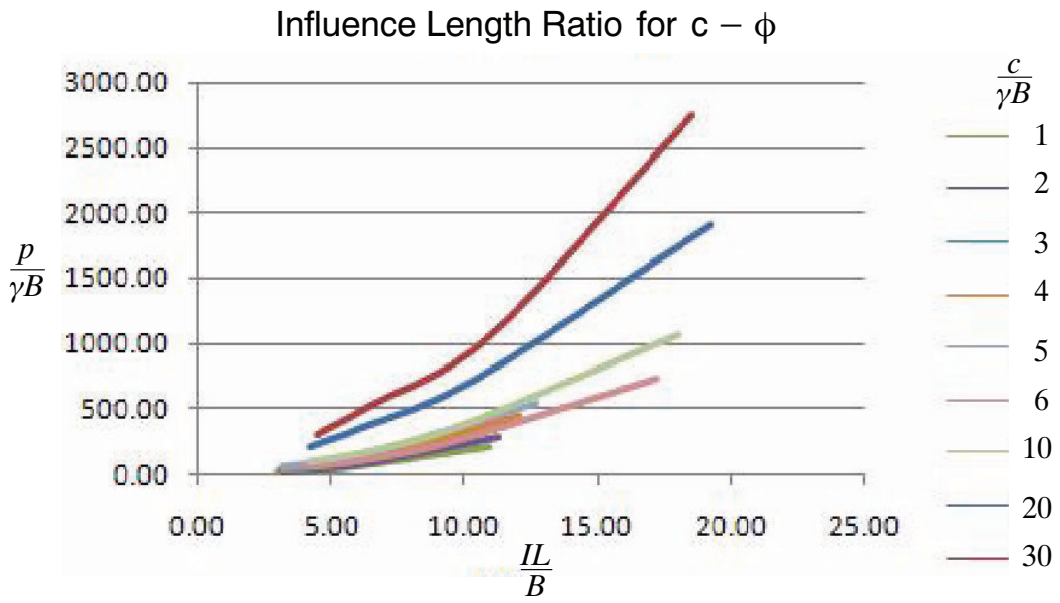

Figure 2-7. Influence length ratio for cohesive-granular material

It is now evident that the failure zone, both in depth and length, is almost double that of sand and clay for cohesive-granular material.

2.3.1 Validation of FLAC Model

Figure 2-8 to Figure 2-10 the comparison between the FLAC level ground model used and results obtained by Terzaghi and Meyerhof's bearing capacity methods. The FLAC model is producing values close to Terzaghi's method indicating that the method is slightly over estimating the solution. As friction angle and dimesnionless strength ratio are increased the solution approches that of Meyerhof.

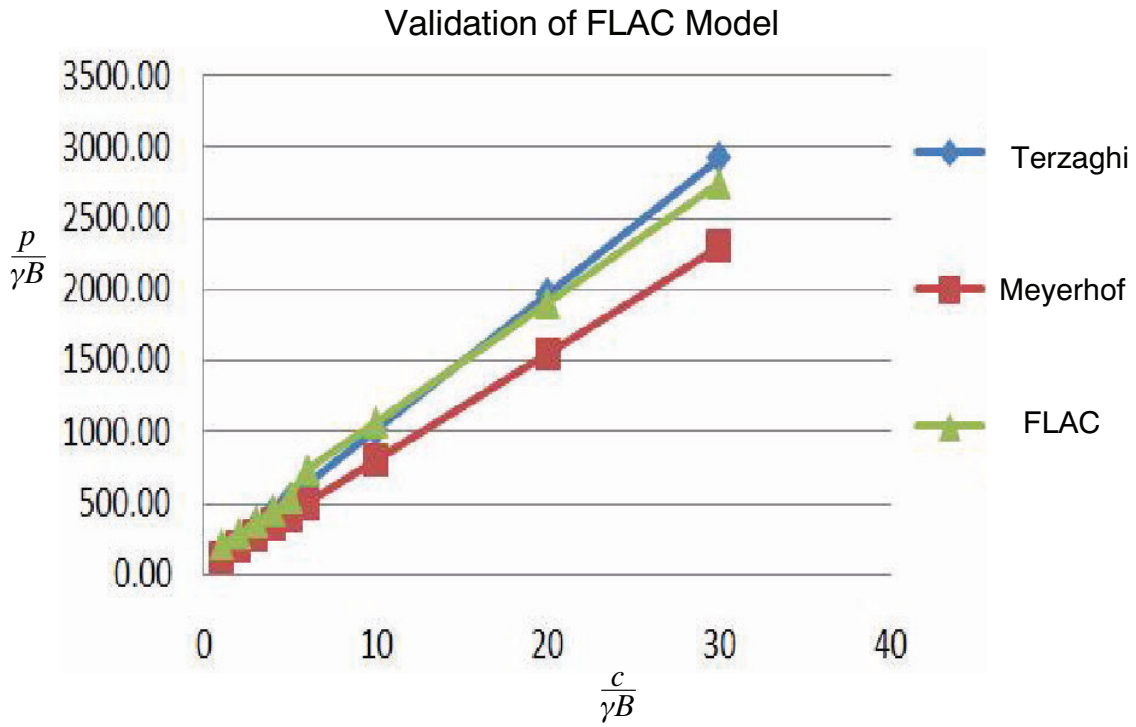

Figure 2-8. Validation of FLAC model for dimensionless strength ratio

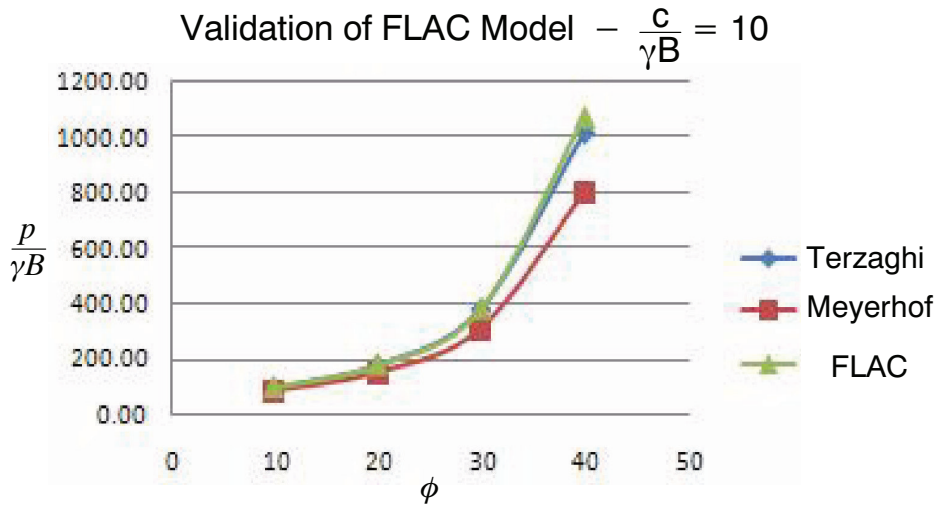

Figure 2-9. Validation of FLAC model for friction angle

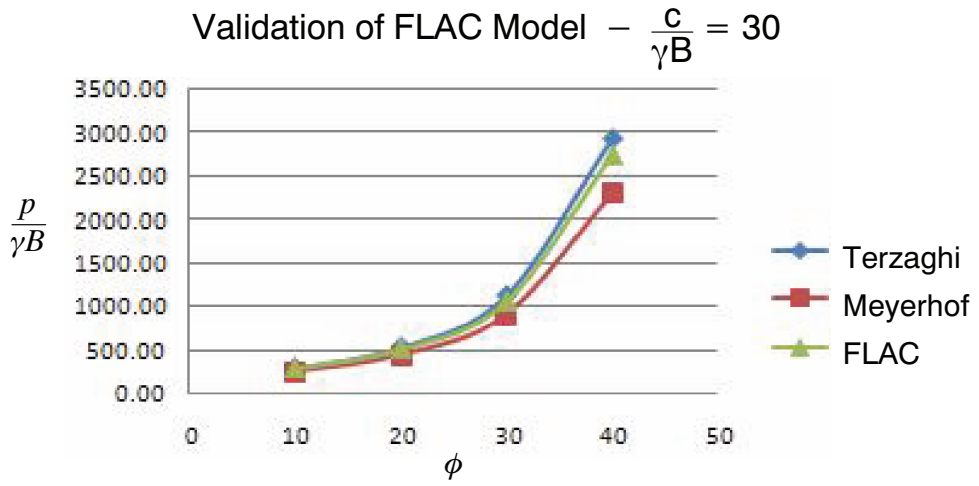

Figure 2-10. Validation of FLAC model for friction angle

2.4 Footing on Level Ground or Footing Near Slope Problem?

The first design consideration when dealing with a footing located near a slope is whether the slope has any influence on the footing. The following charts can be used as an aid to determine, knowing certain parameters, whether the footing is to be treated as a footing on level ground or footing ner slope problem. If it is found that the footing is located on level ground the problem can be solved using established methods such as those discussed in chapter 1. For a footing near slope problem, the following chapters in this research seek to give design aids with high accuracy to solve such problems. Figure 2-11 to Figure 2-18 should be used to decide whether a footing is to be considered as on level ground or near a slope.

2.4.1 Comparison Among Various Slope Height Ratio's

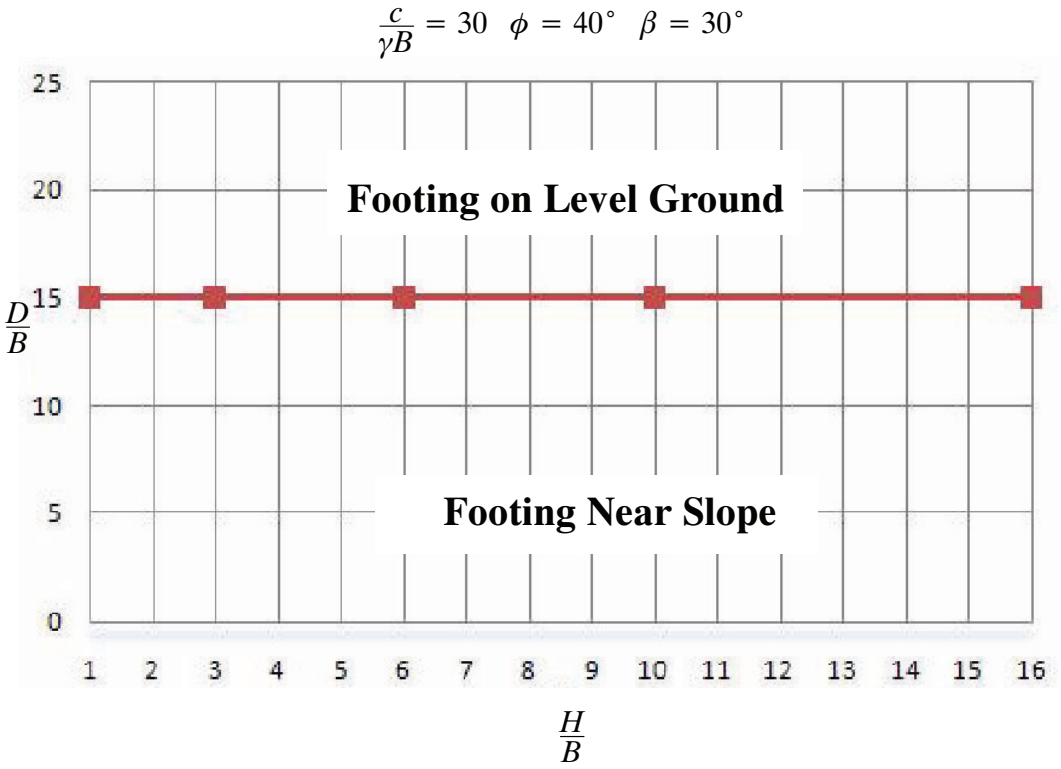

Figure 2-11. Level ground or footing near slope with given slope height ratio and a strong case

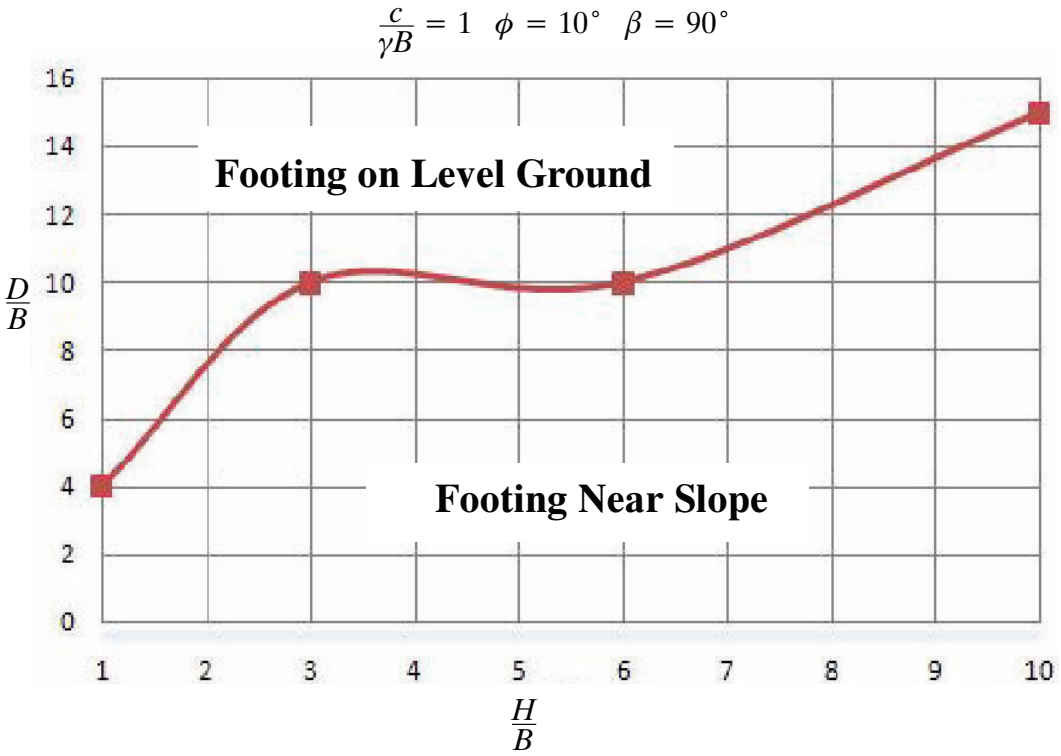

Figure 2-12. Level ground or footing near slope with given slope height ratio and a weak case

2.4.2 Comparison Among Various β

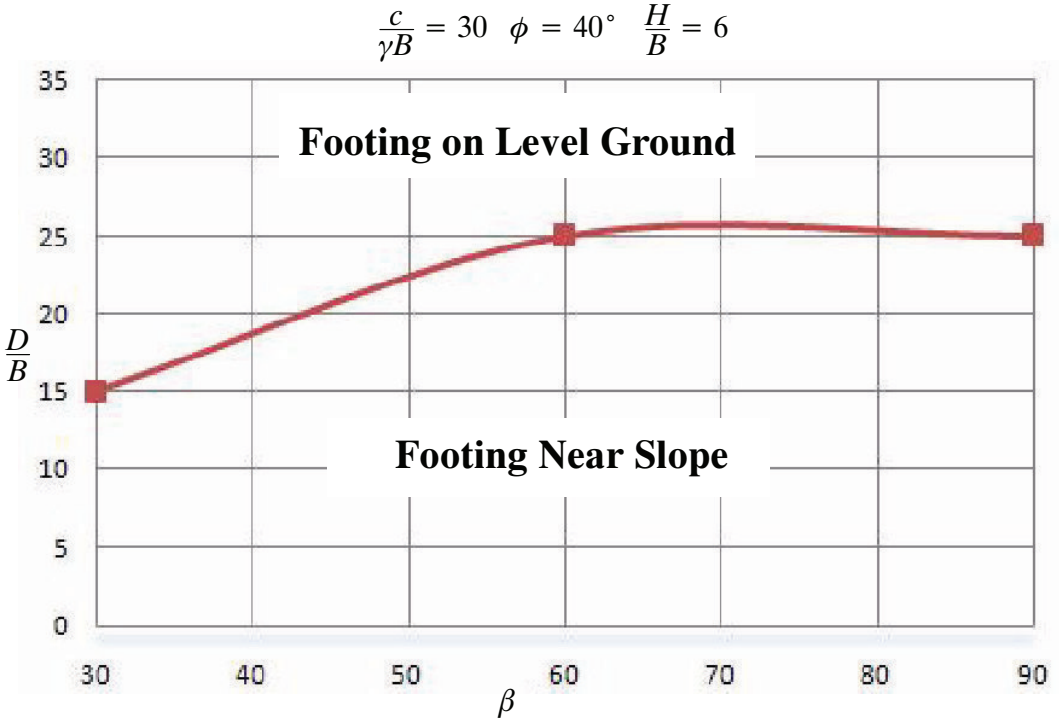

Figure 2-13. Level ground or footing near slope with given slop angle and a strong case

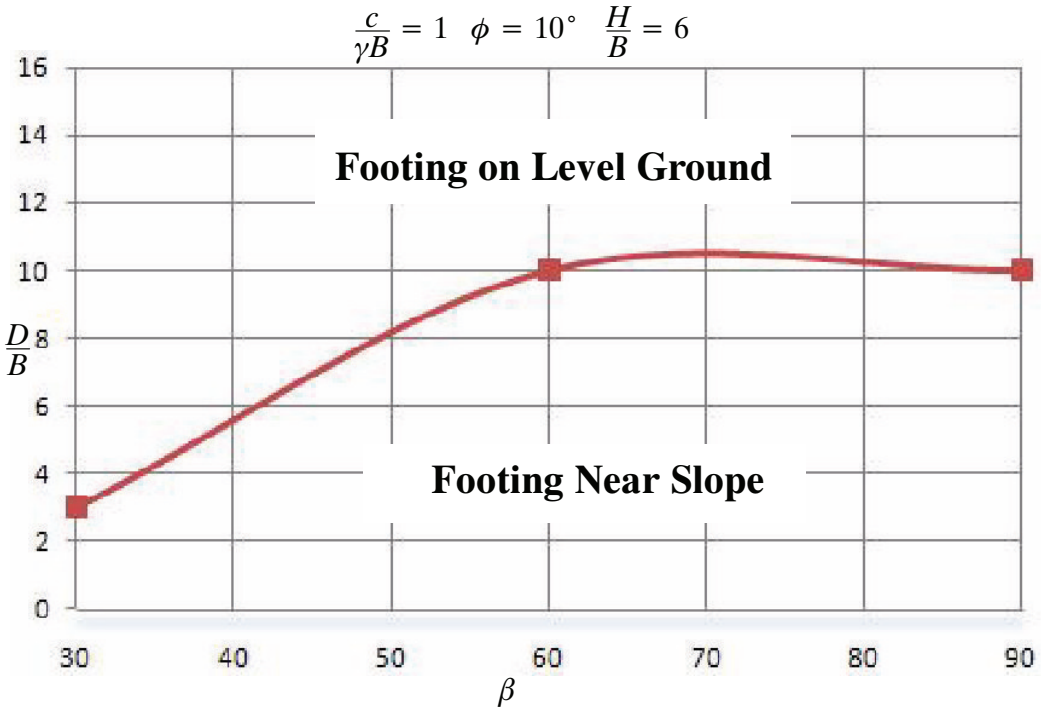

Figure 2-14. Level ground or footing near slope with given slop angle and a weak case

2.4.3 Comparison Among Various Dimensionless Strength Ratio's

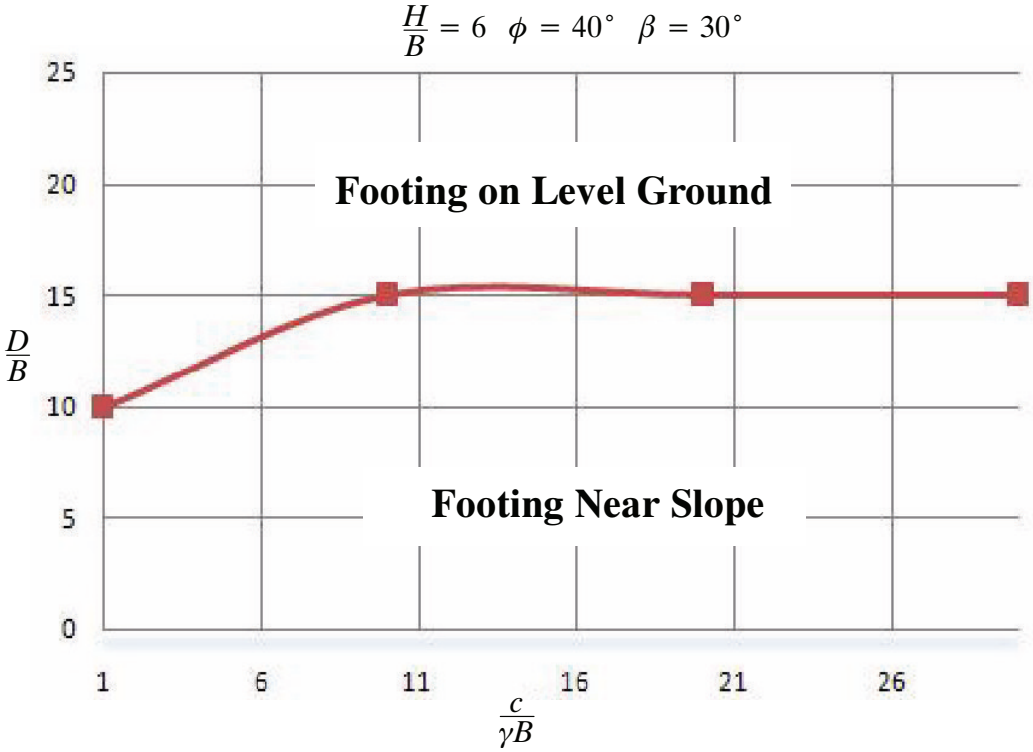

Figure 2-15. Level ground or footing near slope with given dimensionless strength ratio and a strong case

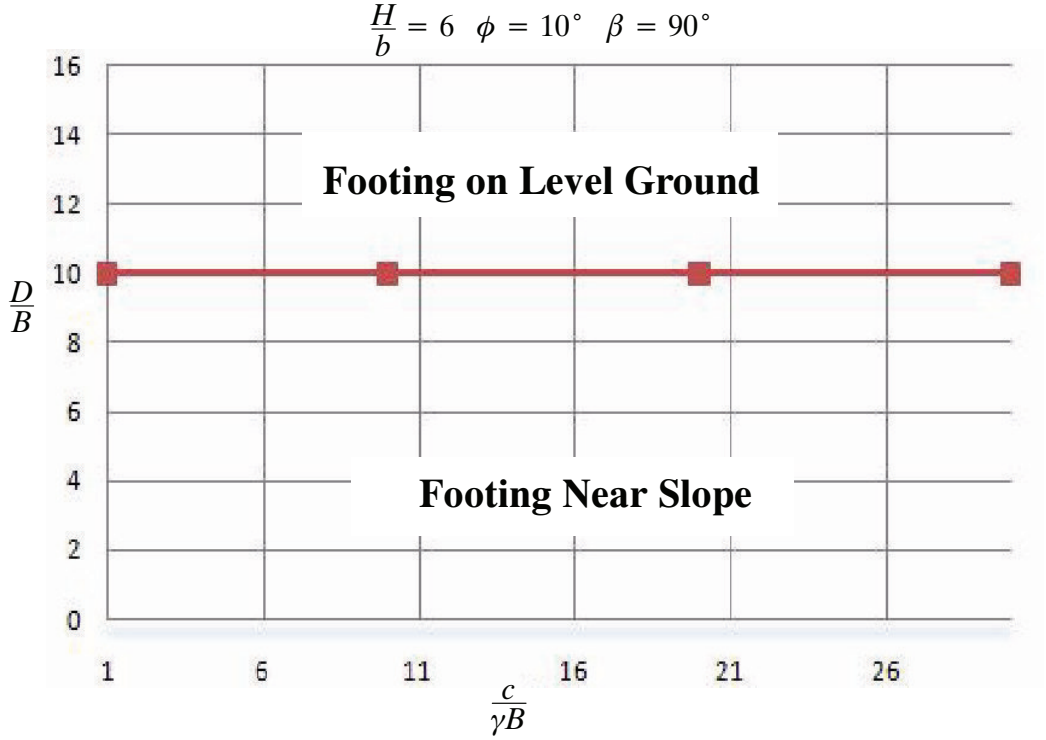

Figure 2-16. Level ground or footing near slope with given dimensionless strength ratio and a weak case

2.4.4 Comparison Among Various Friction Angles

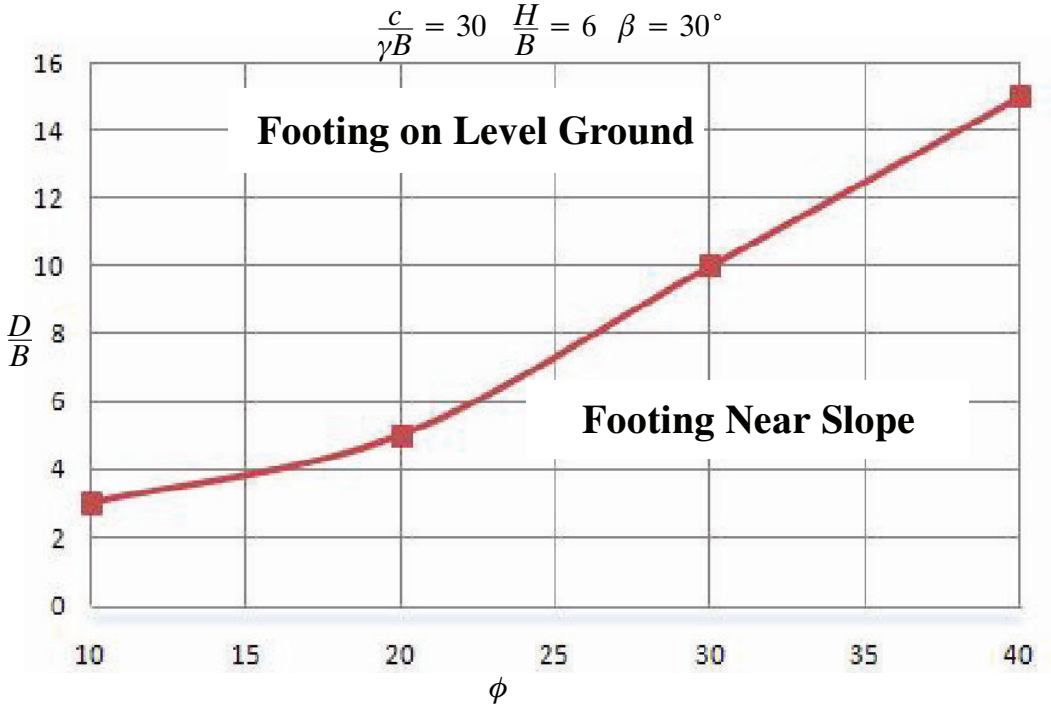

Figure 2-17. Level ground or footing near slope with given friction angle and a strong case

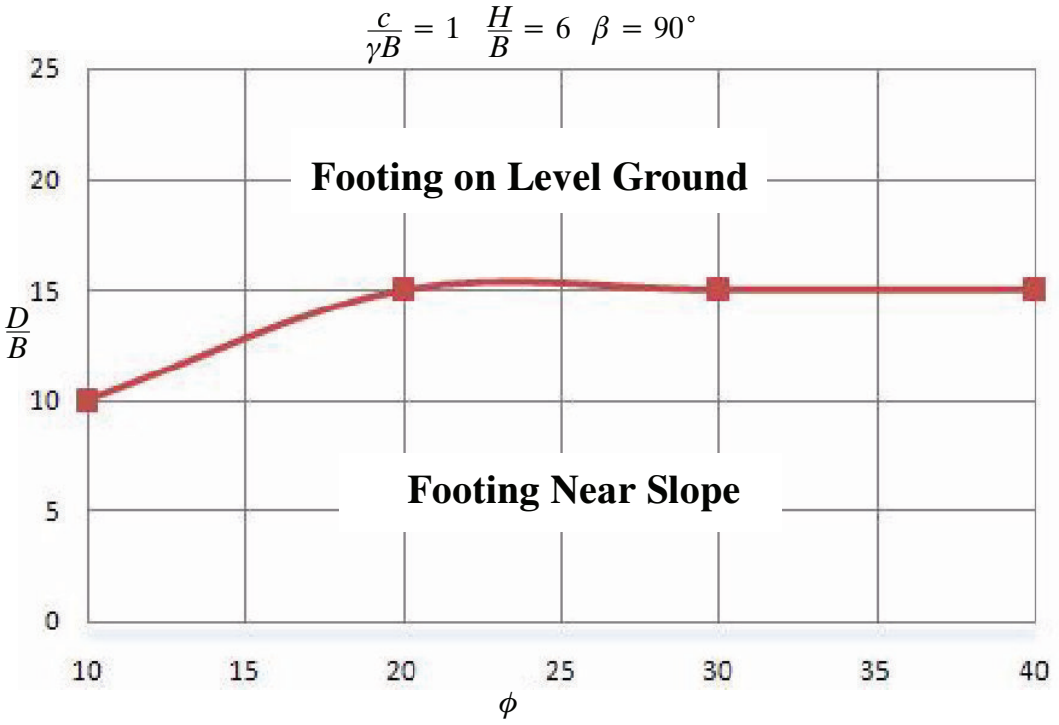

Figure 2-18. Level ground or footing near slope with given friction angle and a weak case

2.5 Adjusted FLAC Script File

Improvements to the script file to be run by FLAC have been made to improve ease of data entry, therefore reduced human error.

From the level ground analysis it was determined that each scenario produces a largely varied failure zone. This meant that for a number of cases the mesh size was too large and taking up uneccesary computational run-time. In the cases where the mesh size was too small the results produced were invalid as well as taking up more run-time. To overcome this issue a new FLAC script file was created which would, based on the inputted slope parameters, create an appropriate mesh size.

2.5.1 Validation of New Script

Figure 3-2 shows the variation in the old FLAC script file, used for the level ground analysis, with the new script file, used for the footing near slope analysis which includes the remainder of this research. These two sets of data are also plotted against results obtained using Terzaghi's method. The results taken from the footing near slope analysis have been taken from the apparent flat ground scenario. This is where the footing distance ratio, D/B, is such that the slope has no influence on the bearing capacity of the foundation. Figure 2-19 shows the comparison of the old script file and the new script file.

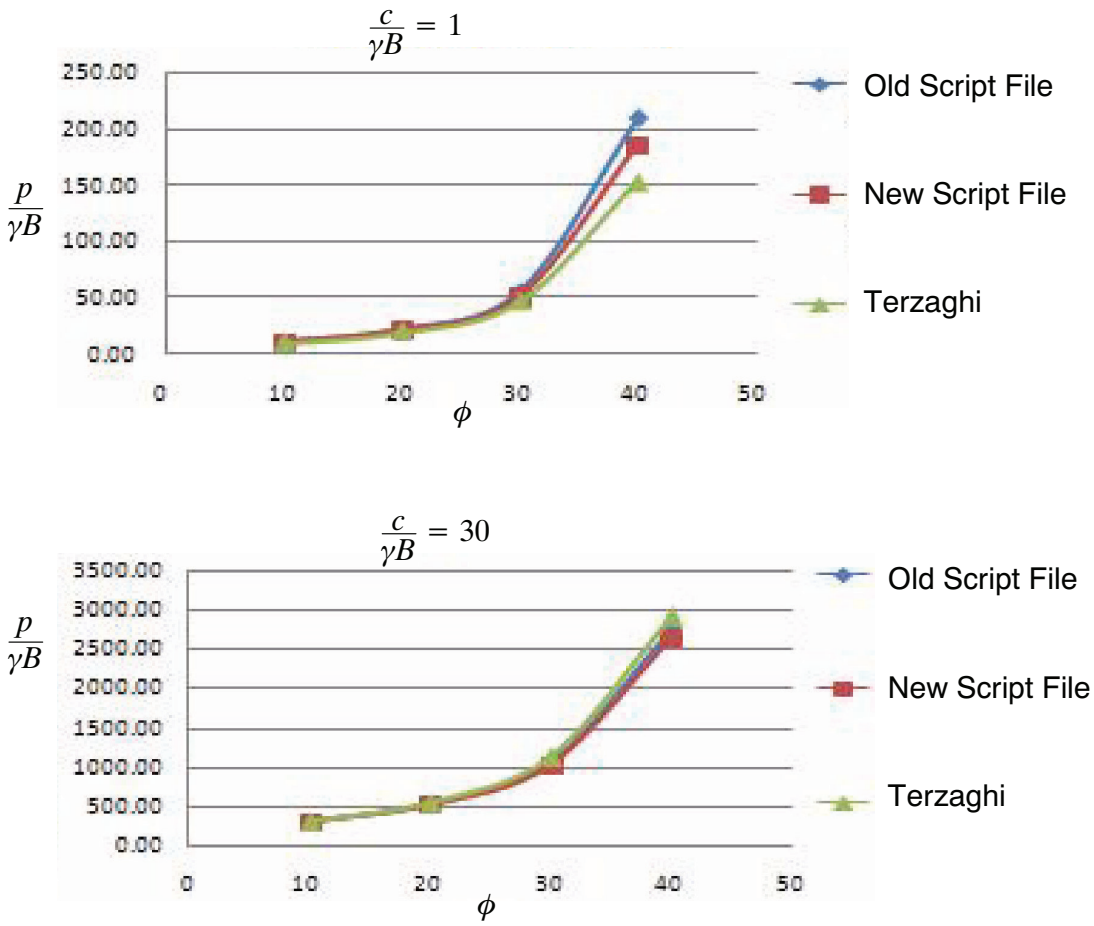

Figure 2-19. Old script file against new script file

The new script file has evidently reduced a small amount of the over-estimation seen in the old script file, but this small amount will make little difference to the accuracy of tthis model.

2.6 Conclusion

With a validated new model, which minimises program run time, and the ability to determine when the footing near slope solution method is required a full parametric study can be undertaken. The next chapters investigate a number of geometrical and material parameters and their effect on the bearing capacity of the footing near slope problem.

Material Properties Effect

3.1 Introduction

This chapter investigates the effect of foundation material properties, being dimensionless strength ratio and friction angle, for a given footing near slope problem.

The common parameters to be used in this chapter are slope angle, $\beta = 30^\circ$, dimensionless strength ratio, $\frac{c}{\gamma B} = 30$, slope height ratio, $\frac{H}{B} = 6$, footing distance ratio, $\frac{D}{B} = 1$, dimensionless surcharge loading, $\frac{q}{\gamma B} = 0$ and friction angle, $\phi = 40^\circ$. For a given scenario of these parameters the normalised bearing capacity for a level ground case is approximately 2650.

This chapter will only investigate cohesive-granular foundation materials, therfore dimensionless strength ratio and friction angle will always be positive. This is opposed to materials where cohesion ($\frac{c}{\gamma B}$) equals zero, such as for sand, and where friction angle (ϕ) equals zero, such as for clay.

3.2 Friction Angle Effect

Friction angle is a measure of the particle shape. A perfectly round shape has a zero internal angle of friction and is the reason they cannot stand in a pile. Sand on the other hand will maintain a cone formation because each particles angular shape does not allow other particles to roll freely past. The friction angle is also the natural angle of repose for a given particle when cohesion equals zero. It is therefore expected that a foundation consisting of a large friction angle will produce a larger normalised bearing capacity of the footing.

3.2.1 Comparison Among Various Footing Distance Ratios

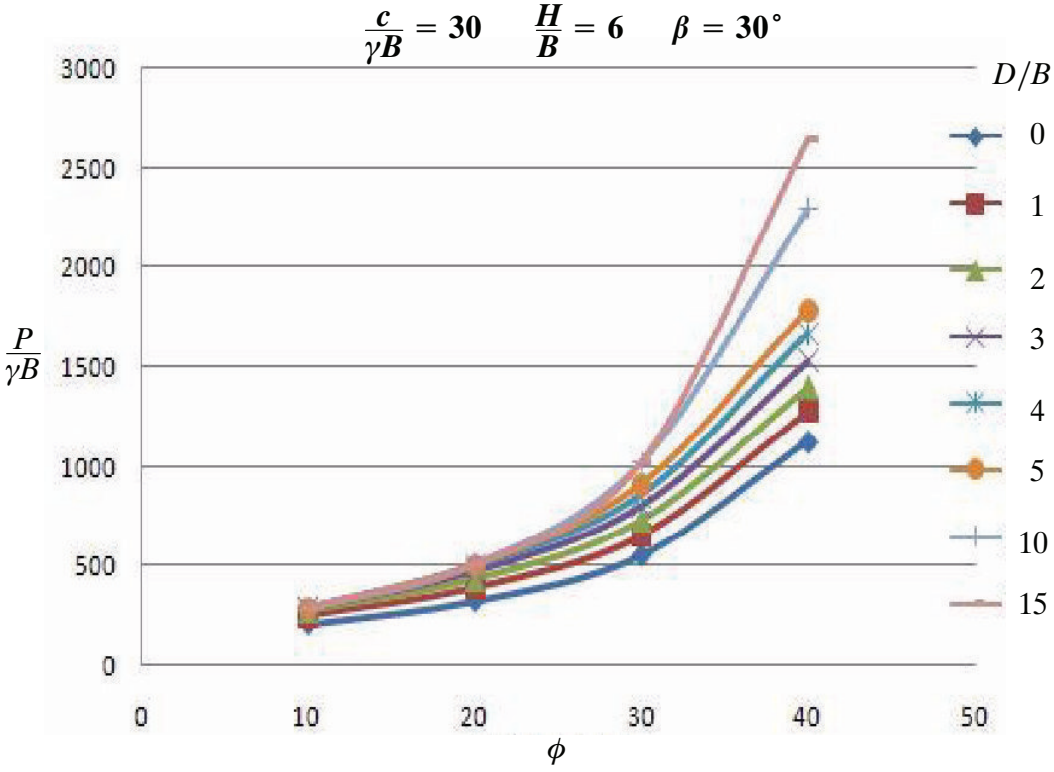

Figure 3-1. Effect of friction angle and footing distance ratio

The results shown in Figure 3-1 for the effect of friction angle with varying footing distance ratio display a converging trend for the normalised bearing capacity as friction angle is decreased. A great effect is evident between $\phi = 30^\circ$ and $\phi = 40^\circ$ with the largest increse of normalised bearing capacity, especially as D/B approches level ground condition. It is also evident for small friction angles that a level ground state is reached with much smaller D/B values as the data trends start to overlap one another.

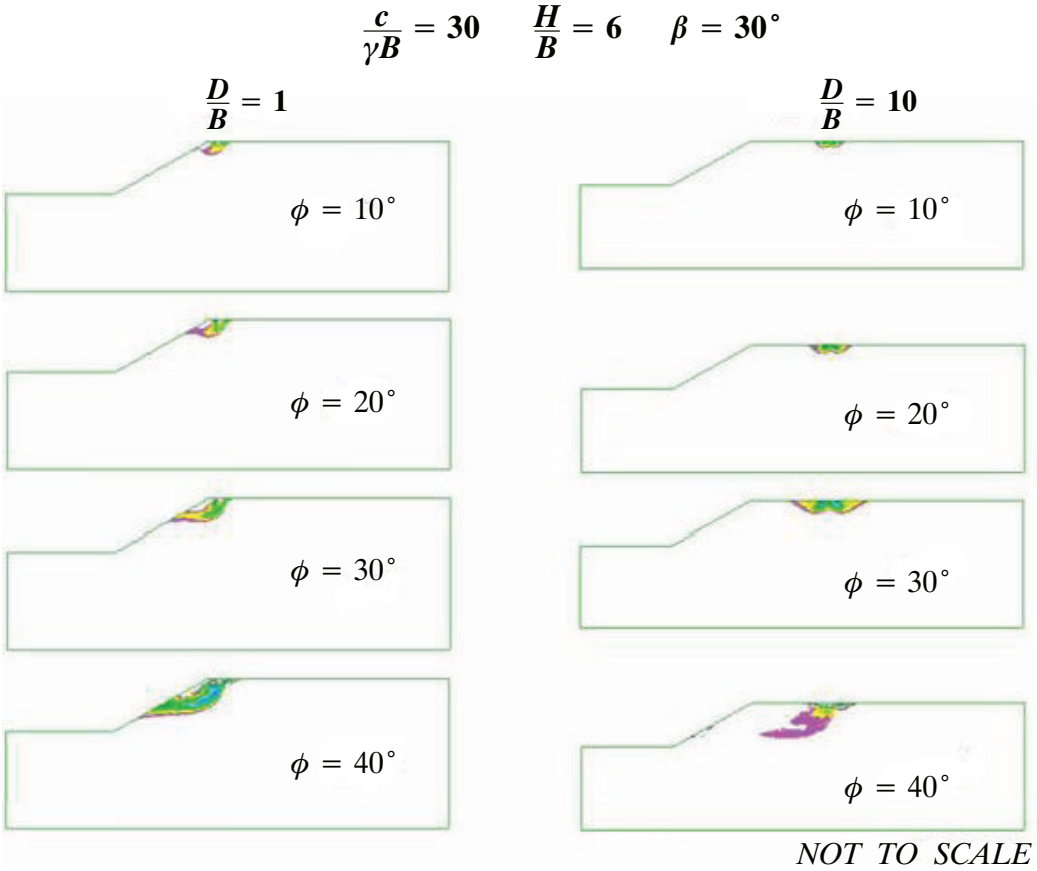

Figure 3-2. Contour plots of friction angle and footing distance ratio

The contour plots in Figure 3-2 confirm the level ground condition experienced for smaller friction angles and larger D/B values. The case shown indicates that as friction angle is increased, with all other parameters staying the same, the failure mechanism can change from a footing on level ground to a footing near slope problem. An increase in friction angle also causes a larger failure surface and hence a greater bearing capacity as validated in Figure 3-1.

3.2.2 Comparison Among Various Slope Angles

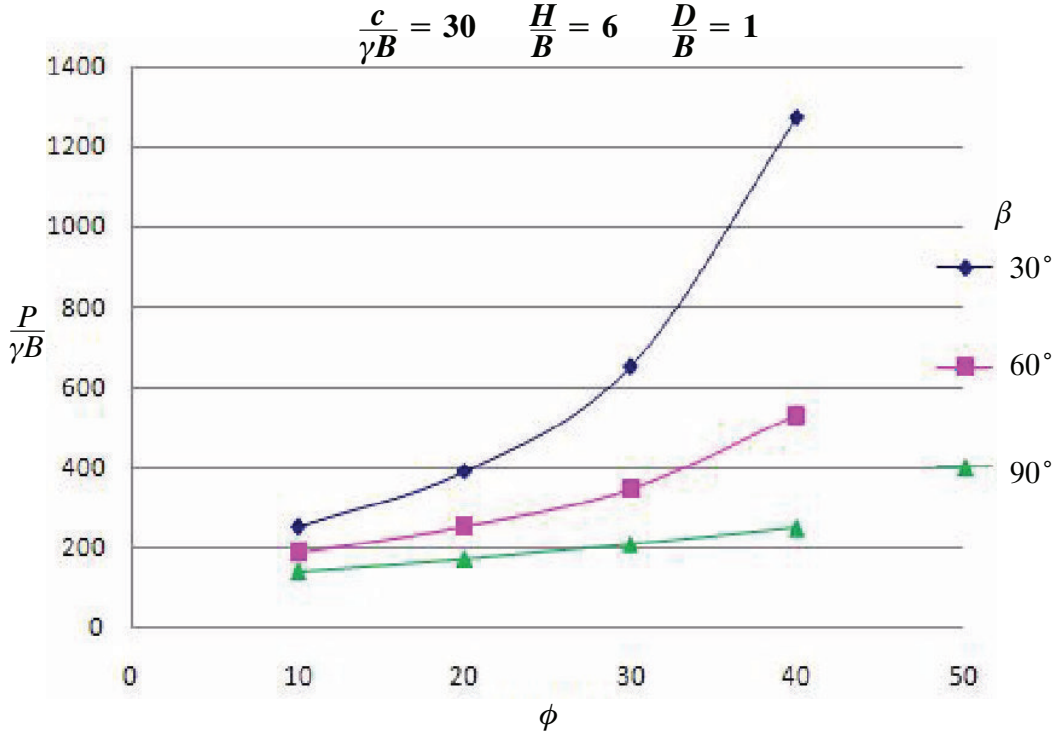

Figure 3-3. Effect of friction angle and slope angle

Again the effect of friction angle shows a converging trend for small friction angles with a change in slope angle. It is evident that the effect of friction angle is not great for a 90 degree slope due to its geometrical instability, however a 30 degree slope is strongly effected by a change in friction angle as shown in Figure 3-3. The normalised bearing capacity for a 30 degree slope with $\phi = 40^\circ$ is approximately double any other condition represented in Figure 3-3.

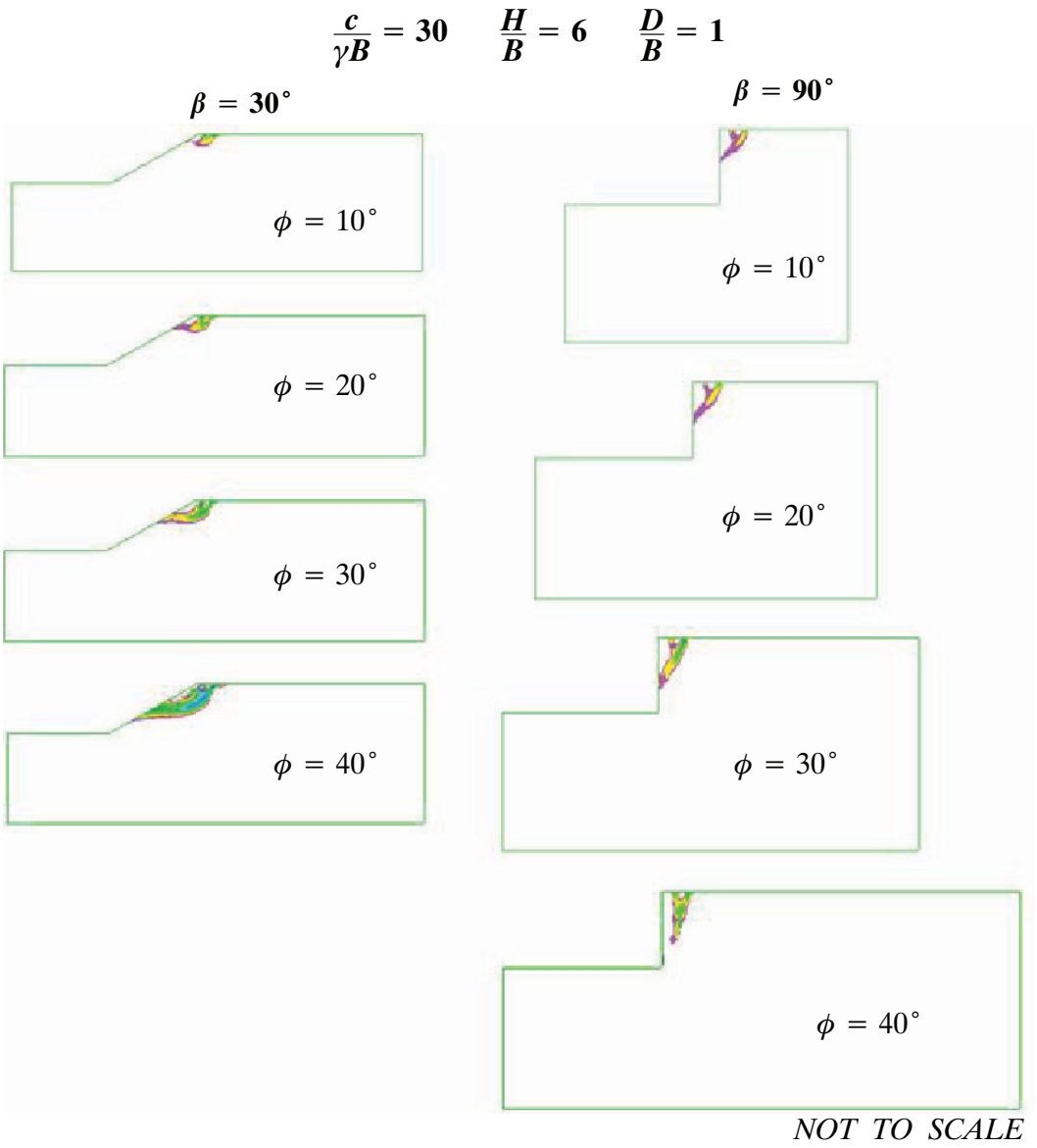

Figure 3-4. Contour plots of friction angle and slope angle

As expected from Figure 3-3 a much smaller failure zone occurs for a 90 degree slope and the vertical nature of the slope produces a weaker, vertical shear failure which results in a much smaller bearing capacity. Because the case represented has a very small footing distance ratio the variation in the failure surface for a 90 degree slope is also very small.

3.2.3 Comparison Among Various Dimensionless Strength Ratios

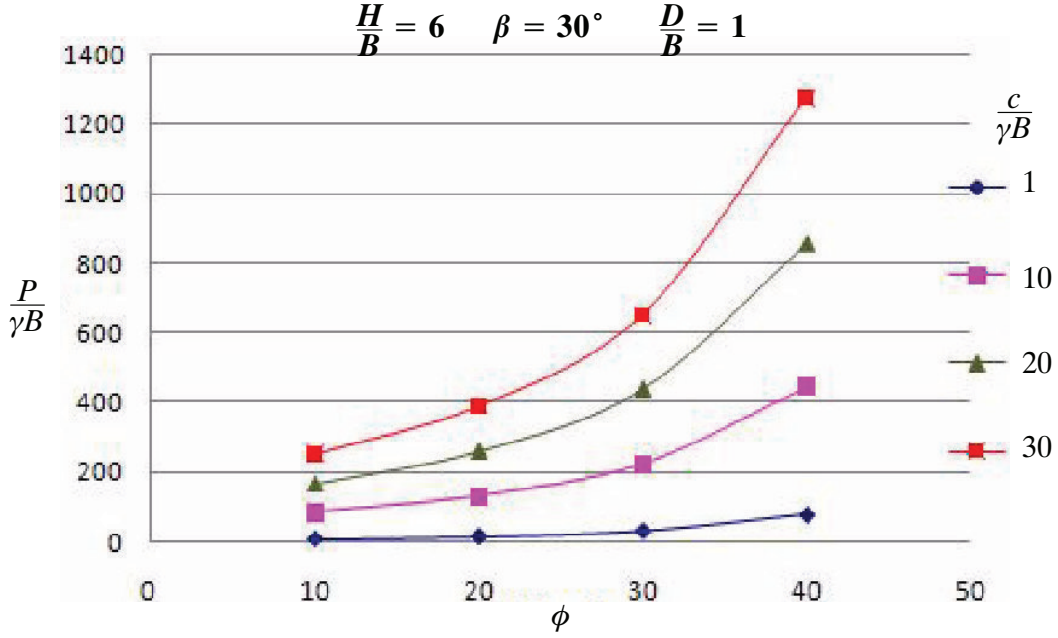

Figure 3-5. Effect of friction angle and dimensionless strength ratio

Figure 3-5 shows that when comparing the effect of friction angle and dimensionless strength ratio a less converging trend is produced to that of the other parameters. A general increse is seen in the normalised bearing capacity with both an increase in friction angle and dimensionless strength ratio. It is evident that a very weak foundation consists of a material with $\phi = 10^\circ$ and $\frac{c}{\gamma B} = 1$ where the normalised bearing capacity is almost zero.

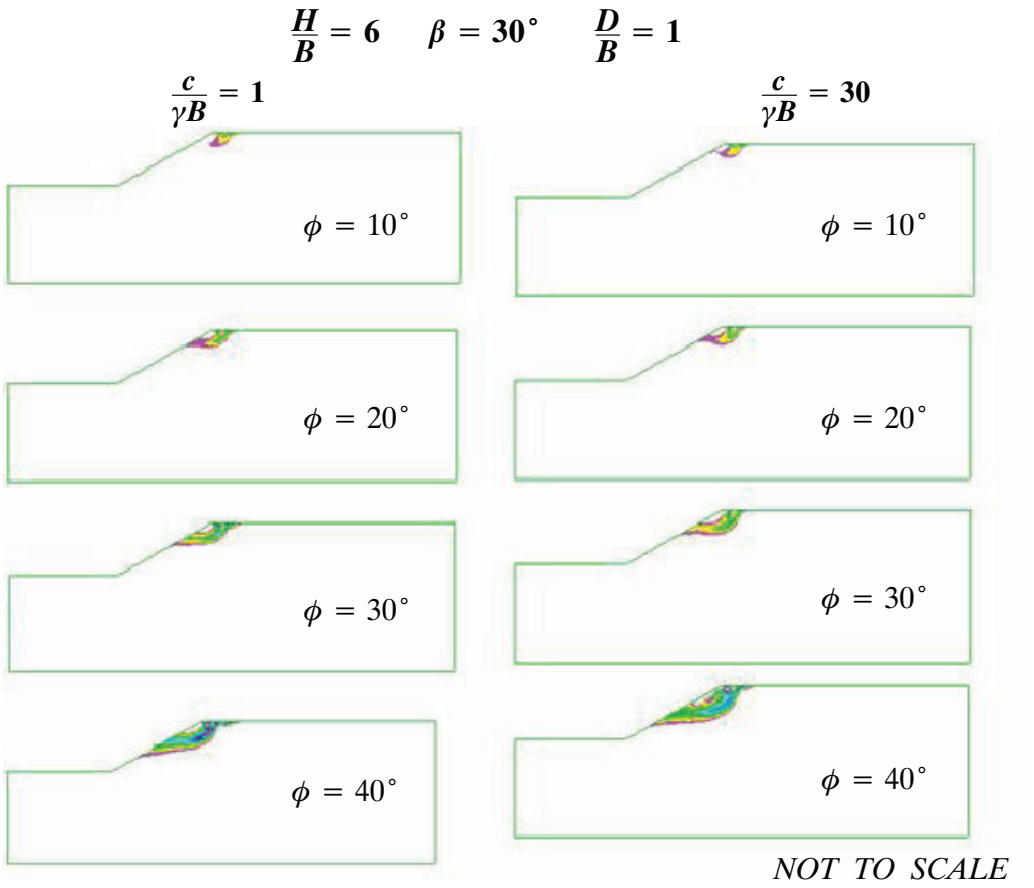

Figure 3-6. Contour plots offriction angle and dimensionless strength ratio

The failure zones shown in the contour plots of Figure 3-6 represent the increase in the normalised bearing capacity as friction angle is incresed. However, the contour plots do not represent the increase in the normalised bearing capacity which is experienced due to an increase in dimensionless strength ratio. This is because the slip surface remains the same but the load with which the foundation can support, hence the bearing capacity, is reduced with decreased dimensionless strength ratio. This scenario is further explained in the next section for the effect of dimensionless strength ratio.

3.2.4 Comparison Among Various Slope Height Ratios

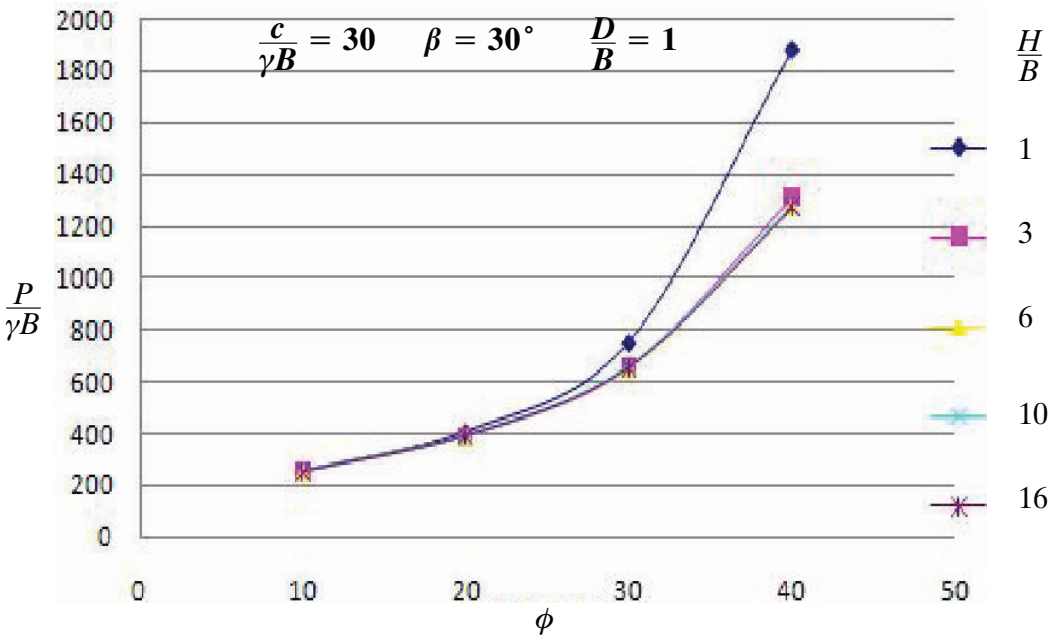

Figure 3-7. Effect of friction angle and slope height ratio

Figure 3-7 shows that for H/B values equal to and greater than three there is no effect from change in H/B. Similar to previous cases the normalised bearing capacity increases as friction angle increases. The effect of H/B is more clearly displayed in the contour plots of Figure 3-8.

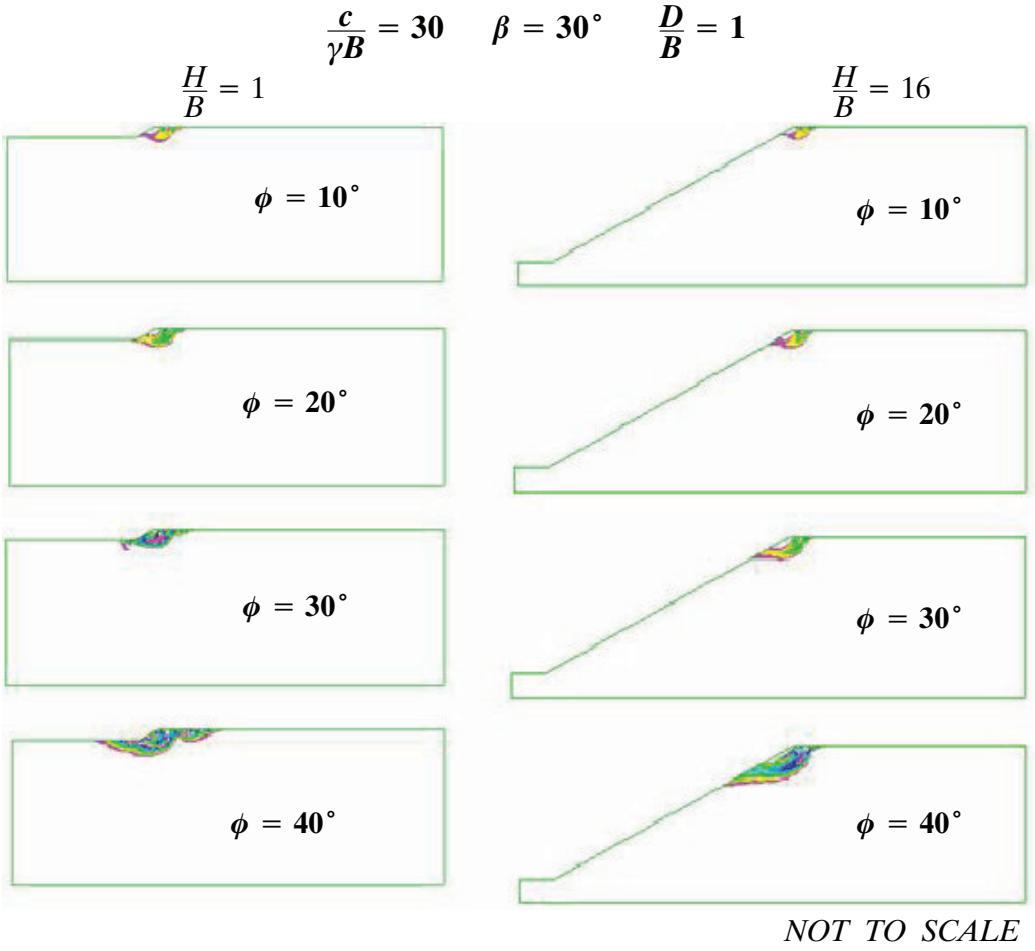

Figure 3-8. Contour plots offriction angle and slope height ratio

With reference to Figure 3-7 the contour plots in Figure 3-8 show that for large H/B the failure surface is always above-toe. For small H/B where $\phi = 10^\circ$ the failure surface is also above-toe and for $\phi = 20^\circ$ the failure surface is at-toe. Once the failure surface reaches at-toe any further increase in H/B has no effect on the normalised bearing capacity. This is why the data trends in Figure 3-7 over-lap one another.

3.2.5 Conclusions

For the effect of friction angle there was a definite convergence of results toward very low friction angles. This convergence is always non-linear meaning that as the friction angle is increased the rate of change of the normalised bearing capacity increases. This concludes that in a practical situation consisting of a particular foundation material with a small friction angle there would be little benefit in modifying any other parameters to increase bearing capacity. An increase in the friction angle of a foundation material will result in

an increase in the normalised bearing capacity with any other combination of parameters so long as those parameters remain constant.

3.3 Cohesion Effect

Cohesion is the shear strength of soil, a measure of the forces which hold the soil particles together. Optimum moisture provides a significant cohesion as does some natural minerals which leache into the soil. Heat and long-term surcharge pressure fuse particles together resulting in increased cohesion. Clays are very cohesive materials and as a material becomes more sandy cohesion is reduced. In this section cohesion is represented by dimensionless strength ratio and it is expected that when increased the normalised bearing capacity will increase as well.

3.3.1 Comparison Among Various Footing Distance Ratios

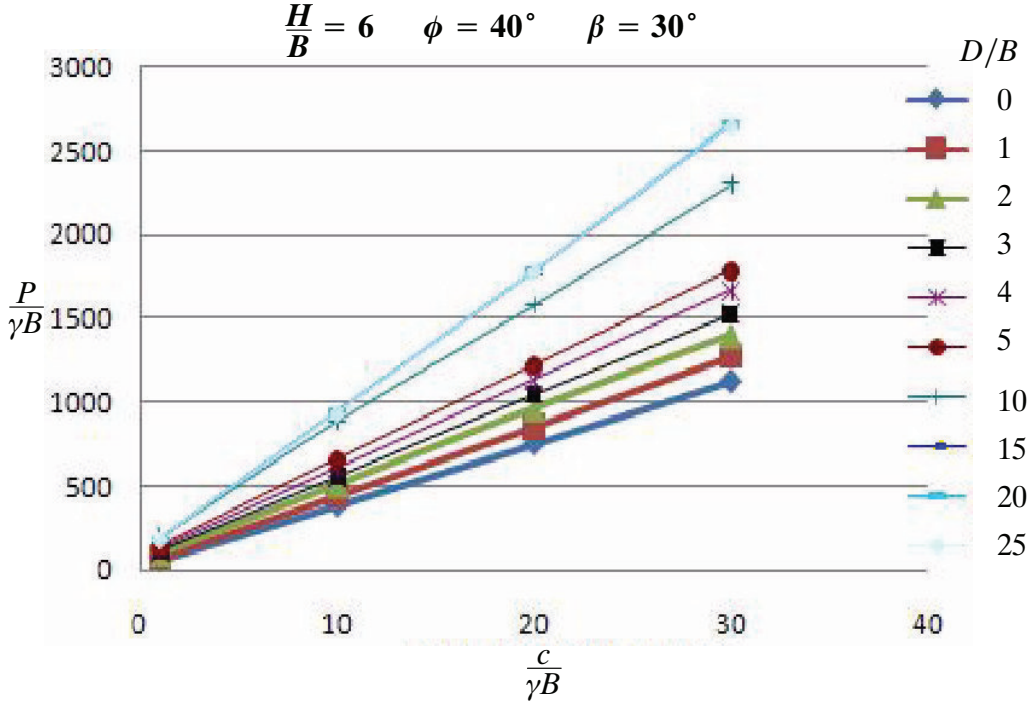

Figure 3-9. Effect of dimensionless strength ratio and footing distance ratio

The data trends in Figure 3-9 show that as dimensionless strength ratio is increased the normalised bearing capacity increases linearly. Also it is noted that for a given dimensionless strength ratio the normalised bearing capacity increases at approximately the same rate for equal increases in the footing distance ratio. It can be seen that the values converge when the dimensionless strength ratio is very small, therefore there is very little difference in the normalised bearing capacity between a footing close to a slope or a footing

on level ground. As D/B gets very large a level ground condition is reached. This is evident from the overlapping of the trend lines for D/B = 15, 20 and 25.

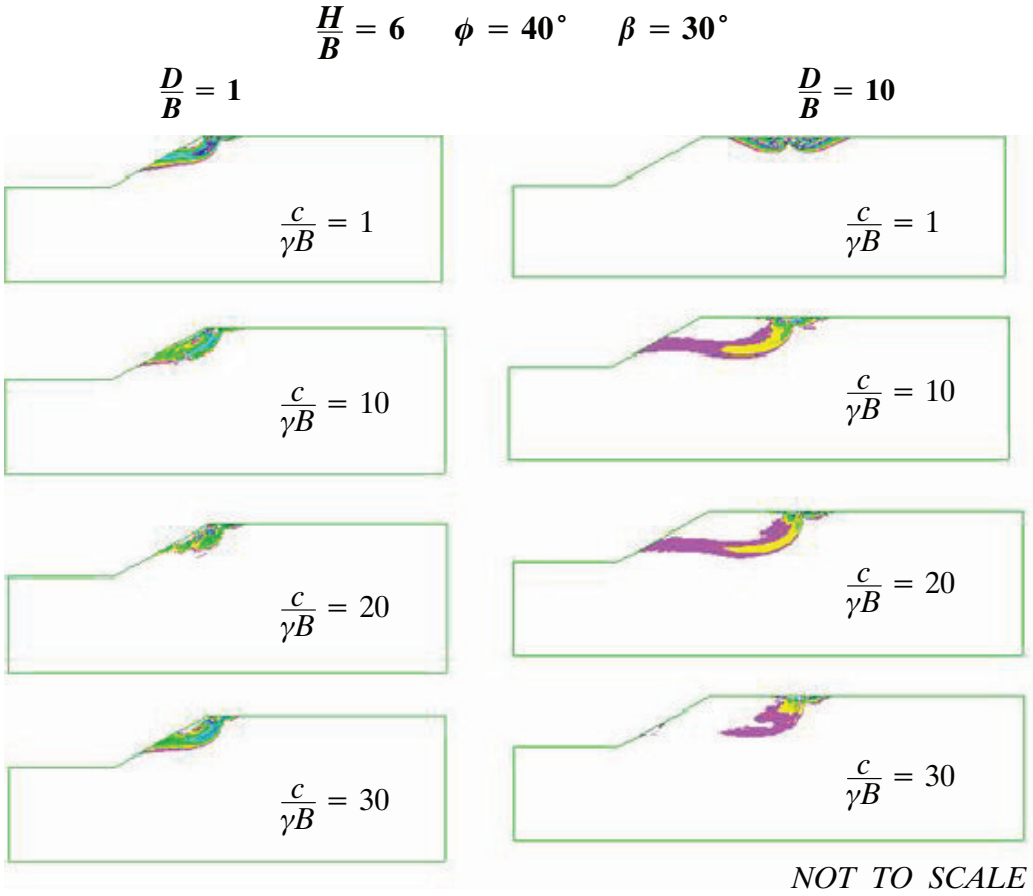

Figure 3-10. Contour plots of dimensionless strength ratio and footing distance ratio

It has been noted throughout this research that the contour plots for varying dimensionless strength ratio's generally produce the same failure surfaces. This is because the strength of the foundation material will determine the load which will cause failure not the shape of the slip surface. However, for this particular case for very small dimensionless strength ratio and large footing distance ratio a level ground condition is encountered. It is noted that once it becomes a footing near slope problem the failure surface only changes slightly.

3.3.2 Comparison Among Various Slope Angles

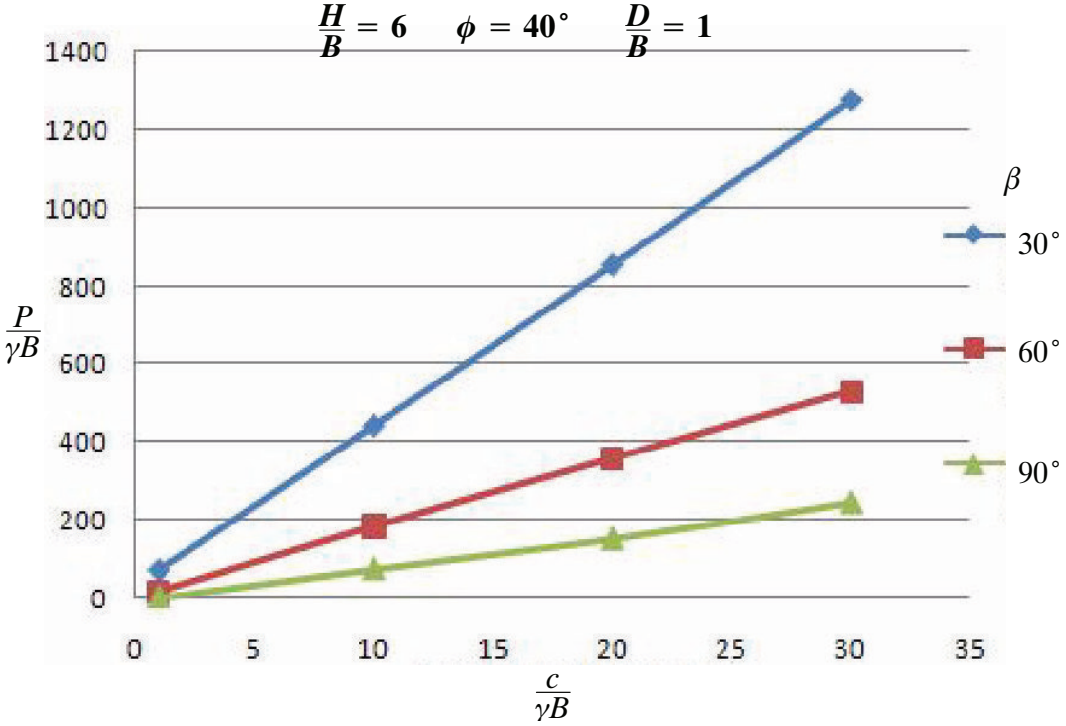

Figure 3-11. Effect of dimensionless strength ratio and slope angle

Again a linear trend is produced in Figure 3-11, with results converging when dimensionless strength ratio becomes very small. This scenario, comparing dimensionless strength ratio with slope angle, shows that the increase in the normalised bearing capacity is not equal with equal increases in slope angle. There is a much greater difference between $\beta = 60^\circ$ and $\beta = 30^\circ$ than there is between $\beta = 90^\circ$ and $\beta = 60^\circ$.

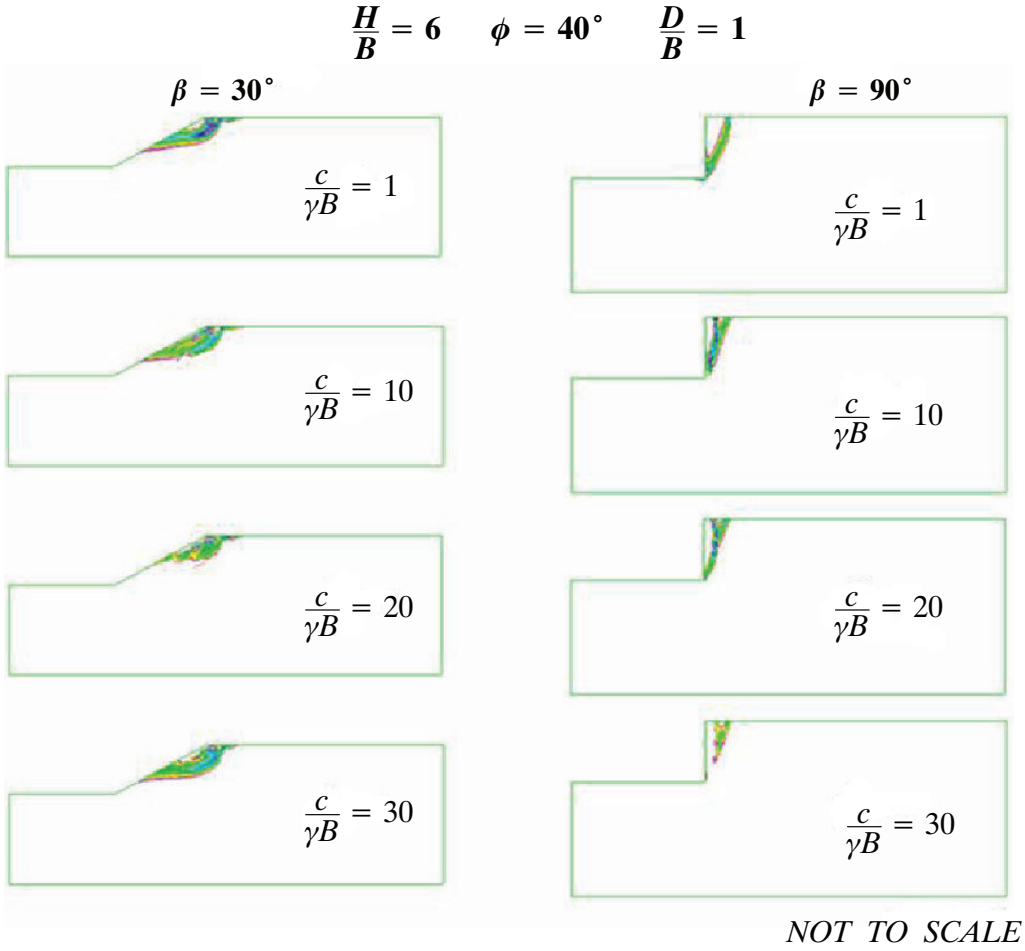

Figure 3-12. Contour plots of dimensionless strength ratio and slope angle

Figure 3-12 displays a further example of the very little change in the failure surface for varying dimensionless strength ratio. It can be noted that for $\beta = 90^\circ$ the failure surface produced is slightly below-toe.

3.3.3 Comparison Among Various Slope Height Ratios

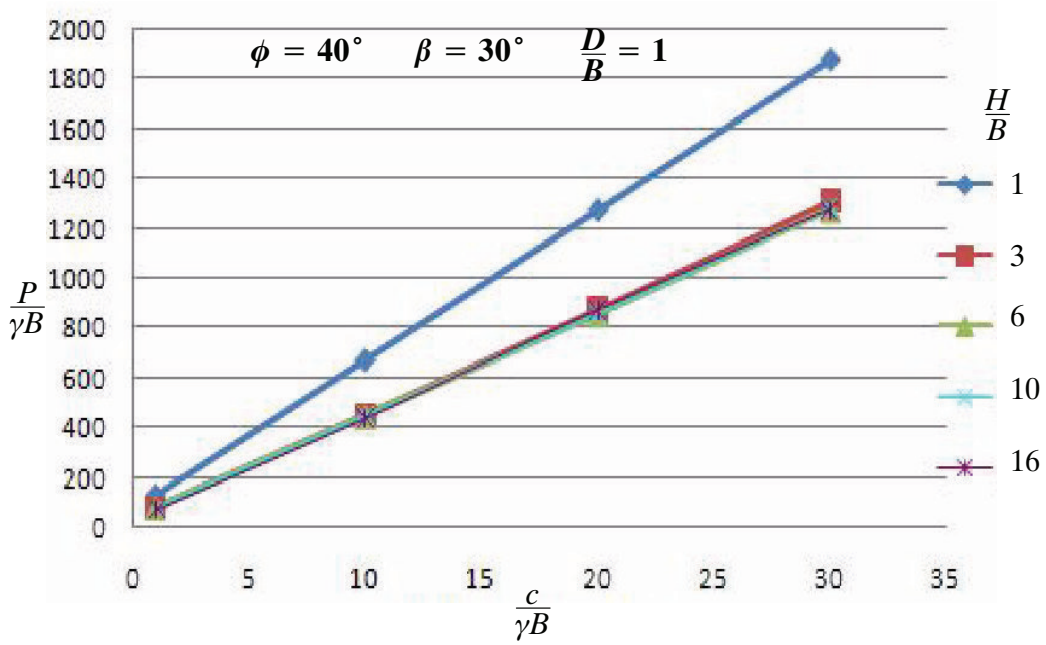

Figure 3-13. Effect of dimensionless strength ratio and slope height ratio

Similar to the other scenarios presented for the effect of dimensionless strength ratio, Figure 3-13 displays a linear trend with a convergence towards small dimensionless strength ratio. However, for H/B = 3 and greater the results obtained are the same because above-toe failure is reached and therefore further increase in H/B has no further effect.

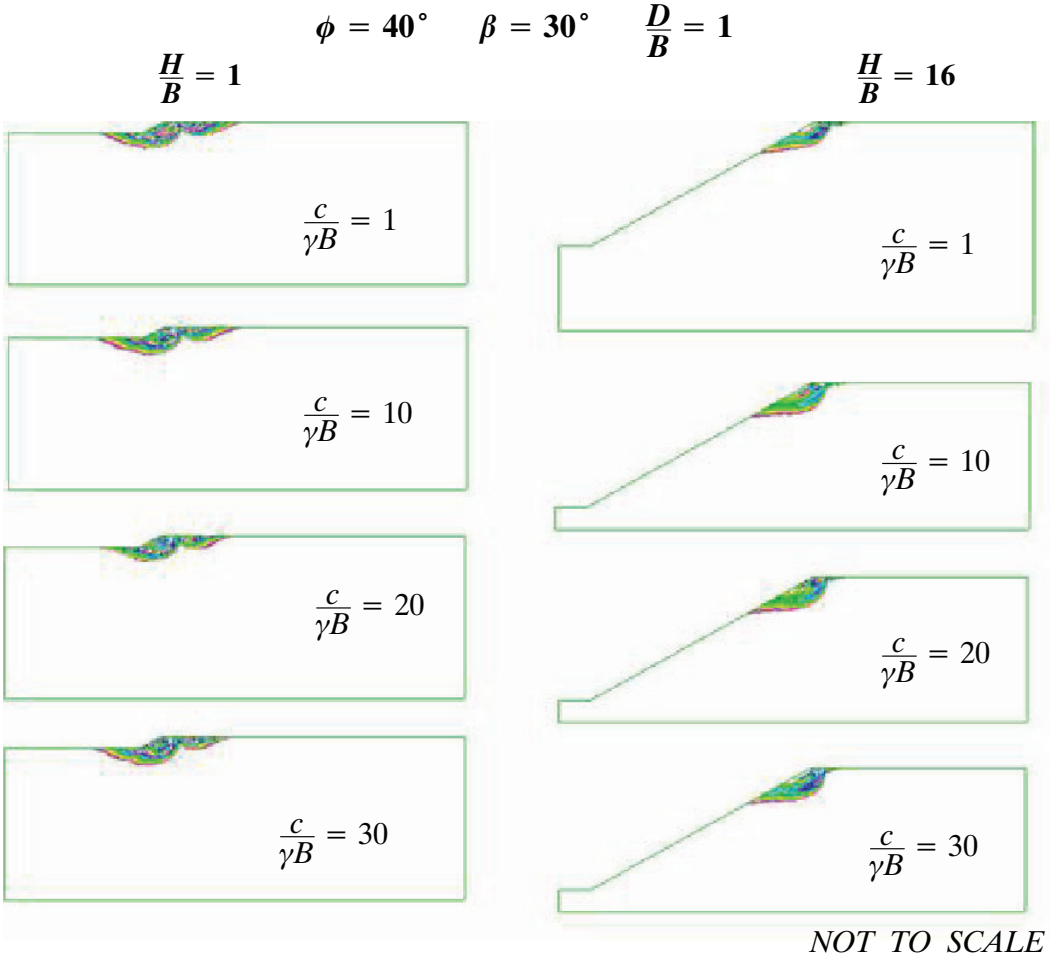

Figure 3-14. Contour plots of dimensionless strength ratio and slope height ratio

Again for the study of dimensionless strength ratio and compared with slope height, the failure surface displays minimal variance as seen in previous dimensionless strength ratio studies.

3.3.4 Comparison Among Various Friction Angles

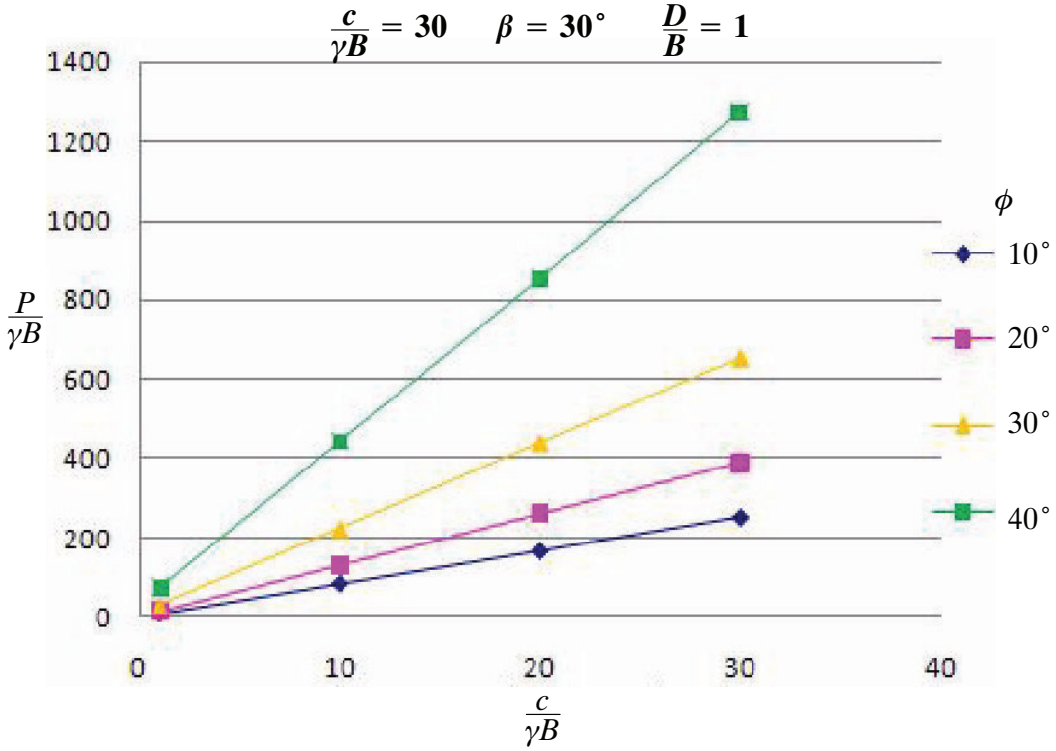

Figure 3-15. Effect of dimensionless strength ratio and friction angle

The effect of dimensionless strength ratio and friction angle again displays the general trend, in Figure 3-15, of a linear increase in the normalised bearing capacity from a convergence at a small value of dimensionless strength ratio. As friction angle increases so to does the difference in normalised bearing capacity with significantly larger values for $\phi = 40^\circ$. This concludes that an ideal foundation material has a large friction angle and large dimensionless strength ratio.

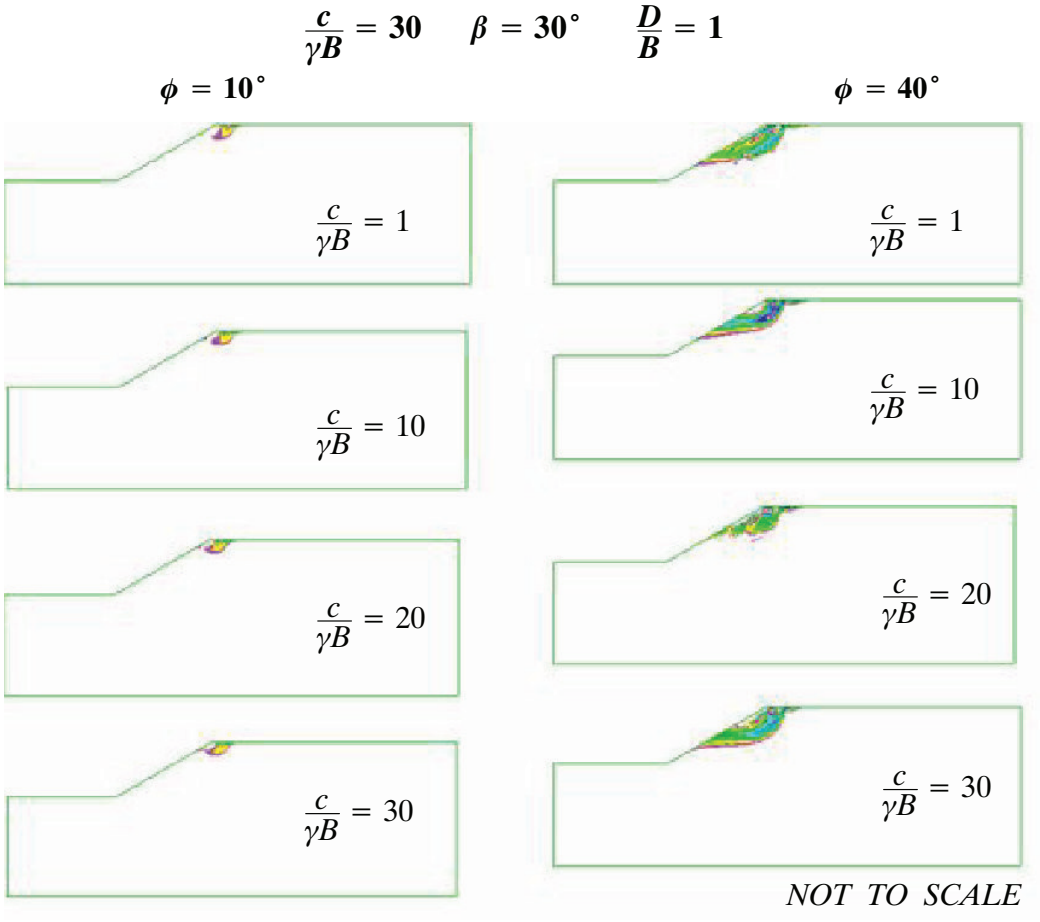

Figure 3-16. Contour plots of dimensionless strength ratio and friction angle

Figure 3-16 shows the continuing trend of the dimensionless strength ratio contour plots where the change in failure surface is insignificant.

3.3.5 Conclusions

This section has made clear conclusions of the effect of dimensionless strength ratio. Increasing the dimensionless strength ratio produces a linear increasing trend in the normalised bearing capacity of the footing near slope problem. When compared with other parameters the trends converge to produce very little difference for a material of small dimensionless strength ratio. It has also been graphically shown that the failure surface does not vary due to change in dimensionless strength ratio, however does vary for all other parameters. Therefore for special cases a difference in the failure surface was seen such as for level ground or below-toe failure.

Geometrical Effect

4.1 Introduction

This chapter investigates the dimensional parameters for the footing near slope problem. Parameters such as slope height, slope angle and location of the footing from the slope strongly influence the overall stability of the slope and footing foundation. Various combinations of these parameters produce a wide range of behavioural trends with great differences in overall bearing capacity. This chapter aims to provide an accurate indication of how each geometrical parameter effects the slope stability whilst varying other geometrical and material parameters.

The common parameters to be used in this chapter are slope angle, $\beta = 30^\circ$, dimensionless strength ratio, $\frac{c}{\gamma B} = 30$, slope height ratio, $\frac{H}{B} = 6$, footing distance ratio, $\frac{D}{B} = 1$, dimensionless surcharge loading, $\frac{q}{\gamma B} = 0$ and friction angle, $\phi = 40^\circ$. For a given scenario of these parameters the normalised bearing capacity for a level ground case is approximately 2650.

This chapter will only investigate cohesive-granular foundation materials, therefore dimensionless strength ratio and friction angle will always be positive. This is opposed to materials where cohesion ($\frac{c}{\gamma B}$) equals zero, such as for sand, and where friction angle (ϕ) equals zero, such as for clay.

4.2 Effect of Slope Angle

This section studies the effect of slope angle on the overall bearing capacity of the slope. It is known that when a slope is steepened, say by excavation, it becomes less stable. This section will give clear trends and values as to which combinations of parameters along with slope angle produce highly stable or unstable slopes. The slope angles which will be studied in this section include $\beta = 30^{\circ}$, $\beta = 60^{\circ}$ and $\beta = 90^{\circ}$.

4.2.1 Comparison Among Various Footing Distance ratios

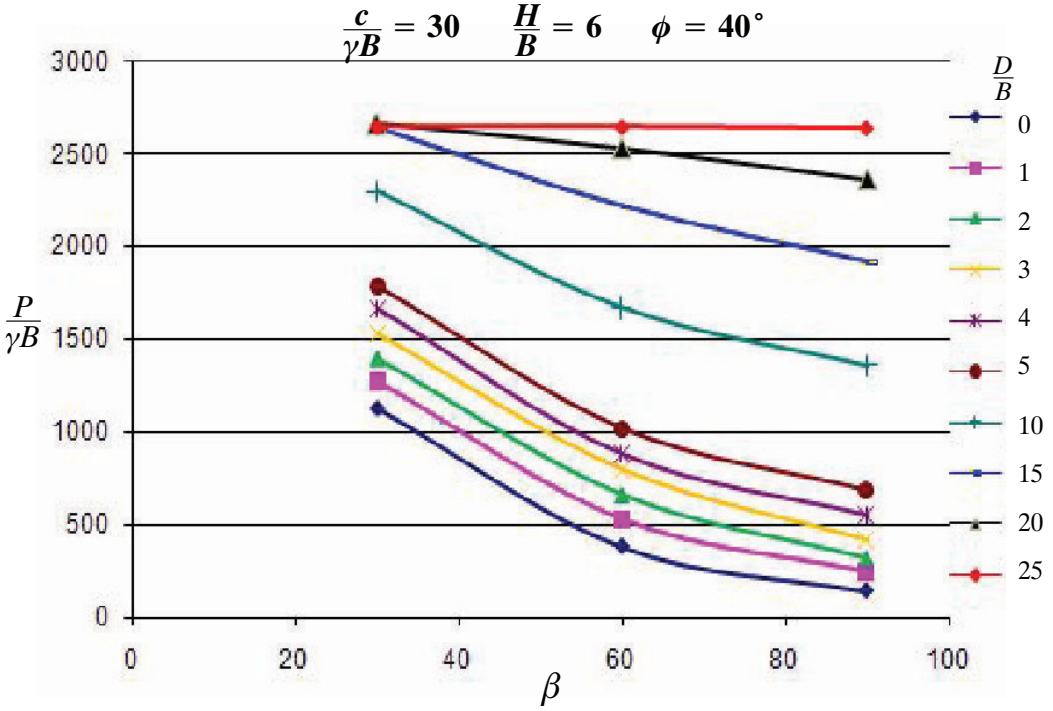

Figure 4-1. Effect of slope angle and footing distance ratio

Figure 5-1 confirms that as a slope becomes steeper it becomes less stable. This is evident in that the normalised bearing capacity is significantly reduced as the slope angle increases. To overcome this reduction figure 5-1 shows that while increasing the slope angle but moving the footing further from the slope a greater bearing capacity of the foundation material is acheived. For example a 30 degree slope with D/B = 2 has approximately the same bearing capacity as a 90 degree slope with D/B = 10. From a design perspective it is interesting to note for a 30 degree slope with D/B = 15 the behaviour is such that the slope has no influence on the bearing capacity and the problem is considered as a level ground problem. Therefore, there would be no benefit from moving the footing any further from the slope. For the same position a 90 degree slope still has quite a large effect on the bearing capacity.

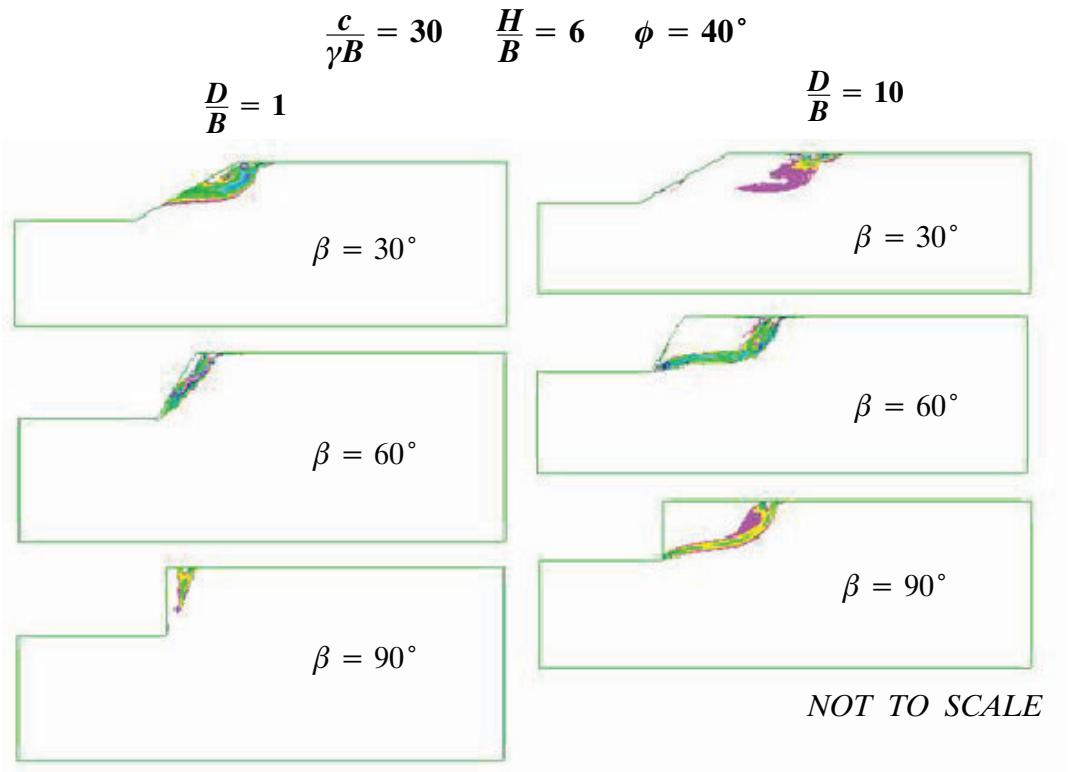

Figure 4-2. Contour plots of slope angle and footing distance ratio

Figure 5-2 shows contour plots for the effect of slope angle compared with varied D/B. These contours clearly show the key trends for this scenario. When the footing is moved away from the slope the failure zone required to reach the surface of the slope is much greater producing a larger bearing capacity. Also as the slope angle is increased the area of the slope is decreased therefore the failure zone is decreased resulting in a much smaller bearing capacity.

4.2.2 Comparison Among Various Slope Height Ratios

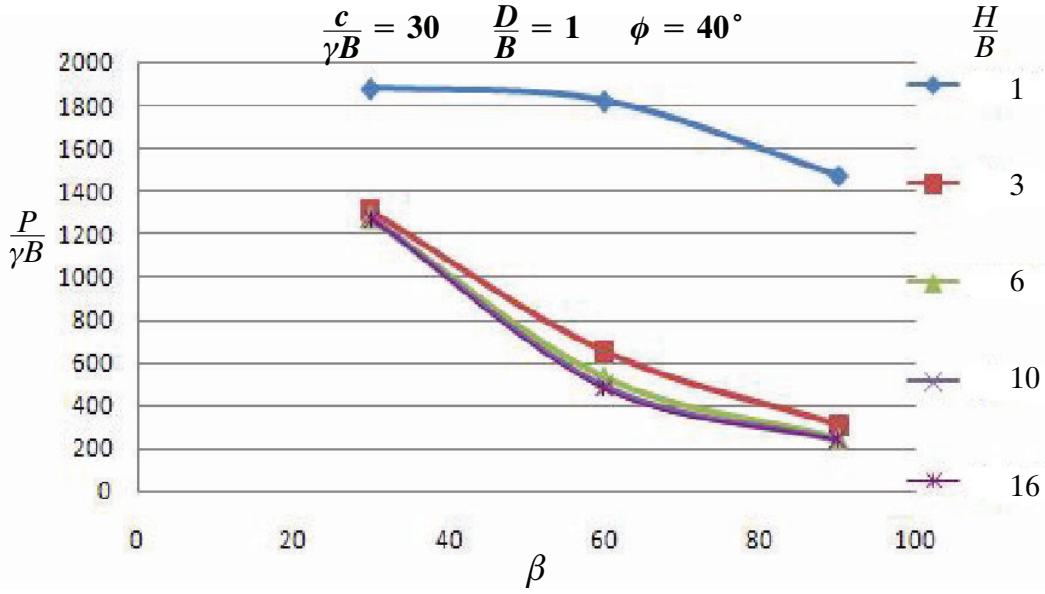

Figure 4-3. Effect of slope angle and slope height ratio

The effect of slope angle is clear again in figure 5-3 with a definite decreasing trend as β is increased. Recall that the normalised bearing capacity for a level ground with the above parameters is approximately 2650. So, even a small slope of H/B = 1 is largely effected.

As H/B approaches level ground the effect on the normalised bearing capacity is much greater for a slope angle of 90˚ to that of a 30˚ or 60˚ slope. For large H/B the decrease in the normalised bearing capacity is similar between a 30˚ and 60˚ slope as well as between a 60˚ and 90˚ slope.

There is a great difference in normalised bearing capacity between H/B = 1 and H/B = 3. From H/B = 6 there is no further effect as H/B is increased. These trends will be more clear in the contour plots of figure 5-4.

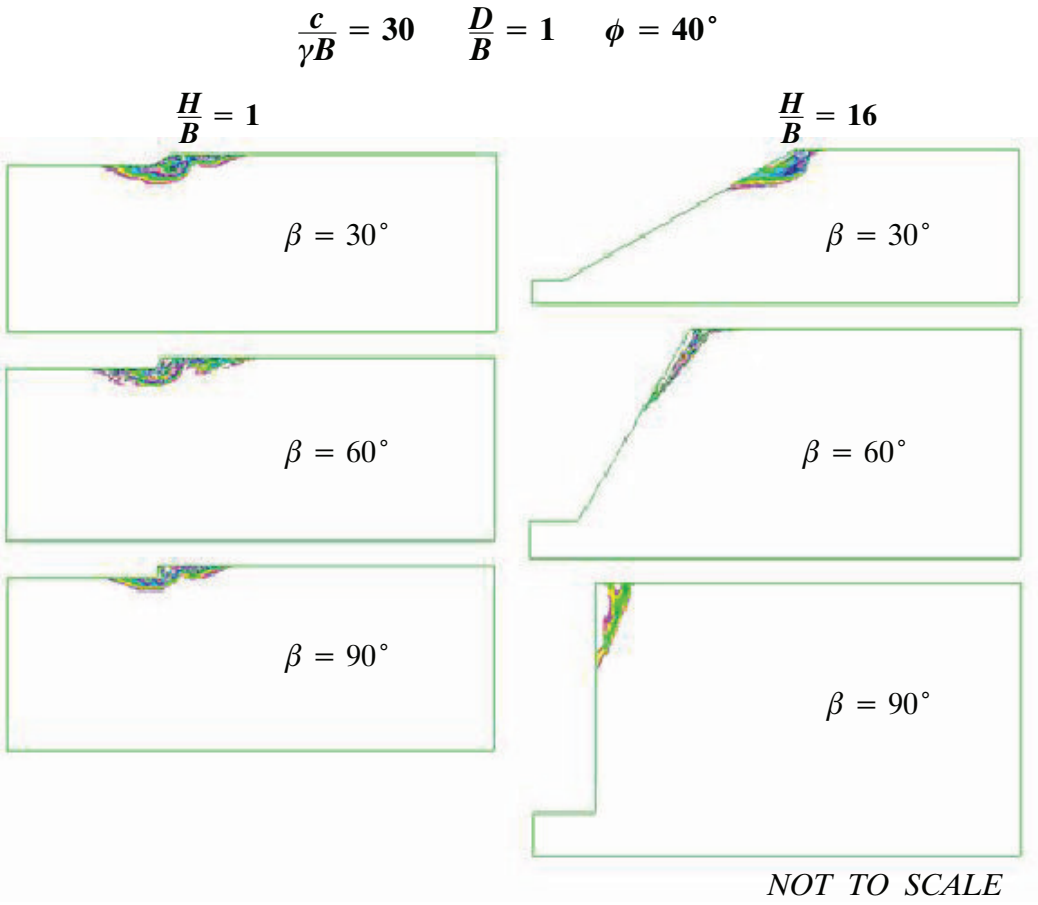

Figure 4-4. Contour plots of slope angle and slope height ratio

The contour plots in figure 5-4 show that for small H/B overall slope stabilility failure occurs where the whole slope is engulfed in the slip surface. Both 30 and 60 degree slopes allow for a larger failure zone due to the nature of the inclination of the slope. This is why the values for the normalised bearing capacity are close for a 30 and 60 degree slope and quite different for the 90 degree slope. This is the trend shown in figure 5-3 where the H/B = 1 line shows a concave down shape. For larger H/B the 30 degree slope experiences a failure in the plastic zone due to local foundation failure which is influenced by the slope. When the slope angle is increased to 60 and 90 degrees the failure experienced is only in the active zone due to the great effect of the slope angle. This is why, in figure 5-3, there is a larger difference between the 30 and 60 degree slope than there is between the 60 and 90 degree slope. This trend shows up as a partial concave up curve in figure 5-3.

There is a great difference between H/B = 1 and H/B = 3 because the failure method is changing from overall slope stability failure to local at-toe failure. From H/B = 6 and greater the failure mechanism is local above-toe failure and this is why there is no further effect as H/B is increased.

4.2.3 Comparison Among Various Dimensionless Strength Ratios

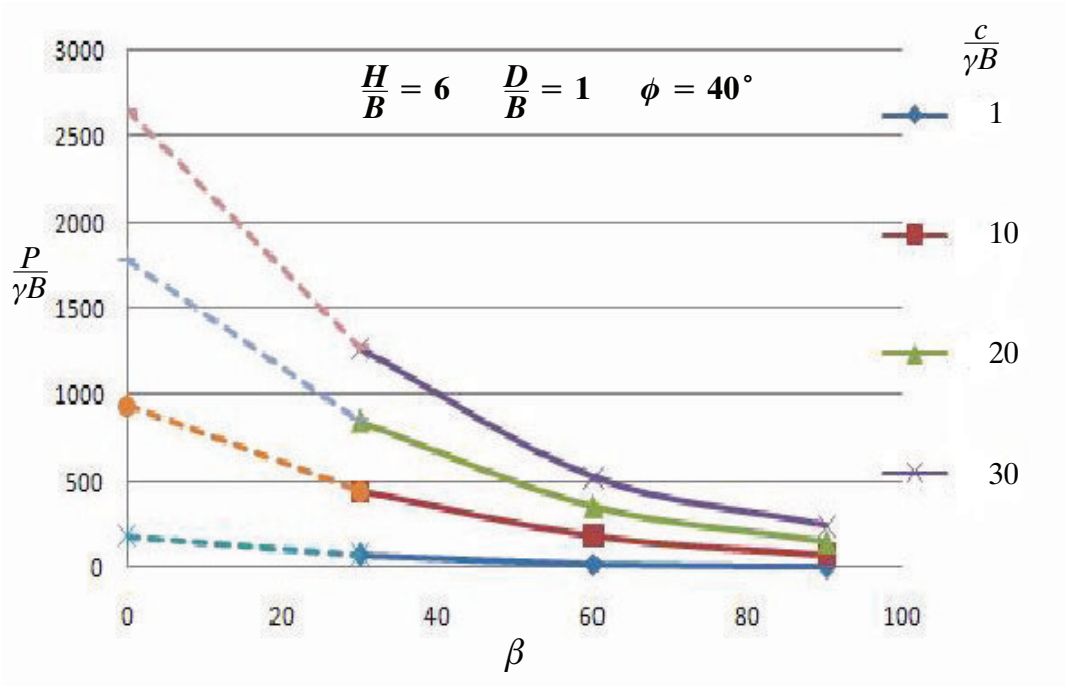

Figure 4-5. Effect of slope angle and dimensionless strength ratio

The clear trends in figure 5-5 are that as the slope angle is increased the normalised bearing capacity decreases and as the dimensionless strength ratio is increased the normailised bearing capacity increases. For each slope angle and various dimensionless strength ratio's the difference in the normalised bearing capacity appears equal and with decreasing slope angle this difference greatly increases. For a design situation with a 90 degree slope, a change in cohesion, reprasented by $\frac{c}{\gamma B}$, would not be of great concern for the overall stability. However for a 30 degree slope, varying cohesion does have a greater effect on the bearing capacity and hence the stability of the slope. This is shown as the convergence of results as the slope angle is increased.

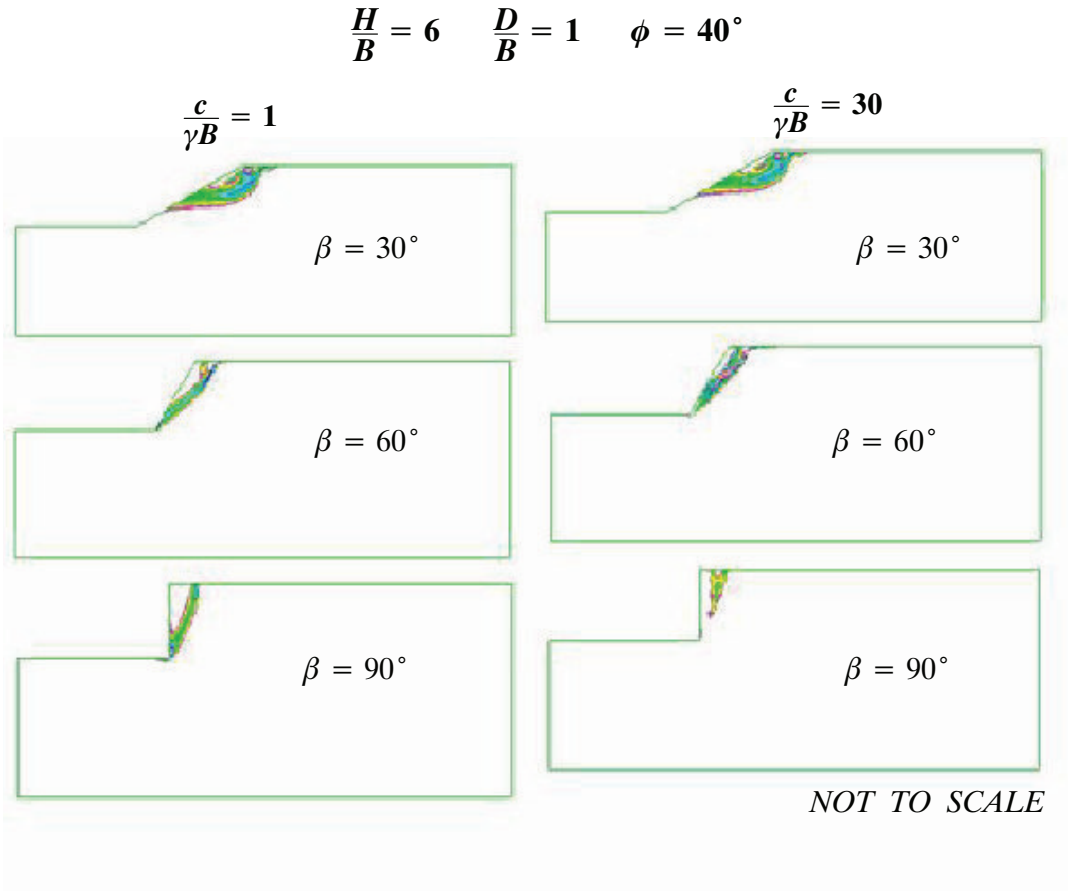

Figure 4-6. Contour plots of slope angle and dimensionless strength ratio

The contour plots in figure 5-6 appear quite similar for a large variance in dimensionless strength ratio. This is because separate scenarios with different cohesion values will exhibit the same failure, however the case with the lower cohesion, or lower $\frac{c}{\gamma B}$ values, will withstand a much less load or fail much sooner if exposed to the same loads. This is due to the material being much weaker and it is the constant friction angle which produces the similar slip surfaces.

4.2.4 Comparison Among Various Friction Angles

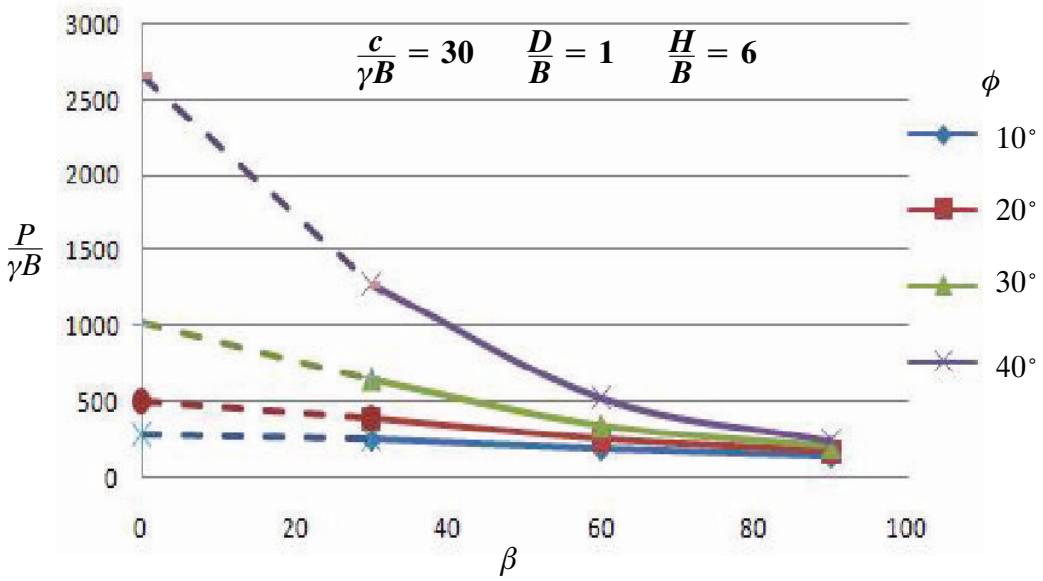

Figure 4-7. Effect of slope angle and friction angle

The conclusion to be made from Figure 5-7 is that the combined effects of slope angle and friction angle are minimal. However, three points should be noted which are $\phi = 30^\circ$ and $\beta = 0^\circ$, $\phi = 40^\circ$ and $\beta = 30^\circ$, $\phi = 40^\circ$ $\beta = 0^\circ$. These points highlight the fact that for large increases in the normalised bearing capacity, friction angle needs to be large along with an approched level ground state.

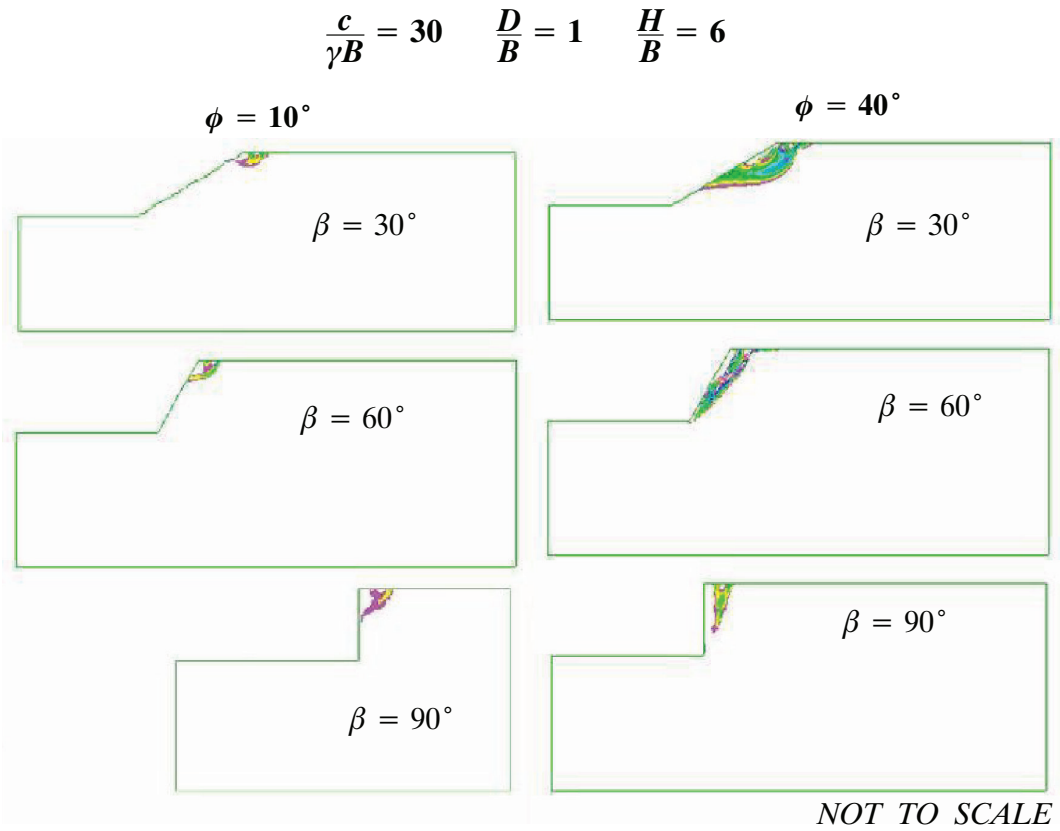

Figure 4-8. Contour plots of slope angle and friction angle

The contour plots from figure 5-8 give a clear picture that for small friction angles the failure zones are much smaller. Because of the small friction angle there is little resistance to shear, this is why the normalised bearing capacity is so small for all three cases and the slope angle has little effect. For high friction angle the material is much stronger and has a greater resistance to shear failure. This is represented by a larger slip surface which also shows the greater effect of the change in slope angle.

4.2.5 Conclusions

There is a clear trend in the effect of slope angle in that the results for all parameters produce partial concave up curves. This proves that $\frac{p}{\gamma B}$ decreases as β increases.

There are some important results obtained from this study that design engineers should consider. When moving a footing further from a slope the effect of slope angle doesn't change only the effect of the footing distance ratio. However, the distance required to reach a level ground state changes with change in slope angle. As H/B and slope angle decrease the condition approaches level ground and therefore approaches the level ground value of normalised bearing capacity. When above-toe failure occurs there is no longer any additional effect of increasing H/B and the effect of slope angle is clear. For dimensionless strength ratio and friction angle values converge as slope angle increases. Therfore there

is limited benefit in modifying the foundation material of a steep slope. Greater benefit is acheived by modifying the slope itself by creating an embankment.

4.3 Effect of Footing Distance Ratio

For this section it is understood that as a footing moves away from a slope the slope itself has less effect on the bearing capacity of the foundation material. It is however, unclear how each of the other parameters of the slope effects the bearing capacity as the footing distance is varied. This section will attempt to make these behaviours more clear for the puspose of geotechnical design.

4.3.1 Comparison Among Various Slope Height Ratios

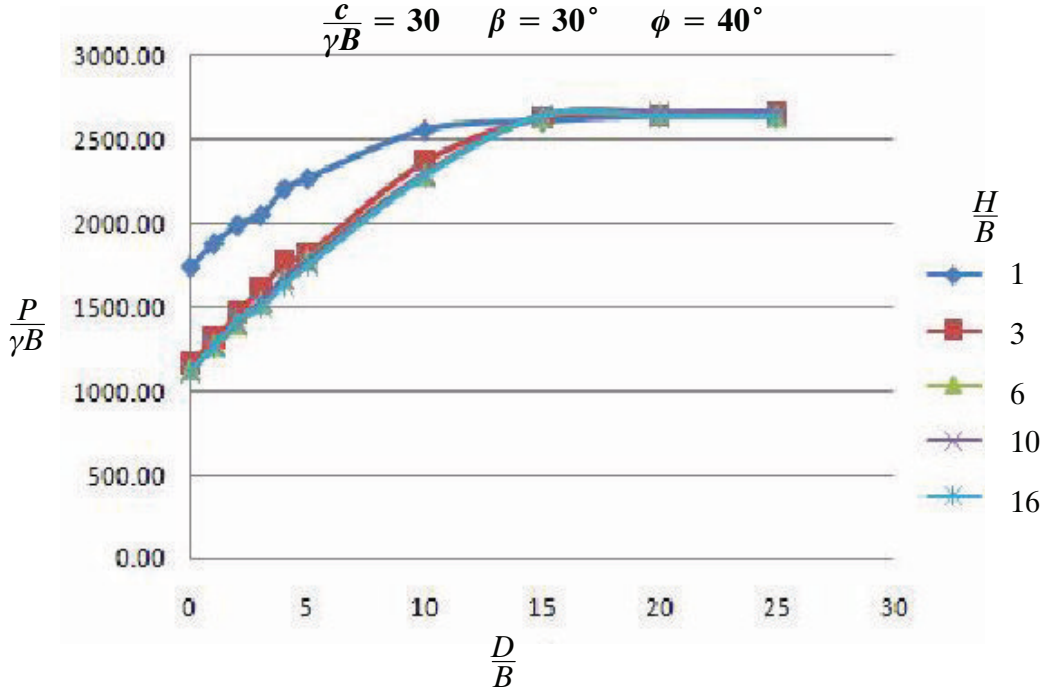

Figure 4-9. Effect of footing distance ratio and slope height ratio

Figure 5-9 shows that as D/B increases while varying H/B the normalised bearing capacity reaches a limit. This limit is due to the material properties for each case being the same and D/B is increased to the point where it becomes an infinite soil mass problem. For this scenario this is reached when D/B = 15. Also it is apparent that for a particular D/B value the H/B values for 6 and above produce exactly the same normalised bearing capacity. Therefore the effect on the normalised bearing capacity is from a change in D/B only for these cases.

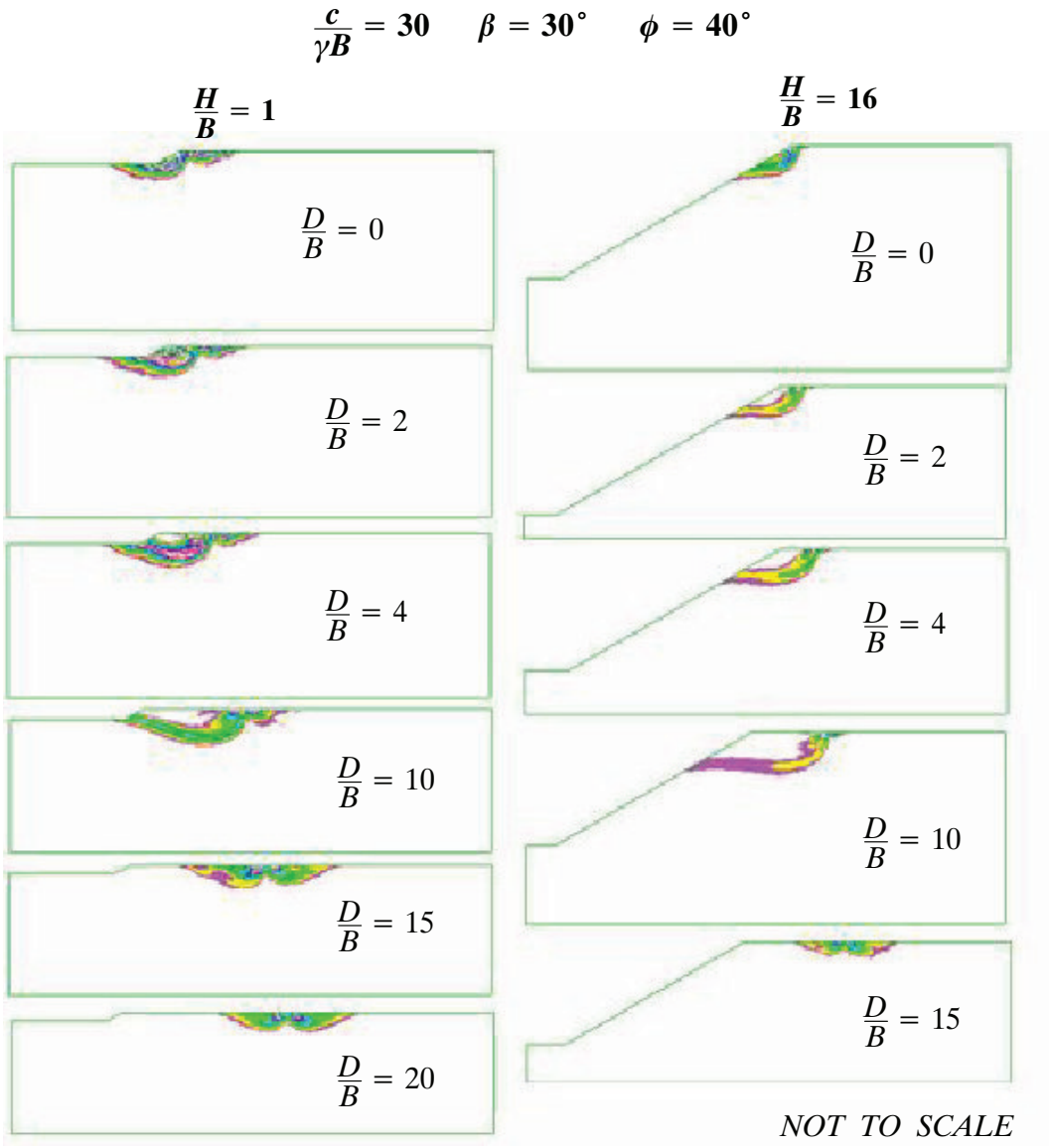

Figure 4-10. Contour plots of footing distance ratio and slope height ratio

The contour plots in figure 5-10 give a clear graphical picture of how the normalised strength ratio increases as D/B increases. For small D/B it is easy to see the difference in the failure zone for the different H/B values which produce different normalised bearing capacity values as seen in figure 5-9. For H/B = 1 the overall slope failure enters the passive zone whereas for H/B = 16 a failure in the plastic zone produces a lower bearing capacity. As D/B increases a much greater force or greater length of time is required for the failure surface to reach the slope. This gives a greater bearing capacity. For D/B = 15 both cases have reached an infinite soil mass problem where the failure zone is symmetrical indicating that the slope has no effect on the bearing capaity. Failure is now due to the foundation material only.

4.3.2 Comparison Among Various Slope Angles

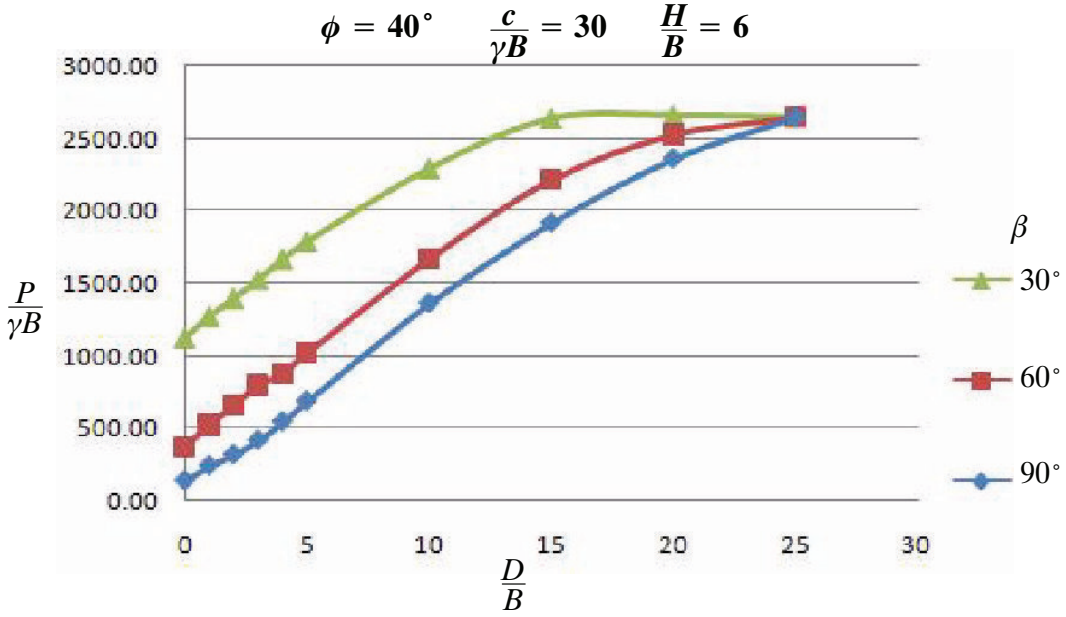

Figure 4-11. Effect of footing distance ratio and slope angle

Figure 5-11 shows a steady increase in the normalised bearing capacity as D/B is increased for each case. The change in slope angle gives a reduced capacity as β is increased. For a 30 degree slope the normalised bearing capacity is not effected after D/B = 15 whereas, for the 60 and 90 degree slopes it is not until D/B = 25 that the slope has no influence. Further results would also show the levelling out affect for the 60 and 90 degree slopes as they reach a level ground scenario.

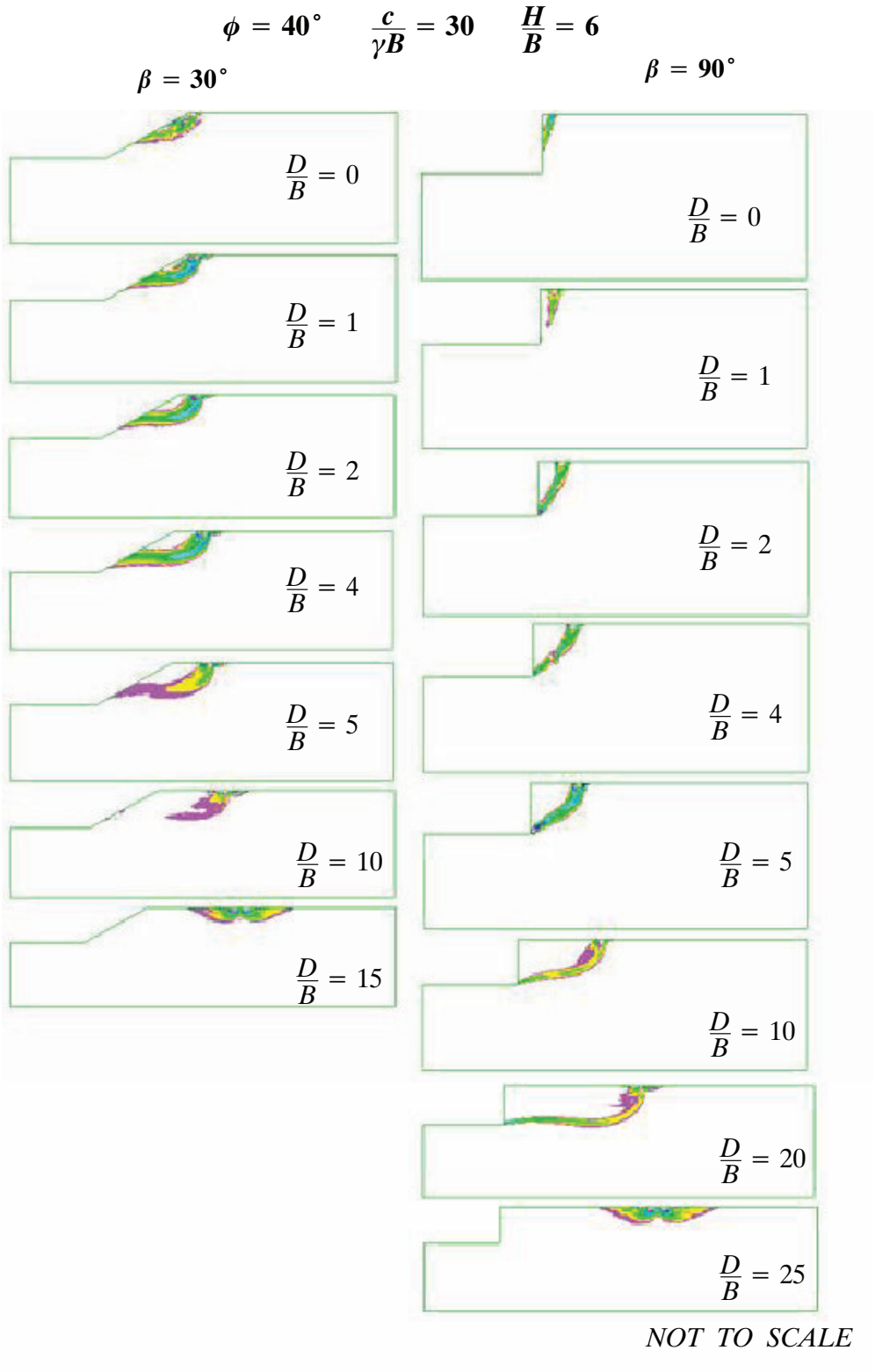

Figure 4-12. Contour plots of footing distance ratio and slope angle

The contour plots in figure 5-12 graphically show a steady increase in the size of the failure zone which represents an increase in the normalised bearing capacity of the scenario. For the 30 degree slope a much stronger failure mechanism is experienced as D/B increases. The local above-toe failure zone starts in a plastic zone and moves through to a passive zone and finally a symmetrical, level ground failure. For the 90 degree slope the above-toe failure in the active zone increases to an at-toe failure in the active zone then through the plastic zone and finally a symmetrical, level ground failure. This graphical representation clearly shows the change in the normalised bearing capacity with increasing D/B as well as different slope angles.

4.3.3 Comparison Among Various Dimensionless Strength Ratios

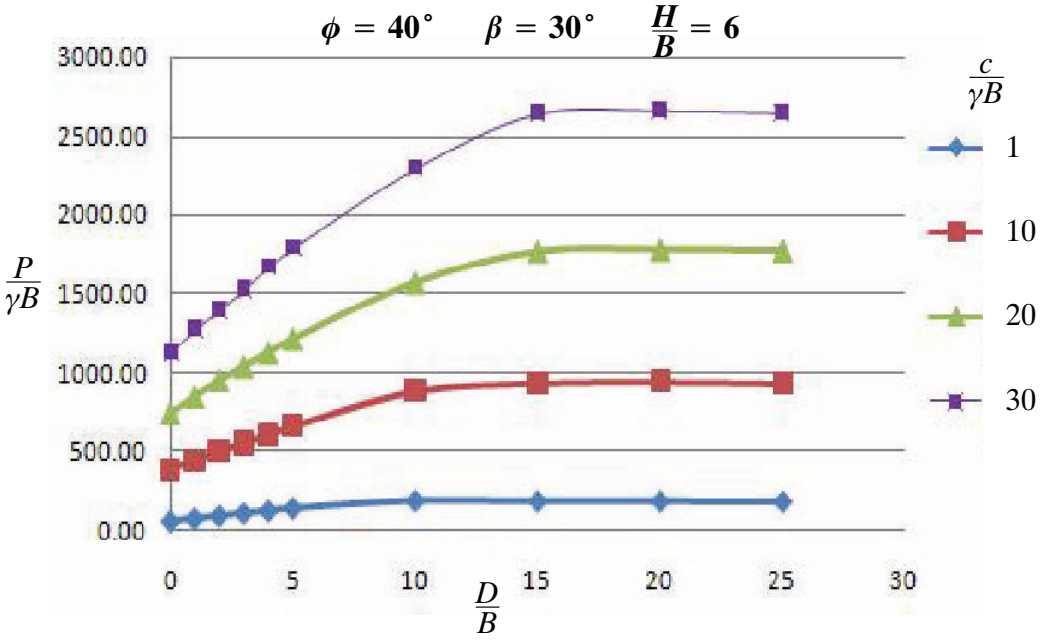

Figure 4-13. Effect of footing distance ratio and dimensionless strength ratio

Analysing the effect of D/B while varying geometrical parameters shows the convergence of results as a level ground problem is reached. However, when comparing against material parameters it is evident that a much weaker material will produce much smaller results. Figure 5-13 shows that same trend is experienced in that the effect of increasing D/B will only continue until a level ground condition. This plot also clearly shows the great effect a change in soil cohesion has on the bearing capacity of a slope. It can be seen that for a dimensionless strength ratio of 1 it is only required that D/B = 10 to obtain a level ground scenario.

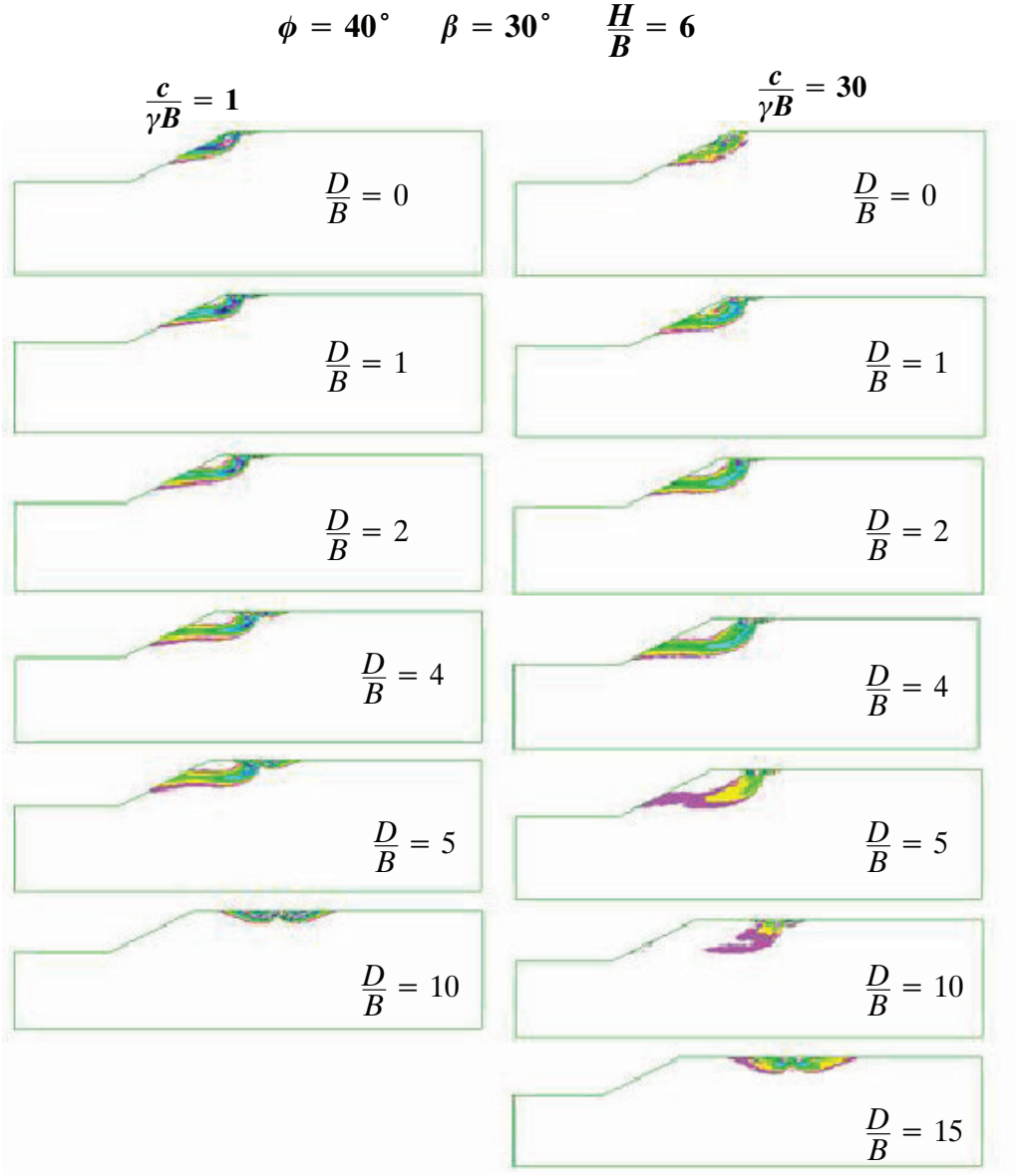

Figure 4-14. Contour plots of footing distance ratio and dimensionless strength ratio

The graphical representaions in figure 5-14 show the behavioural change as D/B is increased. The effect of $\frac{c}{\gamma B}$ is not clear because this parameter represents the strength of the material, therefore a low cohesion material will fail with a much smaller load applied or will fail sooner with the same load. This is why similar failure zones are experienced. However the effect of both D/B and $\frac{c}{\gamma B}$ can be seen in that a symmetrical failure zone is present at D/B =10 for $\frac{c}{\gamma B}$ = 1 and not until D/B = 15 for $\frac{c}{\gamma B}$ = 30.

4.3.4 Comparison Among Various Friction Angles

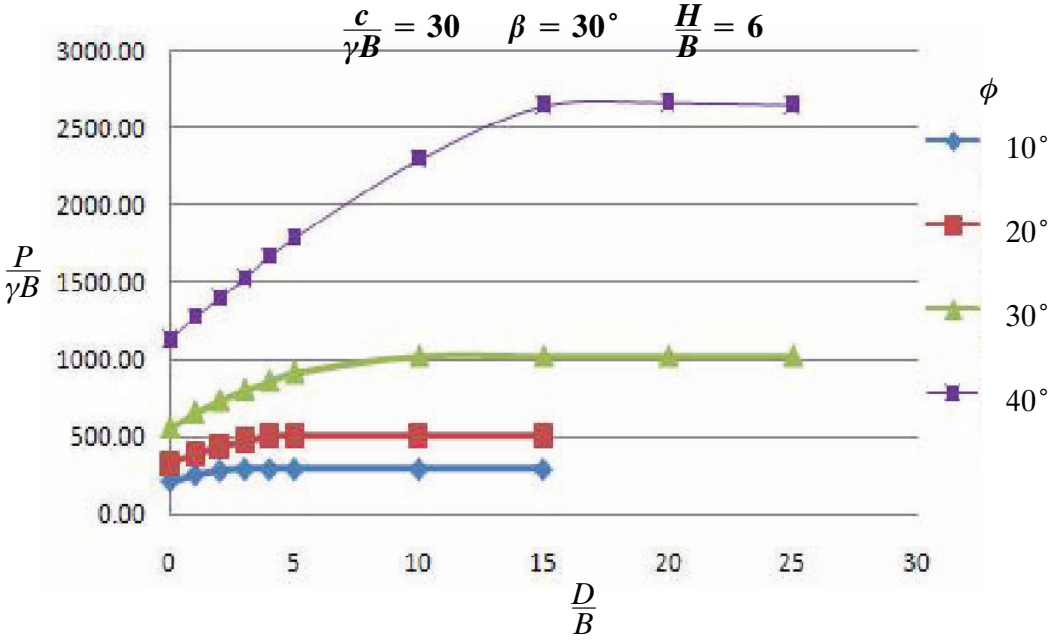

Figure 4-15. Effect of footing distance ratio and friction angle

The linear increase within the data trends of figure 5-15 represents a local bearing capacity failure of the face of the slope. When each curve flattens out it is represening the transition from local bearing capacity failure to level ground, foundation bearing capacity failure. It is clear that foundation materials with higher friction angles produce a higher bearing capacity. The results show that the higher the normalised bearing capacity the greater the influence a nearby slope will have, meaning that a greater ratio of D/B is required to reach a level ground state. Figure 5-15 shows that for a material with $\phi = 40^\circ$ the footing distance ratio (D/B) required to eliminate the effect of the nearby slope is 15. For similar conditions but with a meterial of $\phi = 10^\circ$ the D/B value required is only 3 to reach a level ground state. Therefore for high friction angles the effect of a nearby slope is critical, however a small friction angle results in the material being the critical factor when considering the overall bearing capacity of a nearby slope.

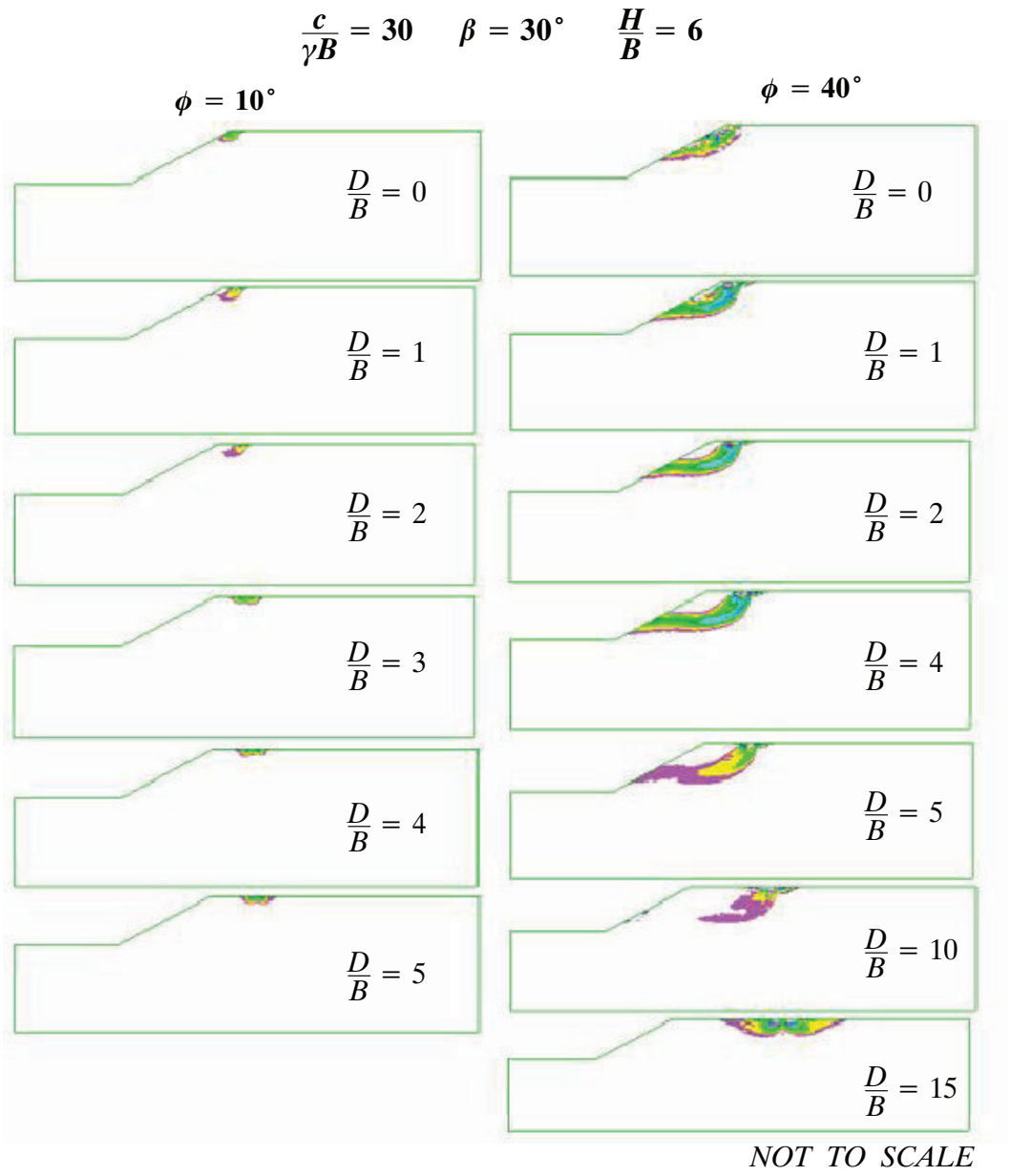

Figure 4-16. Contour plots of footing distance ratio and friction angle

The contour plots in figure 5-16 give a clearer picture of the trends shown in figure 5-15. The failure mechanism of a small friction angle material can be seen to be much smaller than for that of a high friction angle material. Therefore the footing is not required to be moved far from the slope before the failure zone is so weak that it is contained within the level ground. Any further increase in D/B has no effect on the normalised bearing capacity. For a high friction angle material the failure zone is forced much deeper into the foundation material and large loads, long settlement times or a nearby slope are required to produce failure. Because of the large failure zone the effect of the slope on the normalised bearing capacity is much greater. Therefore a much greater D/B value is required before the slope no longer has any influence and this is why there is a great difference in the normalised bearing capacity for a close-by slope and that of an infinitely far slope.

4.3.5 Conclusions

This section, studying the effect of footing distance from a nearby slope, has shown that a number of parameters can greatly influence the rate at which a level ground case is reached when increasing the ratio D/B. With a small friction angle a level ground sceario was reached when D/B = 3, whereas for a particular ninety degree slope the D/B ratio required for a level ground case was twenty-five. This highlights the large effect that the footing distance ratio has on the overall slope stability as well as how other slope parameters can greatly influence this effect.

4.4 Effect of Slope Height Ratio

This section studies the effect of the slope height on the overall bearing capacity of the slope. It is predicted that for small H/B, close to level ground, the failure zone closely resembles that of the level ground case and so to will the bearing capacity. Influences from other parameters on the effect of H/B are outlined in this section.

4.4.1 Comparison Among Various Footing Distance Ratios

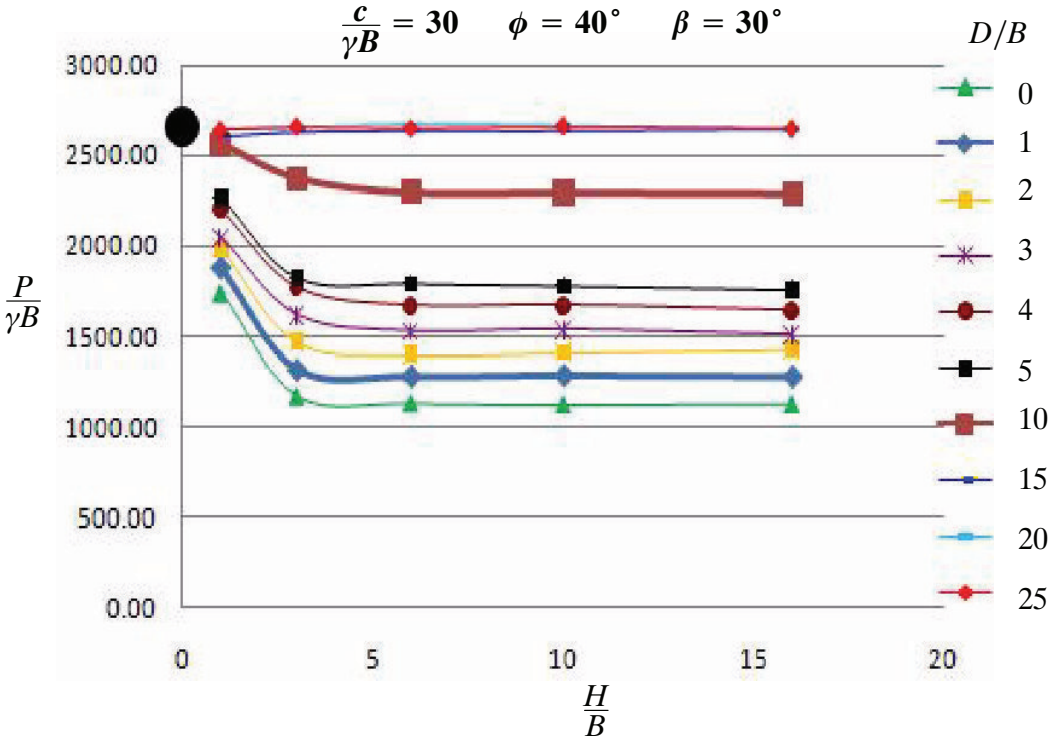

Figure 4-17. Effect of slope height ratio and footing distance ratio

The effect of H/B shows that for large values the normalised bearing capacity does not change. As H/B approaches the values rapidly increase towards the level ground state, represented in figure 5-17 as the black circle. As D/B increases the value at which H/B no longer has any effect is increased as well as the normalised bearing capacity of the slope.

When D/B is very large a level ground starte is reached which is shown by the level lines at the top of the graph.

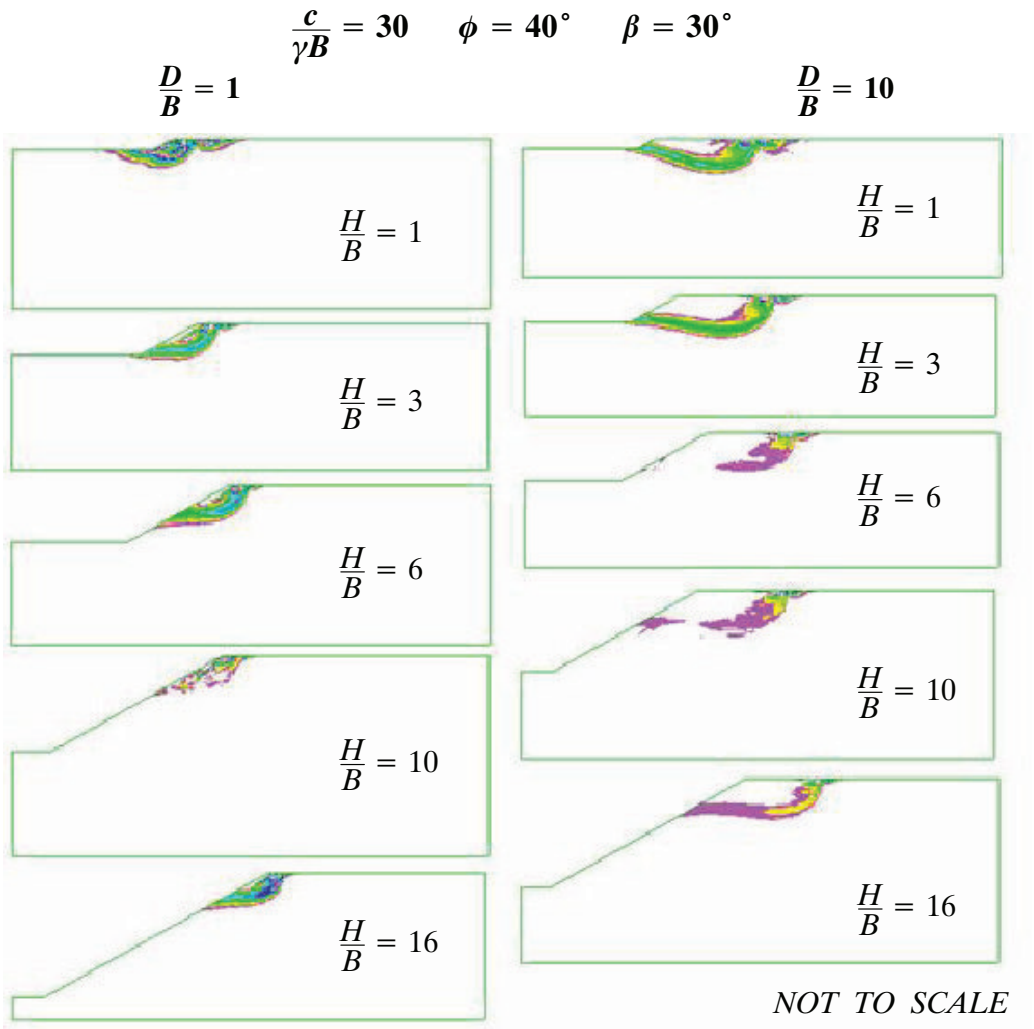

Figure 4-18. Contour plots of slope height ratio and footing distance ratio

In figure 5-18 both maximum shear strain rate contours for H/B = 1 show passive failure zones. It is clear that a large D/B value, such as 10, minimises the effect of H/B due to the strong passive failure zone. It is noted that the normalised bearing capacity is decreasing as the failure mode changes from below-toe to at-toe to above-toe. Once above-toe failure occurs there is no further change in the failure zone.

4.4.2 Comparison Among Various Slope Angles

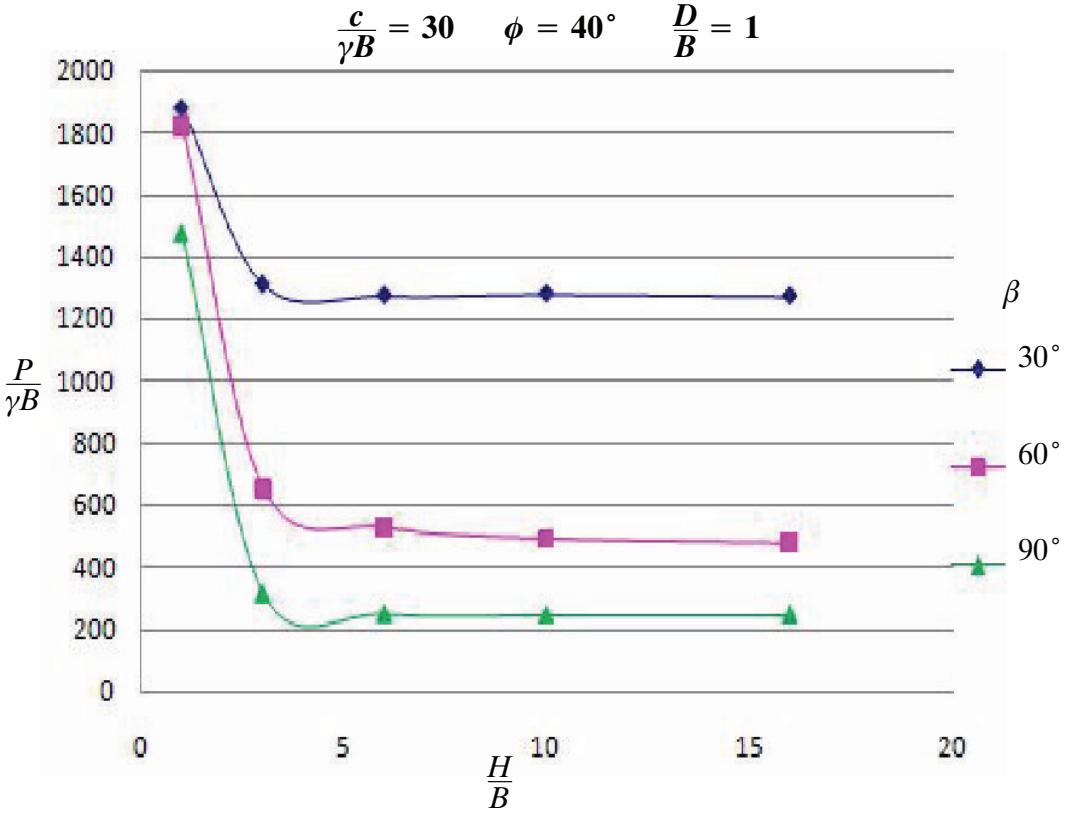

Figure 4-19. Effect of slope height ratio and slope angle

Again it can be seen that for above-toe failure the normalised bearing capacity is constant with change in H/B. For small H/B the influence from change in slope angle is not great, however the influence is quite large as H/B increases. From H/B = 1 to H/B = 3 the slope of $\beta = 90^\circ$ is reduced by approximately 80%. For $\beta = 30^\circ$ and large H/B the slope's normalised bearing capacity is approximately 70% of that of level ground case while for $\beta = 90^\circ$ is approximately 33%. This concludes that the slope angle is very influential on the effect of slope height.

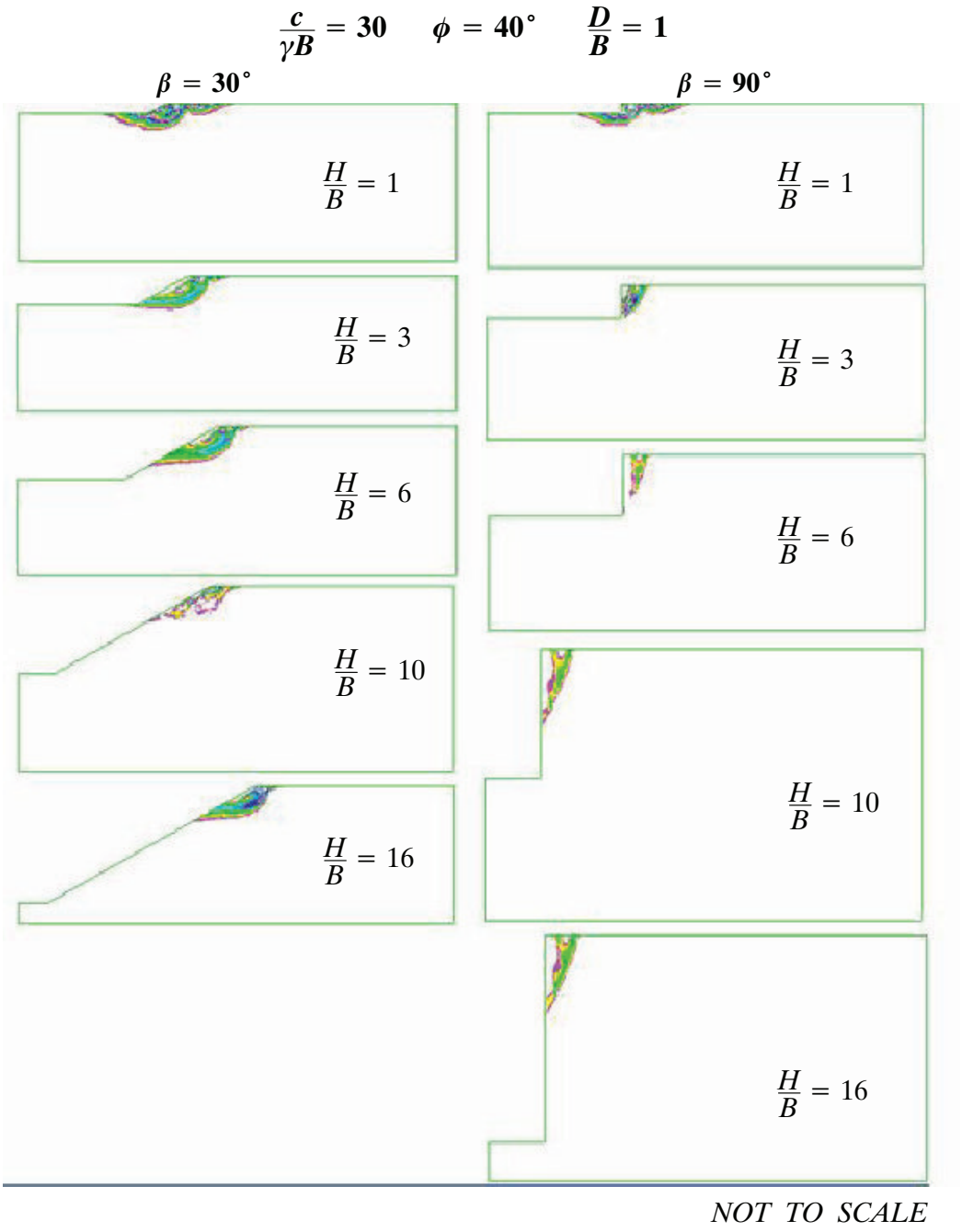

Figure 4-20. Contour Plots of slope height ratio and slope angle

When approaching level ground, for example H/B = 1, Figure 5-20 shows that the influence from the slope angle is not great. However, as H/B increases the slip surface for $\beta = 90^\circ$ is forced down the slope within the active zone of shear failure. This indicates a much lower bearing capacity to that of the slope for $\beta = 30^\circ$. It is also noted that the influence zones are not affected once the failure mechanism is above-toe.

4.4.3 Comparison Among Various Dimensionless Strength Ratios

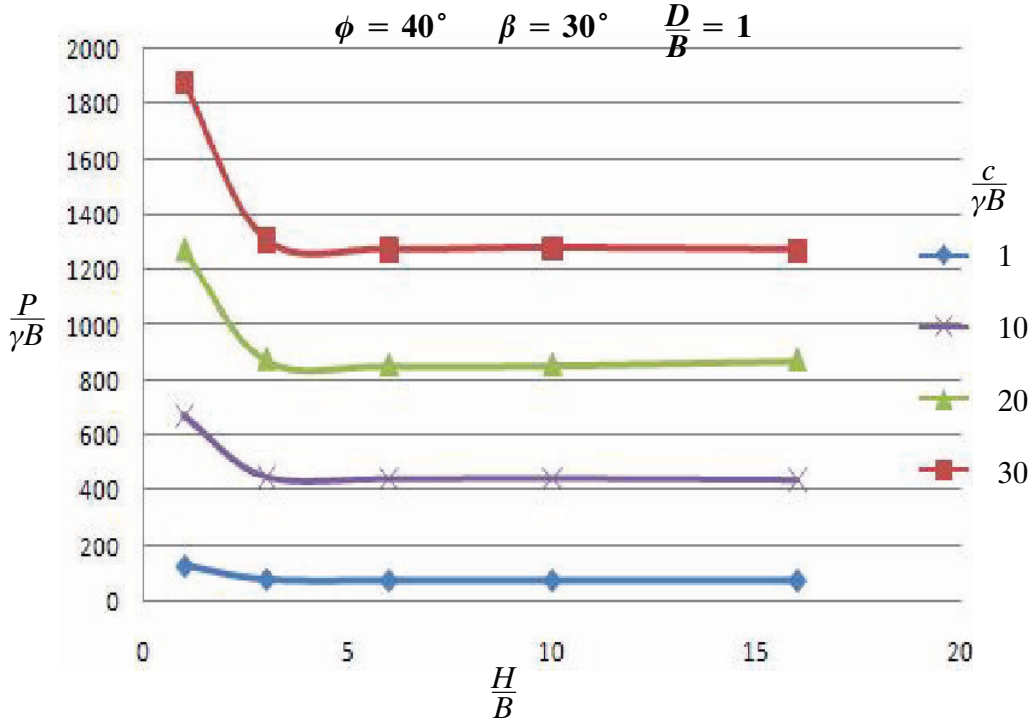

Figure 4-21. Effect of slope height and dimensionless strength ratio

The effect of slope height for this case is indicative of the strength of the material. As the dimensionless strength ratio is decreased so to is the influence of a nearby slope, hence the height of the slope also loses effect. Therefore the effect of H/B is much greater for a strong material rather than a weak material and the effect of H/B until above-toe failure's reached is much greater.

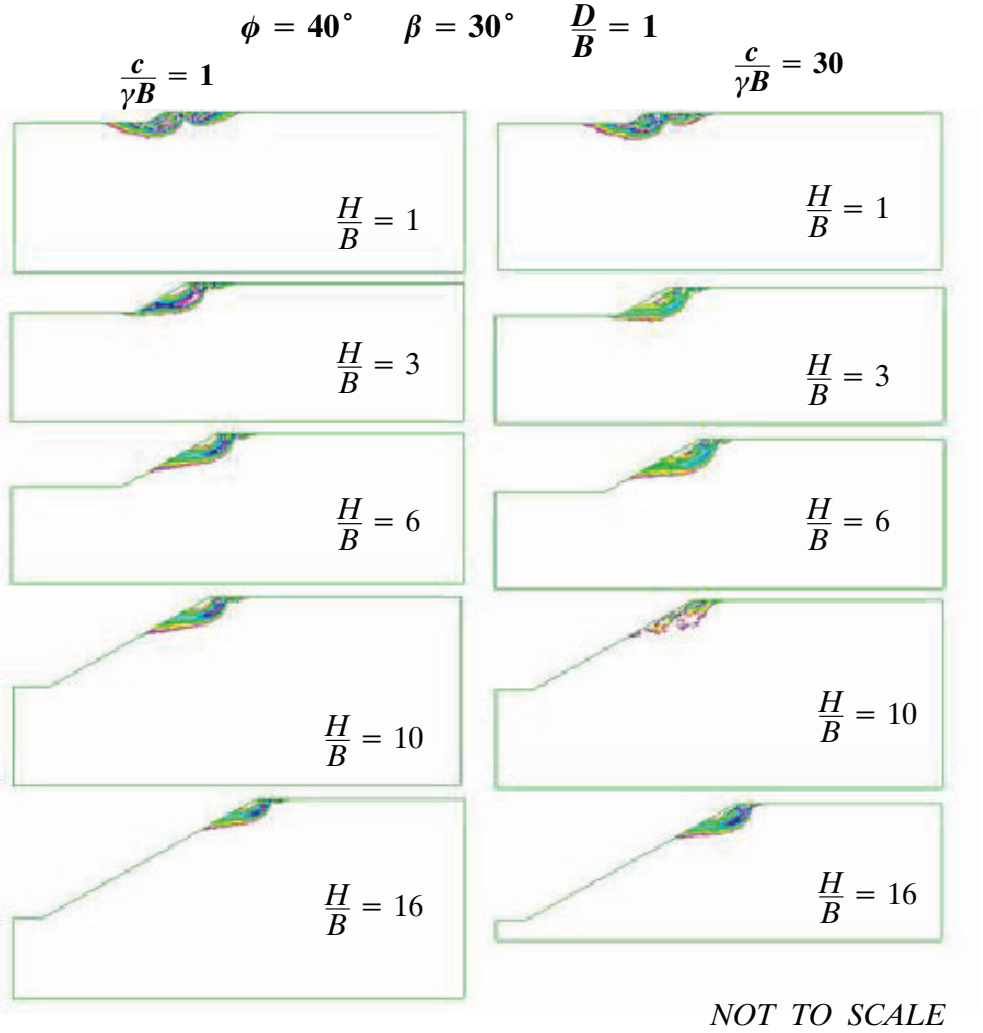

Figure 4-22. Contour plots of slope height ratio and dimensionless strength ratio

As previously discussed the contour plots for dimensionless strength ratio's are not indicative of the solution.

4.4.4 Comparison Among Various Friction Angles

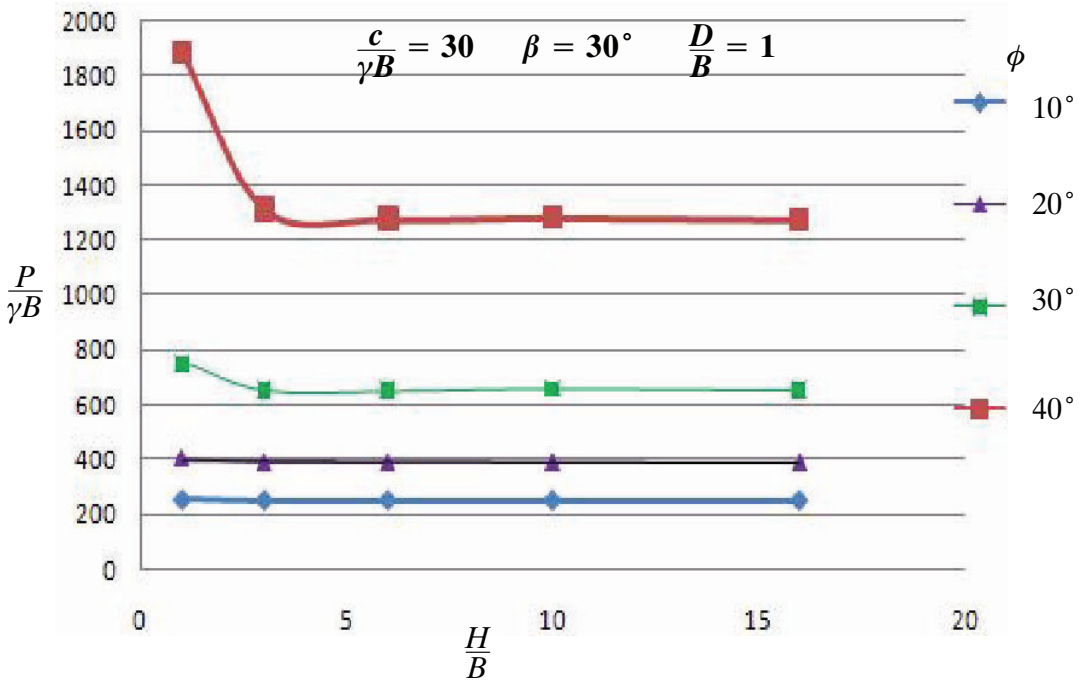

Figure 4-23. Effect of slope height ratio and friction angle

The trends in figure 5-23 clearly show how for small friction angle there is no effect from a change in H/B equal to or greater than 1. For high friction angle there is a large decrease in the normalised bearing capacity between H/B=1 and H/B=3 after which there is no effect from change in H/B due to above-toe shear failure. For small friction angles the effect seen is mainly due to the material rather than the slope hieght.

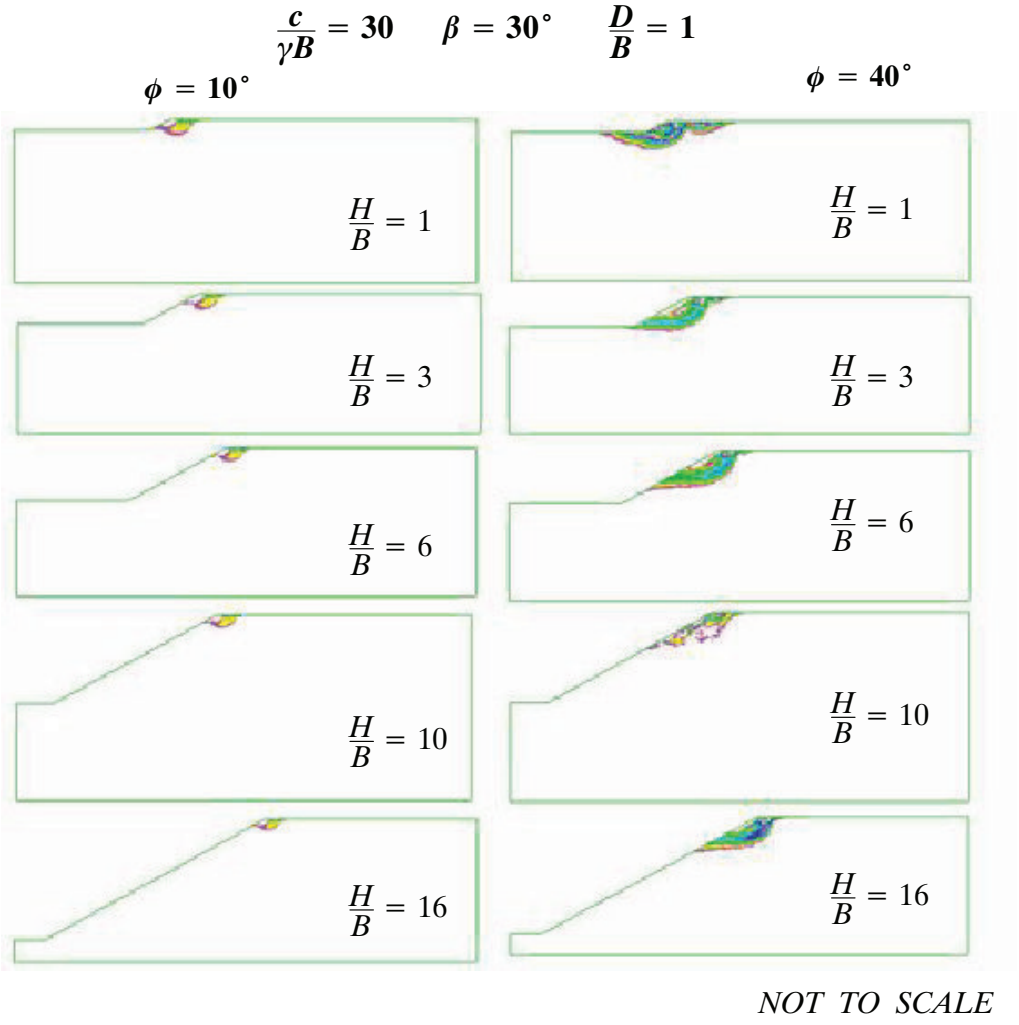

Figure 4-24. Contour Plots of slope height ratio and friction angle

Figure 5-24 shows that the slope material is so unstable for $\phi = 10^\circ$ that the slope's affect is not further influenced with an increas in H/B. This is evident from all the cases having an above-toe failure surface. For an effect to be noticed H/B would need to be very small. When the friction angle is increased the influence on the effect of H/B is apparent. The slopes capacity is higher for H/B=1 and H/B=3 but once the slope height is increased further there is no added affect.

4.4.5 Conclusions

As the slope height increases the normalised bearing capacity decreases until the height has no further influence. The other material and geometrical parameters influence the height at which H/B no longer has any effect as well as the value of the normalised bearing capacity at this state. Weak materials, such as those with small friction angles or dimensionless strength ratio's, aren't strongly affected by slope height.

Development of Additional Research

5.1 Introduction

Due to the size of this research there have been a number of findings which could not be included as a full parametric study. These findings have initiated interesting topics which definately require further investigation. Such topics include the use of well-structured design charts for simplicity in design engineering, the effect of surcharge loading, the effect of a combination of slope stability failure and foundation bearing capacity failure, the investigation of a two-way shear failure mechanism for the footing near slope problem and the effect of dilation angle.

5.2 Design Charts

Design charts are presented to investigate the change in bearing capacity for the footing near slope problem. The following charts, in Figure 6-1 to Figure 6-6, propose a different trend in data to the charts already used throughout this research. The use of x, y, z charts produce much clearer trends and therefore the values within the charts are far easier to read off. It is noted that the more parameters studied the greater the accuracy of these charts as the results are distorted to produce a best-fit trend. An example follows the charts showing how to estimate the ultimate bearing capacity.

5.2.1 Effect of Footing Distance Ratio and Slope Angle

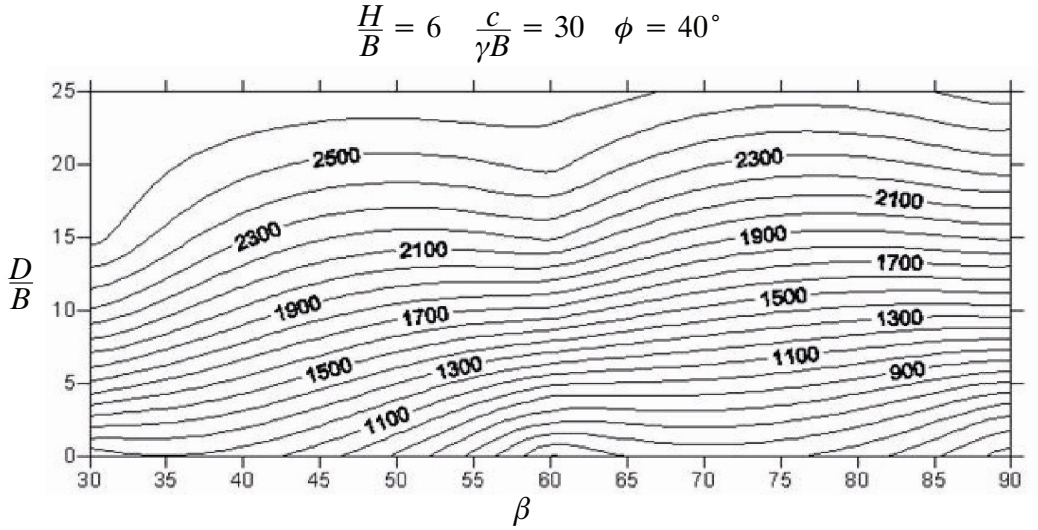

Figure 5-1. Design chart comparing footing distance ratio and slope angle with a strong foundation

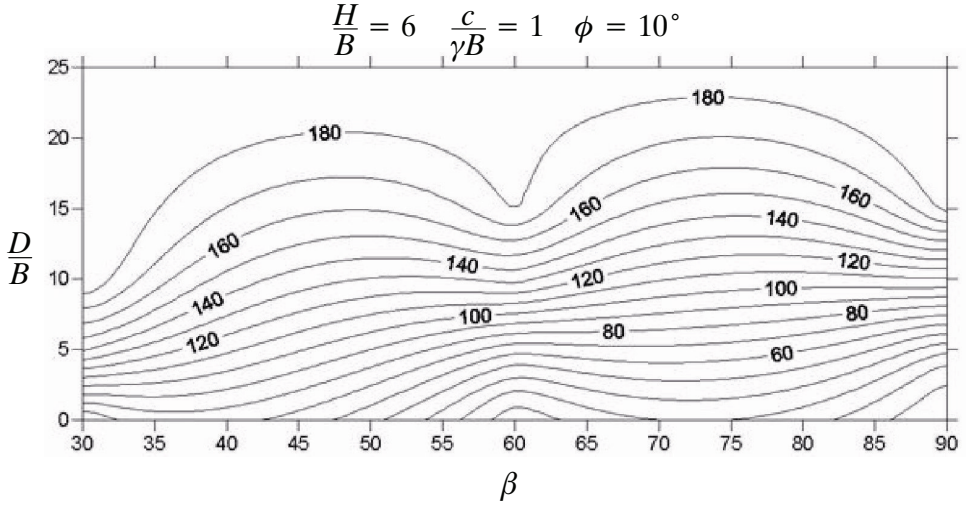

Figure 5-2. Design chart comparing footing distance ratio and slope angle with a weak foundation

5.2.2 Effect of Footing Distance Ratio and Slope Height Ratio

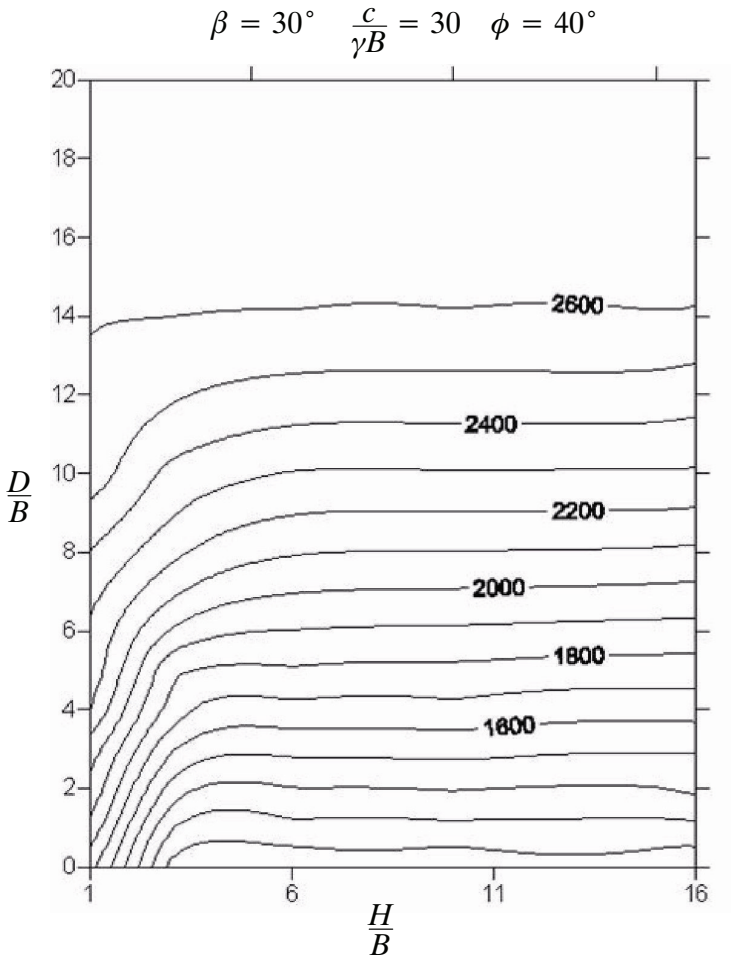

Figure 5-3. Design chart comparing footing distance ratio and slope height ratio with a strong foundation

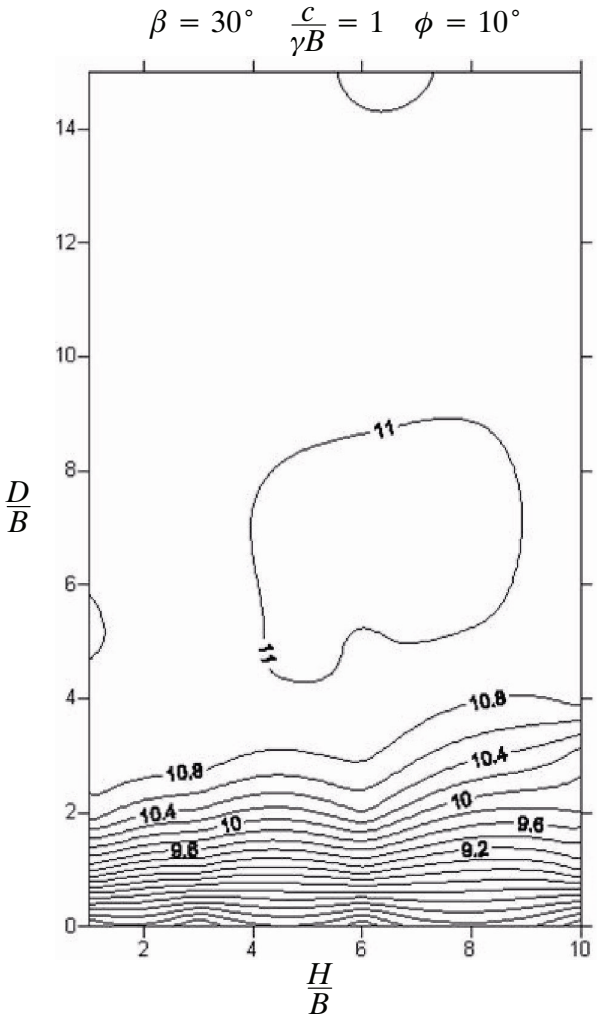

Figure 5-4. Design chart comparing footing distance ratio and slope height ratio with a weak foundation

5.2.3 Effect of Dimensionless Strength Ratio and Friction Angle

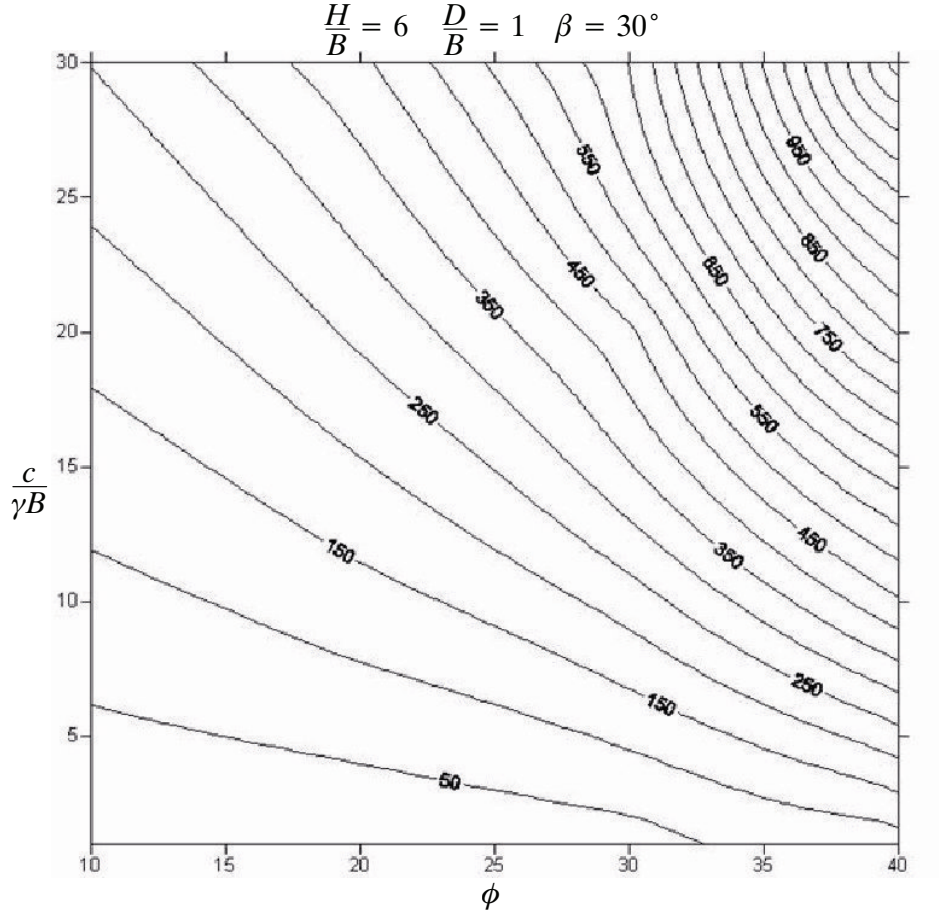

Figure 5-5. Design chart comparing dimensionless strength ratio and friction angle with a small slope angle and small footing distance ratio

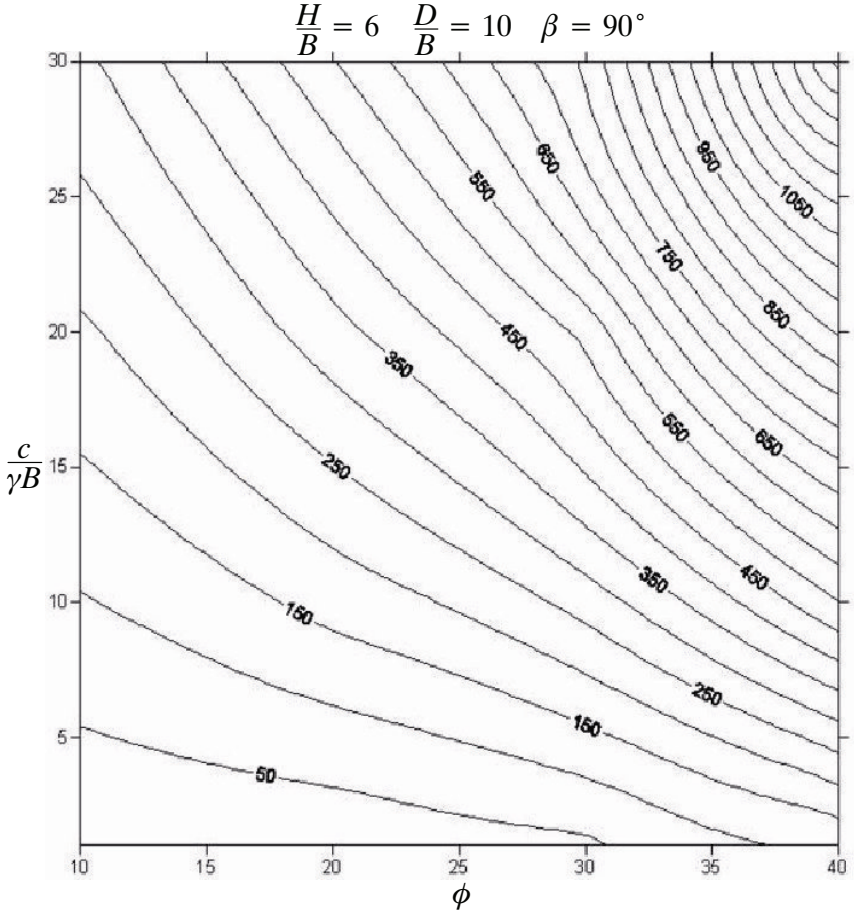

Figure 5-6. Design chart comparing dimensionless strength ratio and friction angle with a large slope angle and large footing distance ratio

5.2.4 Example of Estimation of Bearing Capacity

A surface strip footing of width (B) 1.0 m is located 1.0 m back from the edge of a 30 degree homogeneous granular slope with a slope height (H) of 6.0 m. Assuming a zero depth of foundation embedment (q=0), determine the ultimate bearing capacity (p) given the granular material has a shear strength c_u = 400 kPa, friction angle $\phi = 30^\circ$ and unit weight γ = 20 kN/m^3.

The following procedures are used to determine the ultimate bearing capacity:

- With the given parameters use Figure 6-5.
- Given D = 1 m and B = 1 m, D/B = 1.
- Given H = 6 m and B = 1 m, H/B = 6.
- Given c_u = 400 kPa and unit weight γ = 20 kN/m^3, c_u/γB = 20.
- From Figure 6-5, p/γB $\approx$450.
- p can then be computed p $\approx$9000 kPa.

The actual value for this problem using FLAC analysis was found to be 8617 kPa.

5.3 Surcharge Loading

Foundations are rarely placed on the surface of the ground, but rather at a depth below the ground level. This is to limit the effects of seasonal moisture variations, frost in cold environments, poor surface material including top soil as well as erosion and scour by water. Increasing the depth of a foundation also results in a gain in bearing capacity simply from the weight of soil that has to be removed. This is also supported by Terzaghi's bearing capacity equation with the third term being qN_q , where $q = \gamma D_f$.

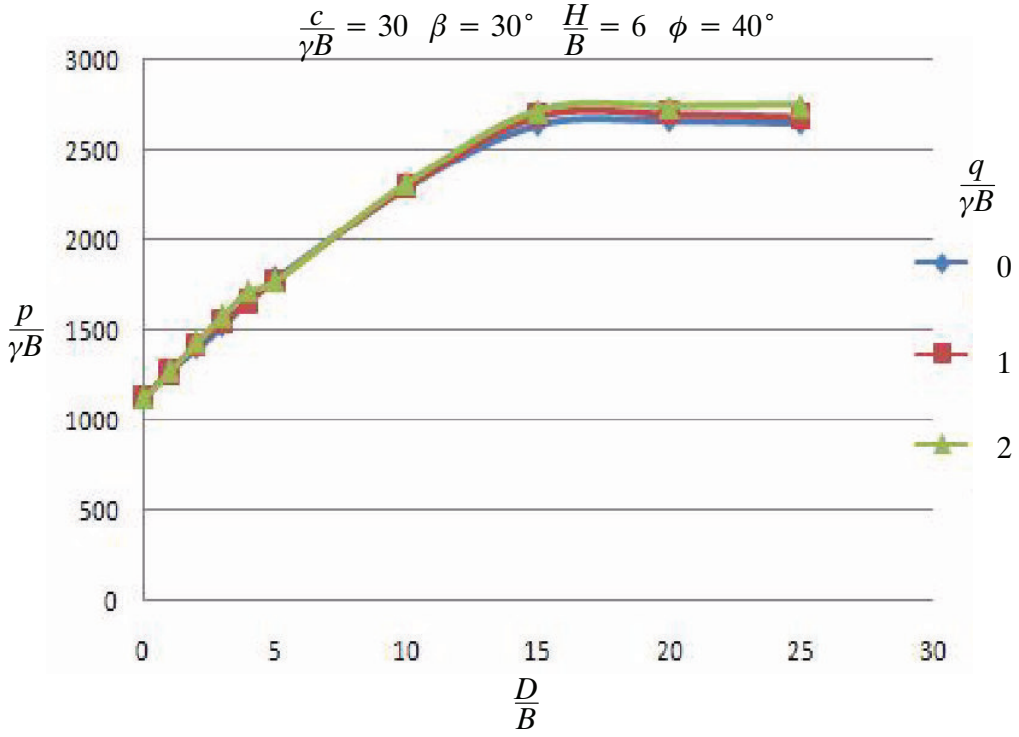

Figure 5-7. Effect of dimensionless surcharge and footing distance ratio

It is evident from Figure 5-7 that the effect of surcharge loading is very minimal for a strong foundation material. It takes a D/B value approaching or at level ground condition for an effect to be apparent, and even then the effect is very small.

Figure 5-8 and Figure 5-9 show that for a small D/B with a strong foundation material varying the slope height or slope angle is not influenced by surcharge loading.

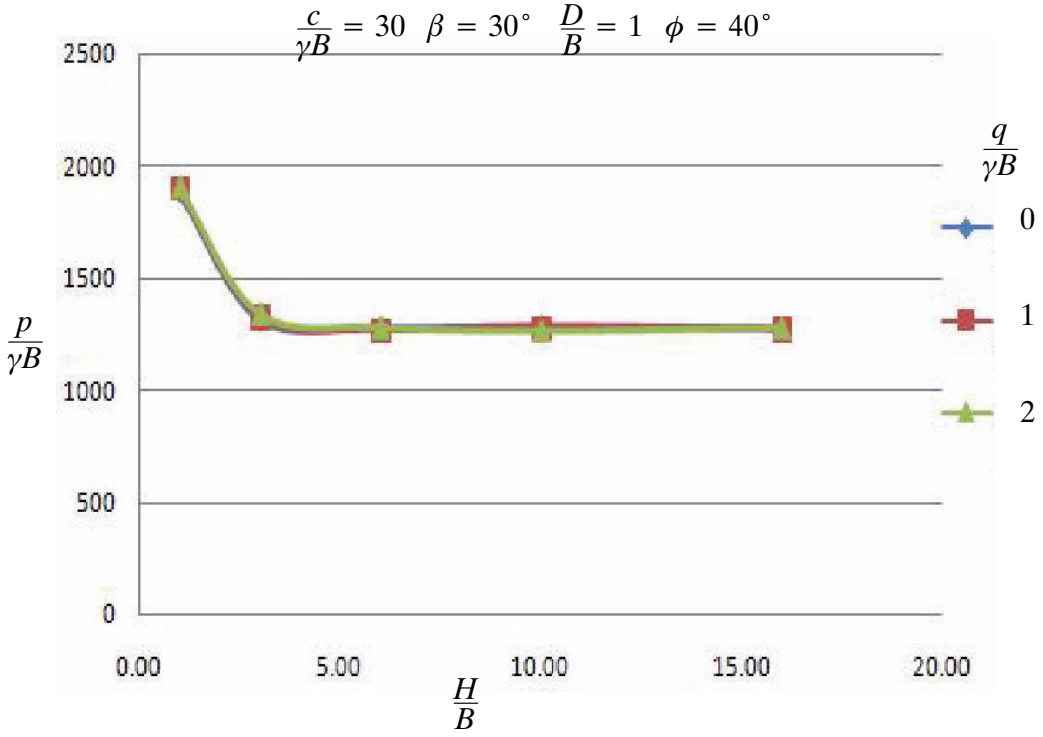

Figure 5-8. Effect of dimensionless surcharge and slope height ratio

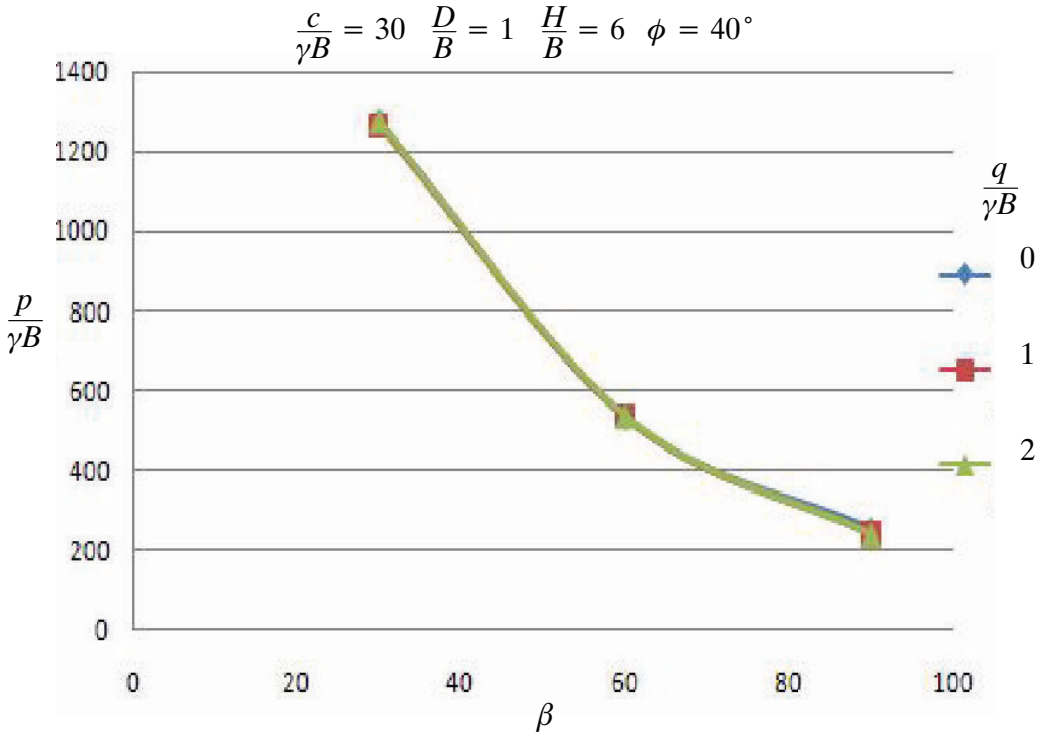

Figure 5-9. Effect of dimensionless surcharge and slope angle

Further to the graphs, Figure 5-10 and Figure 5-11 showing the contour plots give a clear indication of the similar failure surfaces and therefore bearing capacties for varying surchare loading with a strong foundation material.

$$\frac{c}{\gamma B} = 30 \quad \beta = 30^\circ \quad \frac{H}{B} = 6 \quad \phi = 40^\circ$$

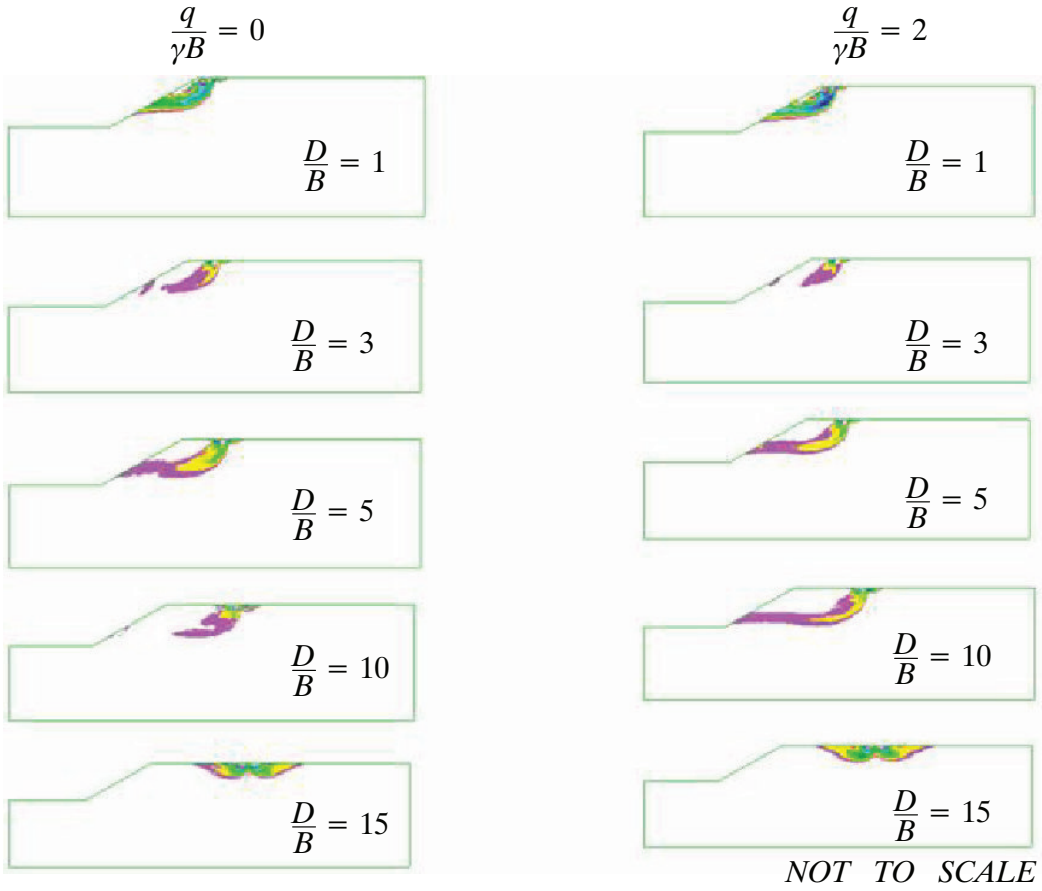

Figure 5-10. Effect of surcharge and footing distance ratio for a strong foundation material and small slope angle

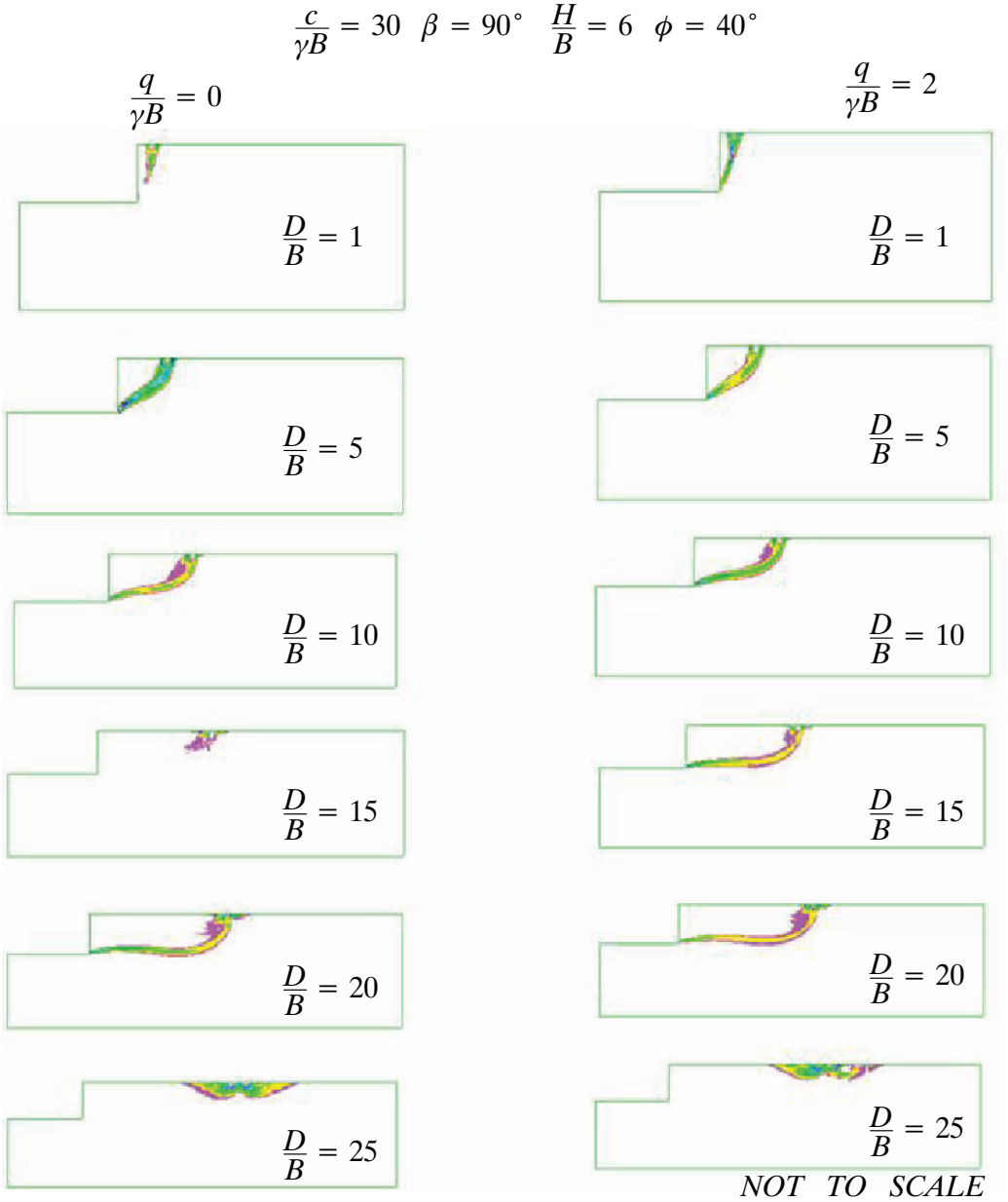

Figure 5-11. Effect of surcharge and footing distance ratio for a strong foundation material and large slope angle

Figure 5-12 and Figure 5-13 show there is a difference in the failure zones for a weak foundation material when varying surcharge loading. However, because the bearing capacities are so small the effect of surcharge is also quite small. Figure 5-12 shows that as D/B is increased for a 30 degree slope the distance required for a level ground state is greater for increased surcharge loading. The larger failure zone represents an increase in the bearing capacity of the footing.

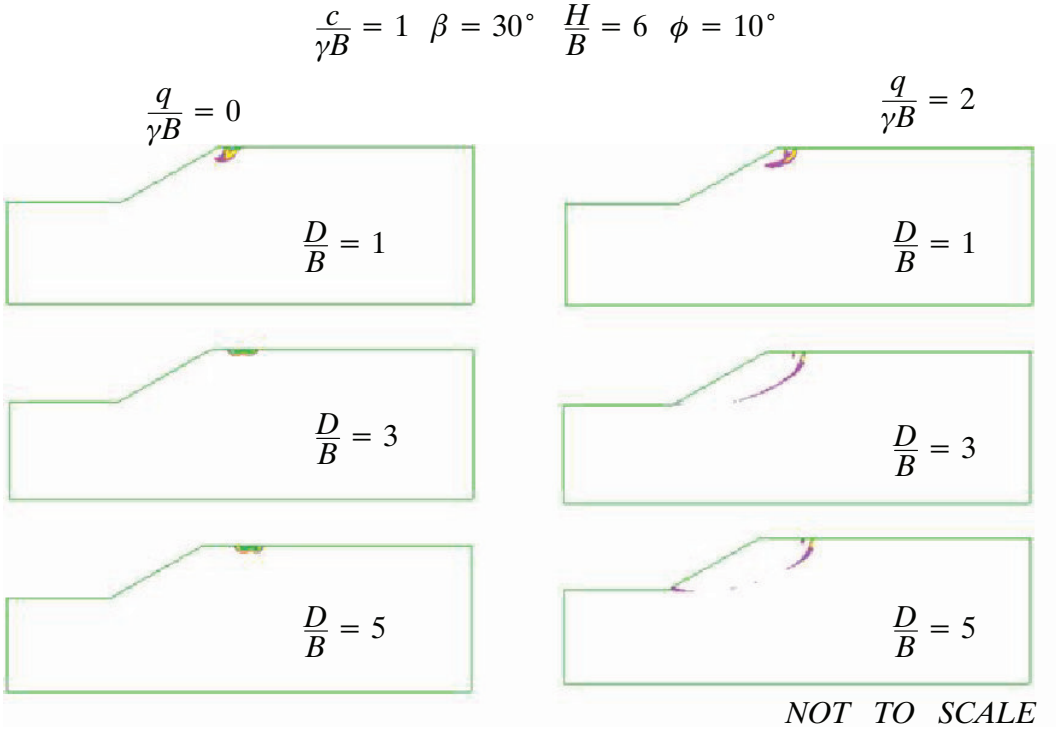

Figure 5-12. Effect of surcharge and footing distance ratio for a weakfoundation material and small slope angle

Due to the weak foundation material and steep slope represented in Figure 5-13 the slope is highly unstable without the addition of surcharge loading. When surcharge loading is applied the slope is still very unstable however the failure surface increases and so to does the bearing capacity. Due to the instability of the slope plotted results do not represent meaningful trends and therefore no graph is used to represent this scenario.

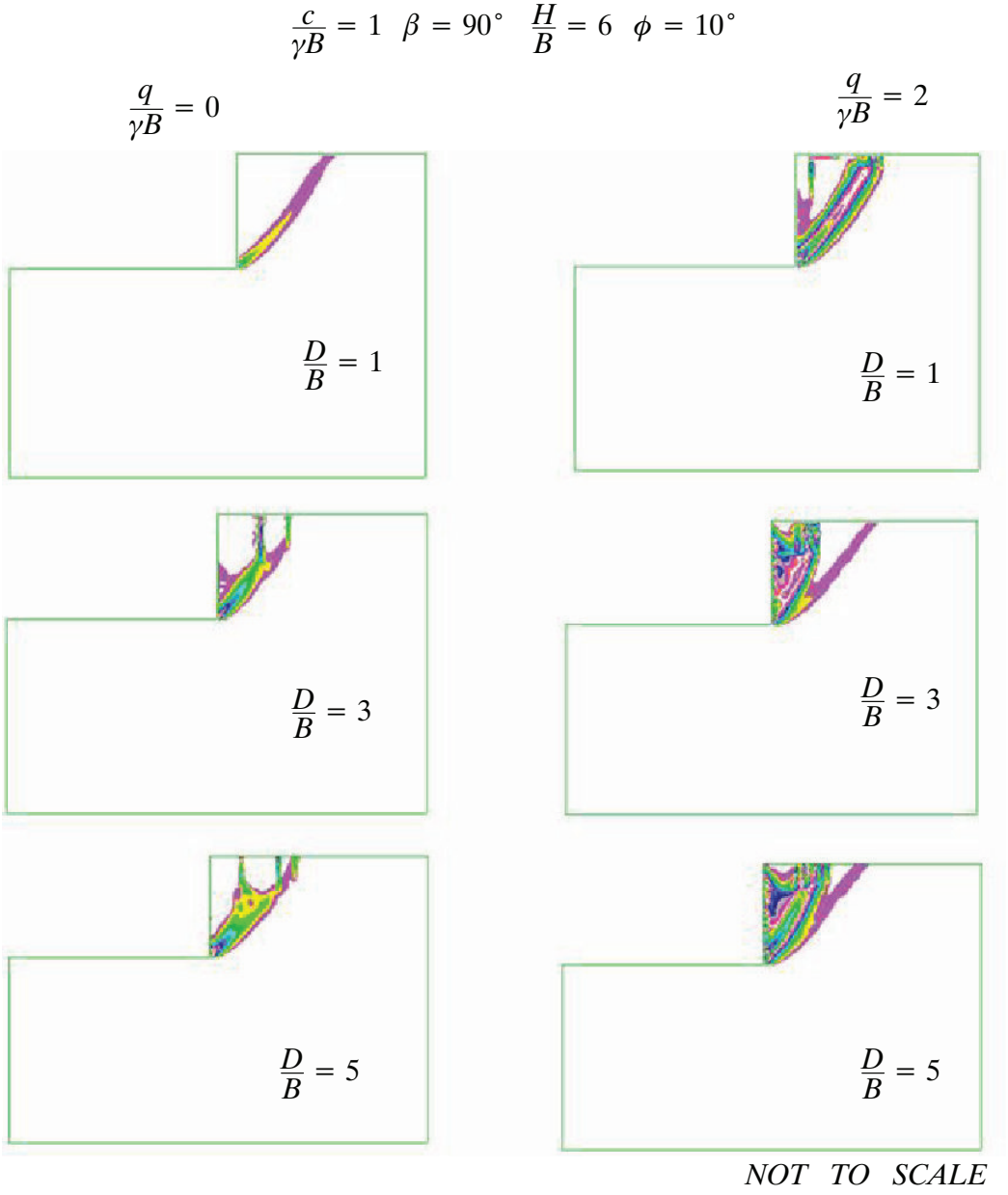

Figure 5-13. Effect of surcharge and footing distance ratio for a weak foundation material and large slope angle

5.4 Combination Shear Failure

It would not be considered desirable to construct a foundation close to an existing slope which, in its existing state, is unstable. Without being able to support its self weight a slope could not support the addition of foundation loading.

Figure 6-10 shows the change in the shear failure mechanism as the footing distance ratio is increased. The general condition required for this scenario is a steep slope and low-strength material.

$$\frac{c}{\gamma B} = 1 \quad \beta = 90^\circ \quad \frac{H}{B} = 10 \quad \phi = 40^\circ$$

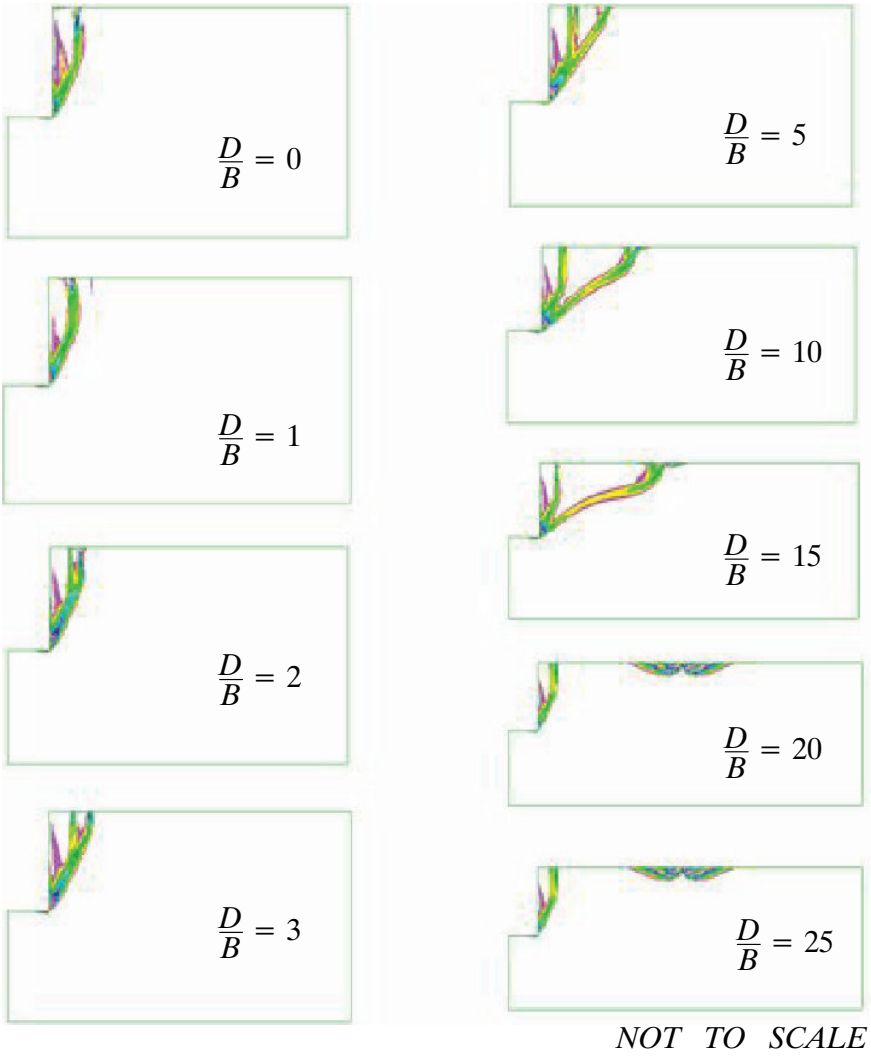

Figure 5-14. Change in combination shear failure with Increasing footing distance ratio

When the footing distance ratio is increased such that a level ground condition is reached, a nearby stable slope has no further influence. Figure 6-11 shows that the foundation bearing capacity is not affected by an unstable slope either. The slight variances in the normalised bearing capacities are due to the nature of the modelling program and not due to the unstable slope.

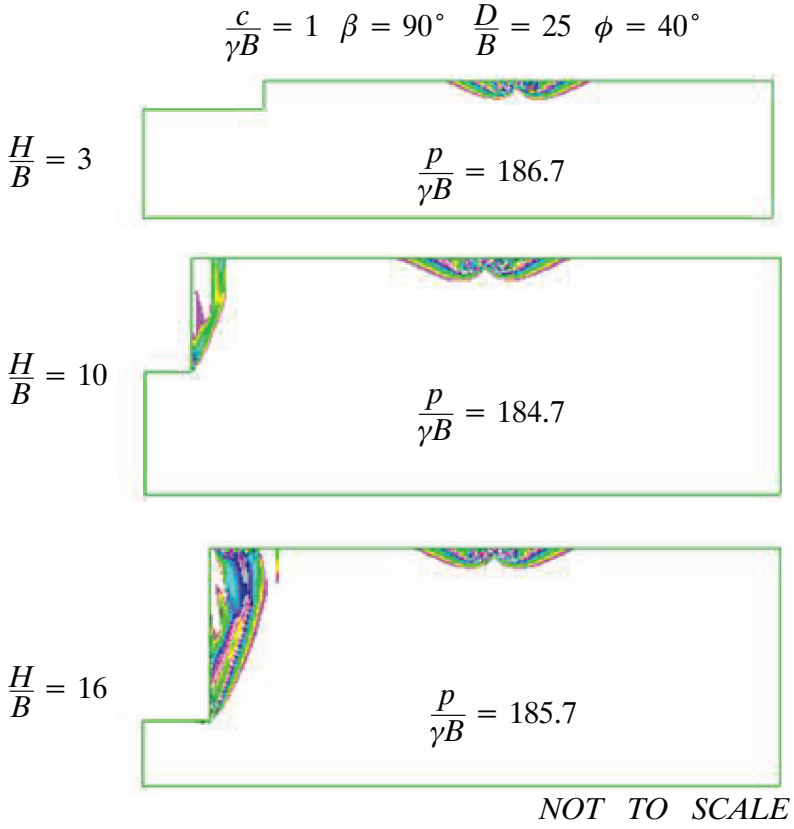

Figure 5-15. Variation in normalised bearing capacity with combination shear failure

5.5 Two-Way Shear Failure Mechanism for a Footing Near Slope

In chapter 1 the proposed shear failure surface for the footing near slope problem was introduced as Figure 1-7. The figure showed a single slip surface towards the slope-face indicating the strong influence a slope has on the bearing capacity of a nearby footing. Figure 5-12 proposes a number of scenario's where the shear failure zone extends in both directions from under the footing. Generally, for this to occur the slope requires one of either a small slope height ratio, large footing distance ratio, weak material, small slope angle. Due to the increased failure zone an increased bearing capacity is expected for two-way shear failure for the footing near slope problem.

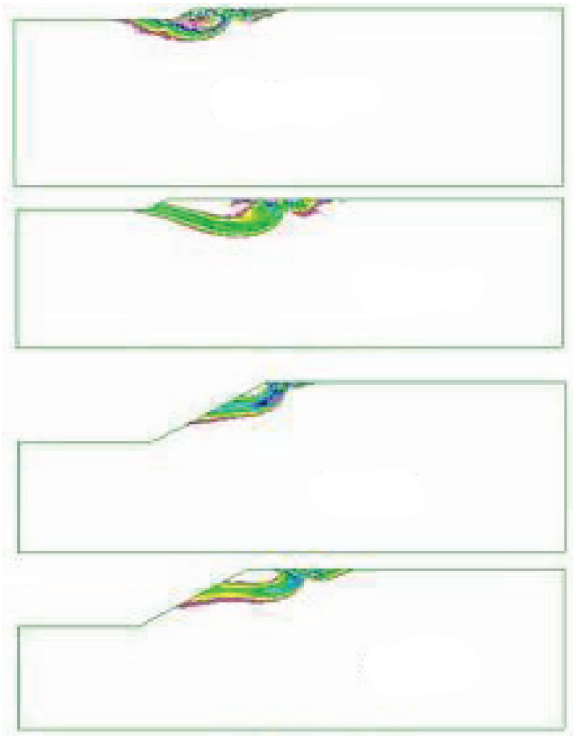

Figure 5-16. Contour plots of two-way shear failure mechanism

5.6 Dilation Angle

Some soils, particularly clays, can shrink and swell significantly when wet or during drying. It is also predicted that large volume changes are experienced during plastic shearing from foundation loading. Classical limit equilibrium methods assume an associated flow rule, which restrics the direction of plastic flow such that $\psi = \phi$. This rule has been used for the previous cases of this research. When $\psi = 0^\circ$ plastic deformation occurs at a constant rate therefore there is no volume change experienced. When $\psi = \phi$ there is no plastic energy dissipation in the material which is physically unreasonable. It is predicted that in reality, especially for granular materials, dilation tends to occur during shear loading therefore the dilation angle ranges between zero and the internal friction angle.

Figure 6-12 to Figure 6-15 shows the variation in normalised bearing capacity with varying dilation angles. Results are compared with varying dimensionless strength ratio's.

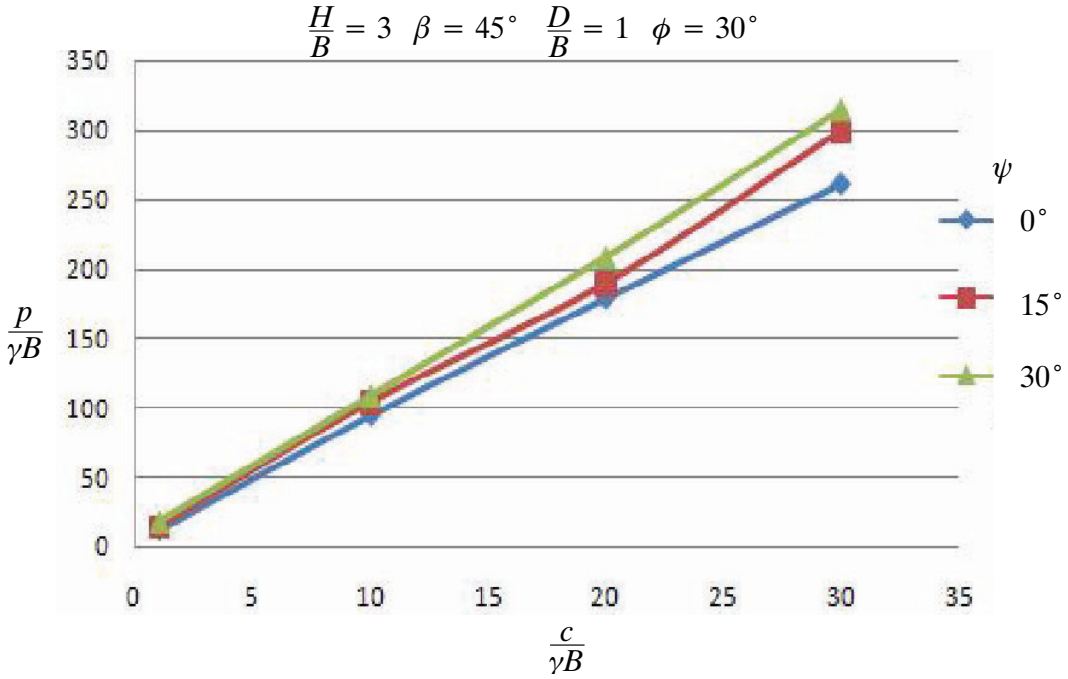

Figure 5-17. Effect of dimensionless strength ratio and dilation angle for 30 degree friction angle

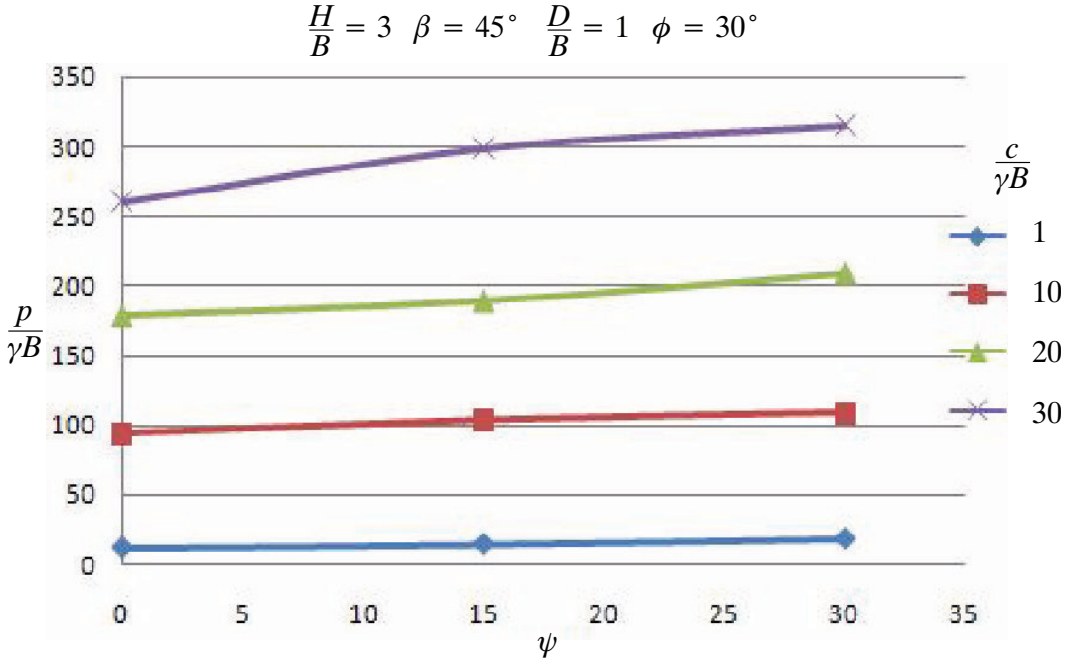

Figure 5-18. Effect of dilation angle and dimensionless strength ratio for 30 degree friction angle

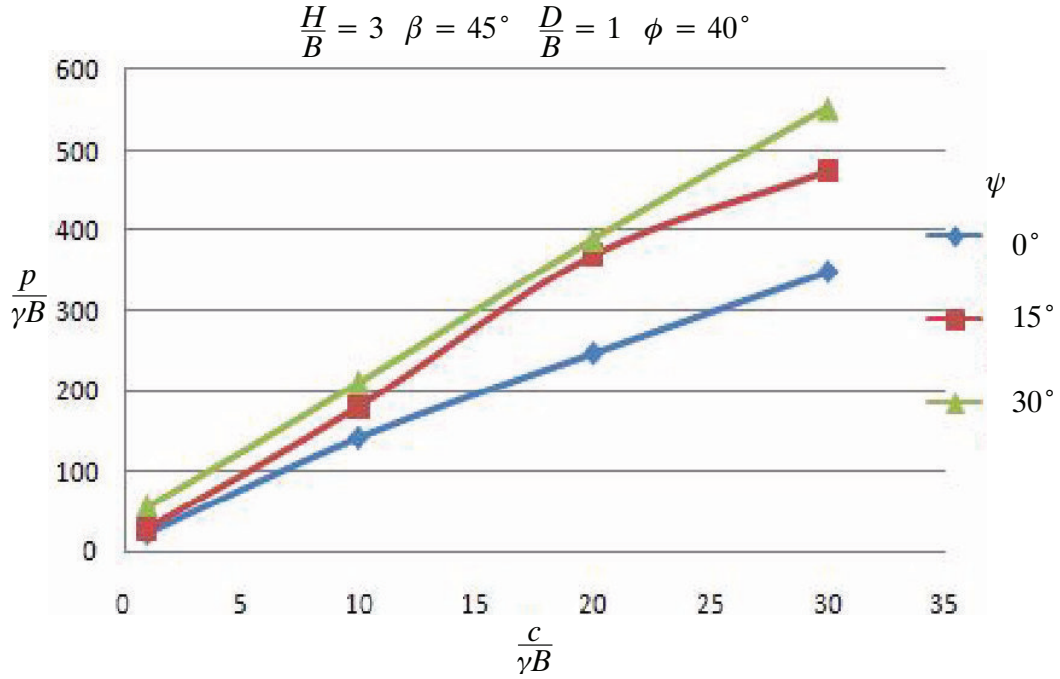

Figure 5-19. Effect of dimensionless strength ratio and dilation angle for 40 degree friction angle

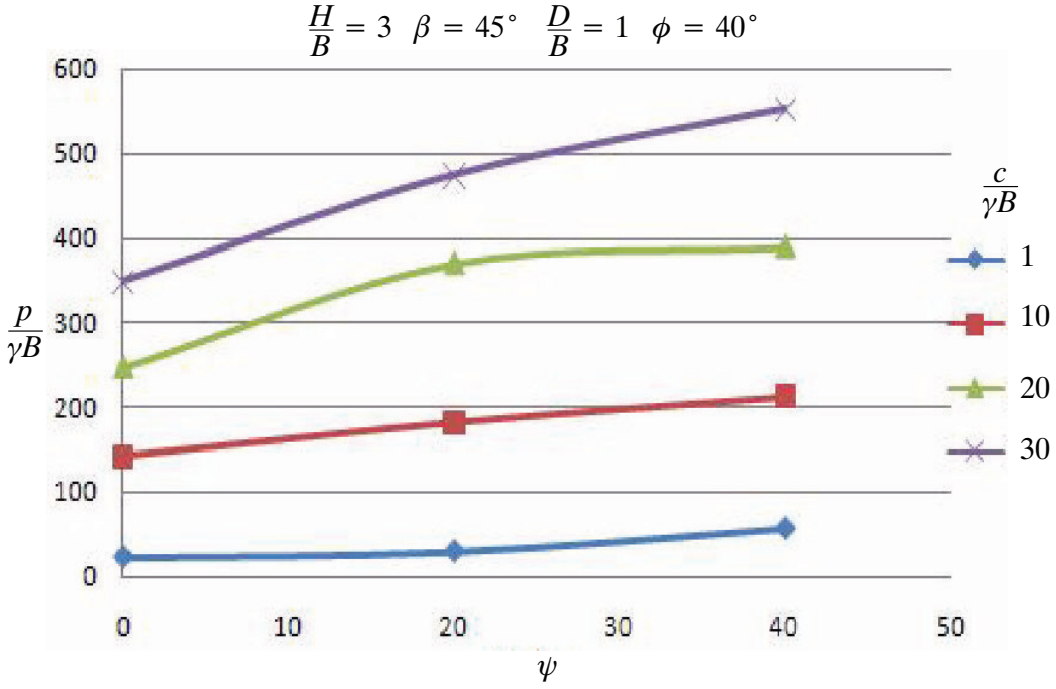

Figure 5-20. Effect of dilation angle and dimensionless strength ratio for 40 degree friction angle

In general, the normalised bearing capacity increases as the dilation angle is increased. Therefore the use of associated flow, as done throughout this research, produces over-estimated bearing capacities of the footing. The important case to note is for high friction angle and high dimensionless strength ratio, where $\phi = 40^\circ$ and $\frac{c}{\gamma B} = 30$. This case is shown in Figure 6-15 and the steep increase can be seen as the dilation angle is increased.

The contour plots shown in Figure 6-16 also indicate a decrese in bearing capacity with decresed dilation angle. This is represented by a decrease in the size of the failure zone which is feasible because zero dilation means zero volume change during plastic shearing, hence the smaller failure zone.

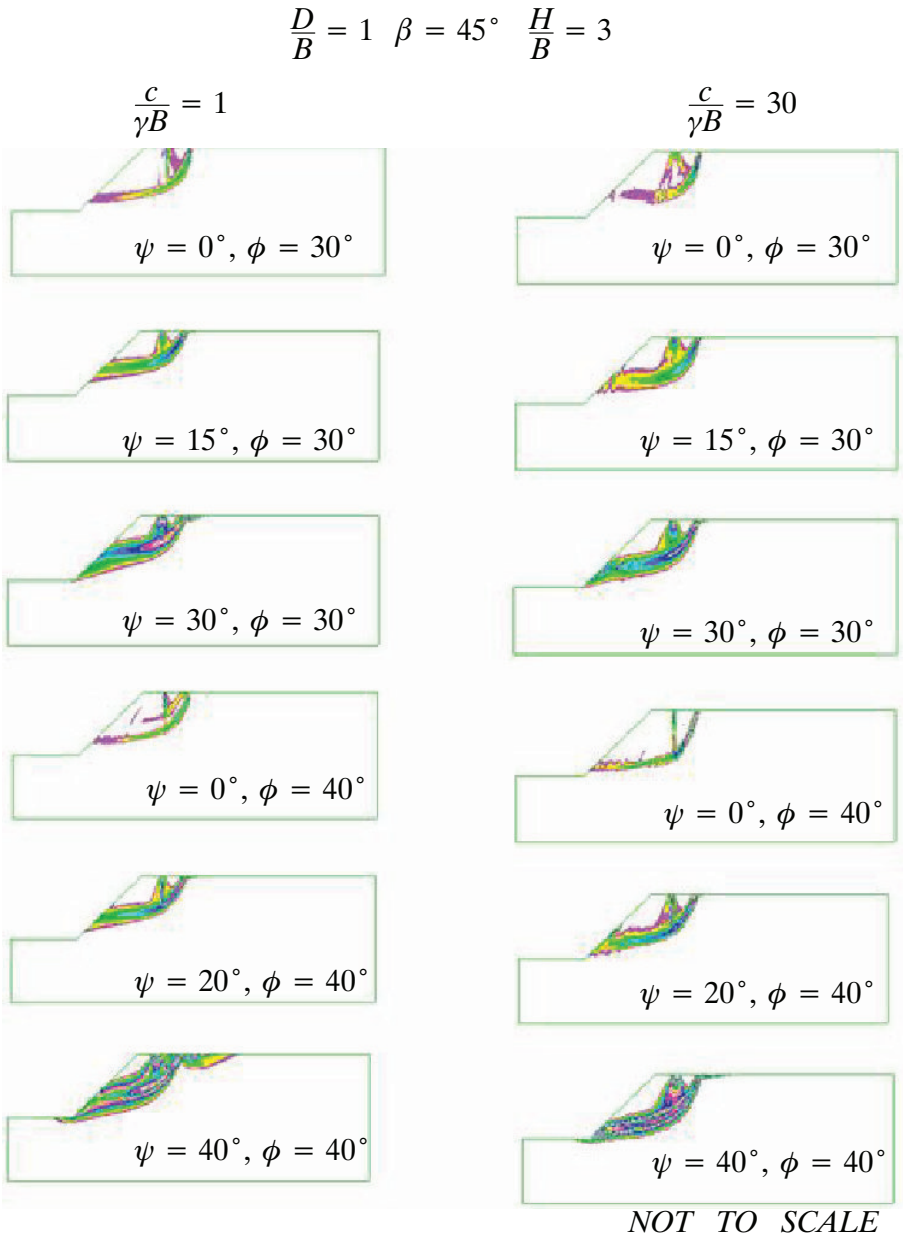

Figure 5-21. Contour plots for change in dilation angle

An interesting point to note is that for zero dilation an initial vertical slip occurs within the filaure zone, particularly for a strong material.

5.7 Conclusion

This chapter has initiated investigations in to a number of key areas of the footing near slope problem. Findings have shown that x,y,z design charts produce greater clarity of results,

however the greater the amount of parameters used the greater the accuracy of the charts. This is because the results are distorted to produce a best-fit situation.

The requirement for a full parametric study of the effect of surcharge loading has become apparent within this chapter. It has been found that there is a significant effect on a weak foundation and very little for a strong foundation. An intermediate study is required to show the progressive effects. Initial studies show an increased normalised bearing capacity as dimensionless surcharge is increased highlighting the importance of the study.

It was found that for a footing considered to be a level ground problem with an unstable slope some distance away the bearing capacity is not affected by the slope. Unstable slopes were only apparent for steep slopes with a very low dimensionless strength ratio. For such a case a very low normalised bearing capacity is achieved even for less steep slopes.

A new shear failure mechanism for the footing near slope problem. Previously a single-direction shear failure zone has been predicted towards the face of the slope, however it has become apparent that the special case of a two-way failure mechanism is possible for the footing on slope problem.

The dilation angle studied verified that as dilation angle increases so to does the normalised bearing capaity of the footing. It has been concluded that when dilation angle equals friction angle, as has been used throughout this research, an over-estimated solution of the bearing capacity is obtained.

Conclusion

6.1 Conclusion

The new script file produced allowed for an efficient and comprehensive parametric study of the footing near slope problem. The effect of geometrical paramaters, such as slope height, footing distance from slope and slope angle were investigated as well has how this effect changed with varying other geometrical and material parameters. A similar study was undertaken for the effect of material parameters including friction angle and cohesion. To produce valuable results all studies were undertaken using dimensionless quantities.

The study of friction angle presented non-linear trends which converge as friction angle is reduced. A small friction angle produces a low normalised bearing capacity and very small failure surface. This highlights the very weak nature of a material containing a small friction angle.

The study of dimensionless strength ratio presented linear trends which converge as the value of dimensionless strength ratio is decreased. The failure surface does not generally vary with change in dimensionless strength ratio but does with all other parameters. However, the normalised bearing capacity changes significantly with a change in dimensionless strength ratio.

The slope height study verified that as the slope height ratio increases the normalised bearing capacity decreases. This occurs until above-toe failure where any further increase has no further affect. Each of the other parameters influence the the height at which above-toe failure occurs.

The footing distance study verified that as the footing distance ratio is increased so to does the normalised bearing capacity until a level ground state is reached. Each of the other

parameters affect the distance at which a level ground state is reached. Stronger materials, a steeper slope and a higher slope require a much greater distance.

The slope angle study verified that as a slope becomes steeper the normalised bearing capacity is decreased. For the geometrical properties the the normailised bearing capacity increases at a steady rate as either footing distance, or slope height is increased with slope angle. For the material properties the normalised bearing capacities negatively converge as the slope angle approaches vertical.

Findings have shown that x,y,z design charts produce greater clarity of results, however the greater the amount of parameters used the greater the accuracy of the charts. This is because the results are distorted to produce a best-fit situation.

It was found that for a footing considered to be a level ground problem with an unstable slope some distance away the bearing capacity is not affected by the slope. Unstable slopes were only apparent for steep slopes with a very low dimensionless strength ratio. For such a case a very low normalised bearing capacity is achieved even for less steep slopes.

A new shear failure mechanism for the footing near slope problem. Previously a single-direction shear failure zone has been predicted towards the face of the slope, however it has become apparent that the special case of a two-wy failure mechanism is possible for the footing on slope problem.

The dilation angle studied verified that as dilation angle increases so to does the normalised bearing capaity of the footing. It has been concluded that when dilation angle equals friction angle, as has been used throughout this research, an over-estimated solution of the bearing capacity is obtained.

6.2 Future Research

Possible directions for future research into this extensive topic were outlined in Chapter 5 - Development of Additional Research. The topics covered were:

- Surcharge loading
- Dilation angle
- Comprehensive set of x,y,z design charts
- Investigation of the two-way shear failure mechanism
- Investigation of combination shear failure of slope stability and foundation bearing capacity failure

Other topics not covered in this research which could produce interesting findings are:

- Footing roughness
- Factor of safety

6.3 Publications

Shiau, J.S., Watson, J.F. & Arnold, M.D. "*Numerical Study of a Shallow Foundation Located near 45 Degree Slopes*", 4th International Conference on Advances in Structural Engineering and Mechanics, May 2008, Korea.

References

2002, FLAC Manuals, Itasca Consulting Group, Minnesota, USA

Craig, R.F. 1997, Soil Mechanics, 6th edn, Spon Press, London, England

Das, B.M. 1999, Shallow Foundations: Bearing Capacity and Settlement, CRC Press, USA

Das, B.M. 1999, Principles of Foundation Engineering, 6th edn, California, USA

Bowles, J.E. 1974, Analytical and Computer Methods in Foundation Engineering

Bowles, J.E. 1996, Foundation Analysis and Design, 5th edn, Illinois, USA

Cernica, J.N. 1995, Geotechnical Engineering: Foundation Design, Youngstown State University

Martins, J.B, 'Numerical Methods in Geomechanics', School of Engineering, University of Minho, Braga, Portugal, 1981

Shiau, J.S., Merifield, R.S., Lyamin, A.V. & Sloan, S.W. 2006, "*Undrained Stability of Footings on Slopes",* Journal of Geotechnical and Geoenvironmental Engineering ASCE, January 2006.

Shiau, J.S., Watson, J.F. & Smith, C.A. "*Foundation located near slope ~A FLAC study*", 1st Int'l. FLAC /DEM Symposium on Numerical Modeling, August 2008, USA

Smith, C.A. & Shiau, J.S. 2007, *"Bearing Capacity of footings near slopes"*, 10th Australia New Zealand Conference on Geomechanics, 556-561.

Appendix

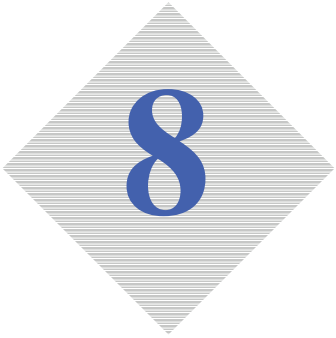

8.1 Appendix A – Project Specification

8.2 Appendix B – Values Corresponding to Charts

Table 8-2. Values corresponding to figure 3-1 for the effect of friction angle with various footing distance ratios

$$H/B = 6,\ \beta = 30^{\circ},\ \frac{c}{\gamma B} = 30$$

$\frac{P}{\gamma B}$ \ ϕ	$\frac{D}{B} = 0$	$\frac{D}{B} = 1$	$\frac{D}{B} = 2$	$\frac{D}{B} = 3$	$\frac{D}{B} = 4$
10	211.62	251.51	276.52	285.85	285.82
20	326.88	389.5	433.47	470.25	498.15
30	554.87	652	729.46	798.23	856.47
40	1126.48	1274.92	1397.84	1527.44	1669.77

$\frac{P}{\gamma B}$ \ ϕ	$\frac{D}{B} = 5$	$\frac{D}{B} = 10$	$\frac{D}{B} = 15$
10	285.87	285.65	285.85
20	503.71	503.78	503.73
30	910.64	1016.81	1016.82
40	1789.53	2294.75	2640.1

Table 8-3. Values corresponding to figure 3-3 for the effect of friction angle with various slope angles

$$H/B = 6,\ D/B = 1,\ \frac{c}{\gamma B} = 30$$

$\frac{P}{\gamma B}$ \ ϕ	$\beta = 30^{\circ}$	$\beta = 60^{\circ}$	$\beta = 90^{\circ}$
10	251.51	186.78	139.96
20	389.5	252.03	170.23
30	652	345.29	205.9
40	1274.92	529.9	246.48

Table 8-4. Values corresponding to figure 3-5 for the effect of friction angle with various dimensionless strength ratios

$$H/B = 6,\ D/B = 1,\ \beta = 30^\circ$$

$\frac{P}{\gamma B}$ \ ϕ	$\frac{c}{\gamma B} = 1$	$\frac{c}{\gamma B} = 10$	$\frac{c}{\gamma B} = 20$	$\frac{c}{\gamma B} = 30$
10	9.15	84.56	167.46	251.51
20	15.81	132.14	260.68	389.5
30	30.84	223.82	439.21	652
40	76.12	444.86	855.16	1274.92

Table 8-5. Values corresponding to figure 3-7 for the effect of friction angle with various slope height ratios

$$\frac{c}{\gamma B} = 30,\ D/B = 1,\ \beta = 30^\circ$$

$\frac{P}{\gamma B}$ \ ϕ	$\frac{H}{B} = 1$	$\frac{H}{B} = 3$	$\frac{H}{B} = 6$	$\frac{H}{B} = 10$	$\frac{H}{B} = 16$
10	253.49	251.8	251.51	251.84	251.59
20	406.03	389.46	389.5	389.67	389.73
30	751.66	654.46	652	659.5	654.24
40	1879.42	1310.95	1274.92	1280.14	1272.98

Table 8-6. Values corresponding to figure 3-9 for the effect of dimensionless strength ratio with various footting distance ratios

$$\phi = 40^\circ,\ H/B = 6,\ \beta = 30^\circ$$

$\frac{P}{\gamma B}$ \ $\frac{c}{\gamma B}$	$\frac{D}{B} = 0$	$\frac{D}{B} = 1$	$\frac{D}{B} = 2$	$\frac{D}{B} = 3$	$\frac{D}{B} = 4$
1	59.39	76.12	93.62	109.47	125.05
10	385.67	444.86	503.68	554.41	606.36
20	751.15	855.16	960.2	1046.8	1134.61
30	1126.48	1274.92	1397.84	1527.44	1669.77

$\frac{P}{\gamma B}$ \ $\frac{c}{\gamma B}$	$\frac{D}{B} = 5$	$\frac{D}{B} = 10$	$\frac{D}{B} = 15$	$\frac{D}{B} = 20$	$\frac{D}{B} = 25$
1	141.78	190.11	186.9	187.19	184.11
10	662.7	886.37	938.89	947.04	936.49
20	1221.02	1577.22	1772.53	1784.32	1777.97
30	1789.53	2294.75	2640.1	2662.28	2647.73

Table 8-7. Values corresponding to figure 3-11 for the effect of dimensionless strength ratio with various slope angles

$$\phi = 40^\circ,\ D/B = 1,\ H/B = 6$$

$\frac{P}{\gamma B}$ \ $\frac{c}{\gamma B}$	$\beta = 30^\circ$	$\beta = 60^\circ$	$\beta = 90^\circ$
1	76.12	20.42	4.49
10	444.86	185.89	77.01
20	855.16	359.29	153.86
30	1274.92	529.9	246.48

Table 8-8. Values corresponding to figure 3-13 for the effect of dimensionless strength ratio with various slope height ratios

$$\phi = 40^\circ,\ D/B = 1,\ \beta = 30^\circ$$

$\frac{P}{\gamma B}$ \ $\frac{c}{\gamma B}$	$\frac{H}{B} = 1$	$\frac{H}{B} = 3$	$\frac{H}{B} = 6$	$\frac{H}{B} = 10$	$\frac{H}{B} = 16$
1	128.21	79.78	76.12	76.1	76.05
10	672.47	452.79	444.86	446.22	440.49
20	1275.57	875.48	855.16	856.76	872.61
30	1879.42	1310.95	1274.92	1280.14	1272.98

Table 8-9. Values corresponding to figure 3-15 for the effect of dimensionless strength ratio with various friction angles

$$\frac{H}{B} = 6,\ D/B = 1,\ \beta = 30^\circ$$

$\frac{P}{\gamma B}$ \ $\frac{c}{\gamma B}$	$\phi = 10^\circ$	$\phi = 20^\circ$	$\phi = 30^\circ$	$\phi = 40^\circ$
1	9.15	15.81	30.84	76.12
10	84.56	132.14	223.82	444.86
20	167.46	260.68	439.21	855.16
30	251.51	389.5	652	1274.92

Table 8–10. Values corresponding to figure 4–1 for the effect of slope angle with various footing distance ratios

$$\frac{H}{B} = 6,\ \phi = 40^\circ,\ \frac{c}{\gamma B} = 30$$

$\frac{P}{\gamma B}$	β	$\frac{D}{B} = 0$	$\frac{D}{B} = 1$	$\frac{D}{B} = 2$	$\frac{D}{B} = 3$	$\frac{D}{B} = 4$
	30	1126.48	1274.92	1397.84	1527.44	1669.77
	60	381.25	529.9	665.38	800.72	880.09
	90	142.19	246.48	323.04	421.3	548

$\frac{P}{\gamma B}$	β	$\frac{D}{B} = 5$	$\frac{D}{B} = 10$	$\frac{D}{B} = 15$	$\frac{D}{B} = 20$	$\frac{D}{B} = 25$
	30	1789.53	2294.75	2640.1	2662.28	2647.73
	60	1024.32	1673.63	2218.35	2528.97	2647.73
	90	690.32	1364.54	1917.41	2360.03	2643.71

Table 8–11. Values corresponding to figure 4–3 for the effect of slope angle with various slope height ratios

$$\phi = 40^\circ,\ D/B = 1,\ \frac{c}{\gamma B} = 30$$

$\frac{P}{\gamma B}$	β	$\frac{H}{B} = 1$	$\frac{H}{B} = 3$	$\frac{H}{B} = 6$	$\frac{H}{B} = 10$	$\frac{H}{B} = 16$
	30	1879.42	1310.95	1274.92	1280.14	1272.98
	60	1820.16	654.96	529.9	494.39	480.29
	90	1471.86	312.03	246.48	242.83	243.3

Table 8–12. Values corresponding to figure 4–5 for the effect of slope angle with various dimensionless strength ratios

$$H/B = 6,\ D/B = 1,\ \phi = 40^\circ$$

$\frac{P}{\gamma B}$	β	$\frac{c}{\gamma B} = 1$	$\frac{c}{\gamma B} = 10$	$\frac{c}{\gamma B} = 20$	$\frac{c}{\gamma B} = 30$
	0	185	940	1785	2650
	30	76.12	444.86	855.16	1274.92
	60	20.42	185.89	359.29	529.9
	90	4.49	77.01	153.86	246.48

Table 8–13. Values corresponding to figure 4–7 for the effect of slope angle with various friction angles

$$\frac{H}{B} = 6,\ D/B = 1,\ \frac{c}{\gamma B} = 30$$

$\frac{P}{\gamma B}$	β	$\phi = 10^\circ$	$\phi = 20^\circ$	$\phi = 30^\circ$	$\phi = 40^\circ$
	30	251.51	389.5	652	1274.92
	60	186.78	252.03	345.29	529.9
	90	139.96	170.23	205.9	246.48

Table 8–14. Values corresponding to figure 4–9 for the effect of footing distance ratio with various slope height ratios

$$Phi = 40^\circ,\ \beta = 30^\circ,\ \frac{c}{\gamma B} = 30$$

$\frac{P}{\gamma B}$	$\frac{D}{B}$	$\frac{H}{B} = 1$	$\frac{H}{B} = 3$	$\frac{H}{B} = 6$	$\frac{H}{B} = 10$	$\frac{H}{B} = 16$
	0	1739.88	1165.13	1126.48	1119.63	1122.30
	1	1879.42	1310.95	1274.92	1280.14	1272.98
	2	1988.08	1465.33	1397.84	1408.33	1426.98
	3	2049.38	1614.34	1527.44	1535.58	1506.35
	4	2205.19	1768.93	1669.77	1671.73	1642.41
	5	2267.26	1820.00	1789.53	1776.36	1754.33
	10	2555.91	2371.43	2294.75	2294.45	2287.73
	15	2608.47	2633.08	2640.10	2639.33	2649.11
	20	2641.42	2650.63	2662.28	2657.85	2644.09
	25	2637.34	2657.63	2647.73	2661.76	2645.66

Table 8-15. Values corresponding to figure 4-11 for the effect of footing distance ratio with various slope angles

$$\phi = 40^\circ,\ \frac{c}{\gamma B} = 30,\ H/B = 6$$

$\frac{P}{\gamma B}$ \ $\frac{D}{B}$	$\beta = 30^\circ$	$\beta = 60^\circ$	$\beta = 90^\circ$
0	1126.48	381.25	142.19
1	1274.92	529.9	246.48
2	1397.84	665.38	323.04
3	1527.44	800.72	421.30
4	1669.77	880.09	548.00
5	1789.53	1024.32	690.32
10	2294.75	1673.63	1364.54
15	2640.10	2218.35	1917.41
20	2662.28	2528.97	2360.03
25	2647.73	2647.73	2643.71

Table 8-16. Values corresponding to figure 4-13 for the effect of footing distance ratio with various dimensionless strength ratios

$$H/B = 6,\ \beta = 30^\circ,\ \phi = 40^\circ$$

$\frac{P}{\gamma B}$ \ $\frac{D}{B}$	$\frac{c}{\gamma B} = 1$	$\frac{c}{\gamma B} = 10$	$\frac{c}{\gamma B} = 20$	$\frac{c}{\gamma B} = 30$
0	59.39	385.67	751.15	1126.48
1	76.12	444.86	855.16	1274.92
2	93.62	503.68	960.20	1397.84
3	109.47	554.41	1046.80	1527.44
4	125.05	606.36	1134.61	1669.77
5	141.78	662.70	1221.02	1789.53
10	190.11	886.37	1577.22	2294.75
15	186.90	938.89	1772.53	2640.10
20	187.19	947.04	1784.32	2662.28
25	184.11	936.49	1777.97	2647.73

Table 8-17. Values corresponding to figure 4-15 for the effect of footing distance ratio with various friction angles

$$\frac{H}{B} = 6,\ \beta = 30^\circ,\ \frac{c}{\gamma B} = 30$$

$\frac{P}{\gamma B}$ \ $\frac{D}{B}$	$\phi = 10^\circ$	$\phi = 20^\circ$	$\phi = 30^\circ$	$\phi = 40^\circ$
0	211.62	326.88	554.87	1126.48
1	251.51	389.50	652.00	1274.92
2	276.52	433.47	729.46	1397.84
3	285.85	470.25	798.23	1527.44
4	285.82	498.15	856.47	1669.77
5	285.87	503.71	910.64	1789.53
10	285.65	503.78	1016.81	2294.75
15	285.83	503.73	1016.82	2640.10
20			1016.71	2662.28
25			1017.24	2647.73

Table 8-18. Values corresponding to figure 4-17 for the effect of slope height ratio with various footing distance ratios

$$\phi = 40^\circ,\ \beta = 30^\circ,\ \frac{c}{\gamma B} = 30$$

$\frac{P}{\gamma B}$ \ $\frac{H}{B}$	$\frac{D}{B} = 0$	$\frac{D}{B} = 1$	$\frac{D}{B} = 2$	$\frac{D}{B} = 3$	$\frac{D}{B} = 4$
1	1739.88	1879.42	1988.08	2049.38	2205.19
3	1165.13	1310.95	1465.33	1614.34	1768.93
6	1126.48	1274.92	1397.84	1527.44	1669.77
10	1119.63	1280.14	1408.33	1535.58	1671.73
16	1122.30	1272.98	1426.98	1506.35	1642.41

$\frac{P}{\gamma B}$ \ $\frac{H}{B}$	$\frac{D}{B} = 5$	$\frac{D}{B} = 10$	$\frac{D}{B} = 15$	$\frac{D}{B} = 20$	$\frac{D}{B} = 25$
1	2267.26	2555.91	2608.47	2641.42	2637.34
3	1820.00	2371.43	2633.08	2650.63	2657.63
6	1789.53	2294.75	2640.10	2662.28	2647.73
10	1776.36	2294.45	2639.33	2657.85	2661.76
16	1754.33	2287.73	2649.11	2644.09	2645.66

Table 8–19. Values corresponding to figure 4–19 for the effect of slope height ratio with various slope angles

$$\phi = 40^\circ,\ D/B = 1,\ \frac{c}{\gamma B} = 30$$

$\frac{P}{\gamma B}$ \ $\frac{H}{B}$	$\beta = 30^\circ$	$\beta = 60^\circ$	$\beta = 90^\circ$
1	1879.42	1820.16	1471.86
3	1310.95	654.96	312.03
6	1274.92	529.9	246.48
10	1280.14	494.39	242.83
16	1272.98	480.29	243.3

Table 8–20. Values corresponding to figure 4–21 for the effect of slope height ratio with various dimensionless strength ratios

$$\phi = 40^\circ,\ D/B = 1,\ \beta = 30^\circ$$

$\frac{P}{\gamma B}$ \ $\frac{H}{B}$	$\frac{c}{\gamma B} = 1$	$\frac{c}{\gamma B} = 10$	$\frac{c}{\gamma B} = 20$	$\frac{c}{\gamma B} = 30$
1	128.21	672.47	1275.57	1879.42
3	79.78	452.79	875.48	1310.95
6	76.12	444.86	855.16	1274.92
10	76.1	446.22	856.76	1280.14
16	76.05	440.49	872.61	1272.98

Table 8–21. Values corresponding to figure 4–23 for the effect of slope height ratio with various friction angles

$$\frac{D}{B} = 1,\ \beta = 30^\circ,\ \frac{c}{\gamma B} = 30$$

$\frac{P}{\gamma B}$ \ $\frac{H}{B}$	$\phi = 10^\circ$	$\phi = 20^\circ$	$\phi = 30^\circ$	$\phi = 40^\circ$
1	253.49	406.03	751.66	1879.42
3	251.8	389.46	654.46	1310.95
6	251.51	389.5	652	1274.92
10	251.84	389.67	659.5	1280.14
16	251.59	389.73	654.24	1272.98

Table 8-22. Values corresponding to figure 5-1, design chart comparing footing distance ratio and slope angle with a strong foundation

$$\frac{H}{B} = 6 \quad \frac{c}{\gamma B} = 30 \quad \phi = 40^\circ$$

$\frac{P}{\gamma B}$	β	$\frac{D}{B} = 0$	$\frac{D}{B} = 1$	$\frac{D}{B} = 2$	$\frac{D}{B} = 3$	$\frac{D}{B} = 4$
	30	1126.481	1274.923	1397.843	1527.436	1669.767
	60	381.25	529.9	665.38	800.72	880.09
	90	142.1927	246.4837	323.0353	421.3045	547.9994

$\frac{P}{\gamma B}$	β	$\frac{D}{B} = 5$	$\frac{D}{B} = 10$	$\frac{D}{B} = 15$	$\frac{D}{B} = 20$	$\frac{D}{B} = 25$
	30	1789.527	2294.753	2640.102	2662.282	2647.734
	60	1024.32	1673.63	2218.35	2528.97	2647.73
	90	690.3159	1364.535	1917.409	2360.033	2643.71

Table 8-23. Values corresponding to figure 5-2, design chart comparing footing distance ratio and slope angle with a weak foundation

$$\frac{H}{B} = 6 \quad \frac{c}{\gamma B} = 1 \quad \phi = 10^\circ$$

$\frac{P}{\gamma B}$	β	$\frac{D}{B} = 0$	$\frac{D}{B} = 1$	$\frac{D}{B} = 2$	$\frac{D}{B} = 3$	$\frac{D}{B} = 4$
	30	59.38972	76.11771	93.61787	109.4734	125.0489
	60	13.55	20.42	29	40.36	50.48
	90	3.10668	4.485389	7.478547	12.82876	20.82172

$\frac{P}{\gamma B}$	β	$\frac{D}{B} = 5$	$\frac{D}{B} = 10$	$\frac{D}{B} = 15$	$\frac{D}{B} = 20$	$\frac{D}{B} = 25$
	30	141.7784	190.1079	186.9012	187.1875	184.1134
	60	63.98	133.84	180.81	181.91	184.11
	90	33.13777	109.0627	183.7605	184.3092	186.3369

Table 8-24. Values corresponding to figure 5-3, design chart comparing footing distance ratio and slope height ratio with a strong foundation

$$\beta = 30^\circ \quad \frac{c}{\gamma B} = 30 \quad \phi = 40^\circ$$

$\frac{H}{B}$	$\frac{D}{B} = 0$	$\frac{D}{B} = 1$	$\frac{D}{B} = 2$	$\frac{D}{B} = 3$	$\frac{D}{B} = 4$
1	1739.878	1879.418	1988.083	2049.378	2205.193
3	1165.133	1310.952	1465.329	1614.337	1768.935
6	1126.481	1274.923	1397.843	1527.436	1669.767
10	1119.626	1280.138	1408.335	1535.583	1671.733
16	1122.298	1272.984	1426.978	1506.347	1642.414

$\frac{P}{\gamma B}$

$\frac{H}{B}$	$\frac{D}{B} = 5$	$\frac{D}{B} = 10$	$\frac{D}{B} = 15$	$\frac{D}{B} = 20$	$\frac{D}{B} = 25$
1	2267.259	2555.914	2608.471	2641.415	2637.342
3	1819.998	2371.433	2633.084	2650.625	2657.626
6	1789.527	2294.753	2640.102	2662.282	2647.734
10	1776.358	2294.45	2639.333	2657.854	2661.758
16	1754.33	2287.727	2649.108	2644.086	2645.665

$\frac{P}{\gamma B}$

Table 8-25. Values corresponding to figure 5-4, design chart comparing footing distance ratio and slope height ratio with a weak foundation

$$\beta = 30^\circ \quad \frac{c}{\gamma B} = 30 \quad \phi = 40^\circ$$

$\frac{P}{\gamma B}$ \ $\frac{H}{B}$	$\frac{D}{B} = 0$	$\frac{D}{B} = 1$	$\frac{D}{B} = 2$	$\frac{D}{B} = 3$	$\frac{D}{B} = 4$
1	7.382008	9.483981	10.75839	10.83038	10.89104
3	7.167661	9.136581	10.36372	10.92769	10.96767
6	7.229989	9.151524	10.41923	10.83697	10.96504
10	7.203732	9.044972	9.799718	10.10446	10.88512

$\frac{P}{\gamma B}$ \ $\frac{H}{B}$	$\frac{D}{B} = 5$	$\frac{D}{B} = 10$	$\frac{D}{B} = 15$
1	10.75204	10.95171	
3	10.88817	10.92774	10.98775
6	10.98079	10.92337	10.76216
10	10.81302	10.92329	10.81887

Table 8-26. Values corresponding to figure 5-5, design chart comparing dimensionless strength ratio and friction angle with small slope angle and small footing distance ratio

$$\beta = 30^\circ \quad \frac{D}{B} = 1 \quad \frac{H}{B} = 6$$

$\frac{P}{\gamma B}$ \ ϕ	$\frac{c}{\gamma B} = 1$	$\frac{c}{\gamma B} = 10$	$\frac{c}{\gamma B} = 20$	$\frac{c}{\gamma B} = 30$
10	9.15	84.56	167.46	251.51
20	15.81	132.14	260.68	389.5
30	30.84	223.82	439.21	652
40	76.12	444.86	855.16	1274.92

Table 8-27. Values corresponding to figure 5-6, design chart comparing dimensionless strength ratio and friction angle with large slope angle and large footing distance ratio

$$\beta = 30^\circ \quad \frac{D}{B} = 1 \quad \frac{H}{B} = 6$$

$\frac{P}{\gamma B}$ \ ϕ	$\frac{c}{\gamma B} = 1$	$\frac{c}{\gamma B} = 10$	$\frac{c}{\gamma B} = 20$	$\frac{c}{\gamma B} = 30$
10	10.61	96.37	191.23	285.82
20	18.31	169.64	332.74	496.62
30	41.43	271.47	513.9	761.18
40	109.06	499.32	906.8	1364.54

Table 8-28. Values corresponding to figure 5-7 for the effect of surcharge with various footing distance ratio's

$$\frac{H}{B} = 6, \ \beta = 30^\circ, \ \frac{c}{\gamma B} = 30$$

$\frac{P}{\gamma B}$ \ $\frac{D}{B}$	$\frac{q}{\gamma B} = 0$	$\frac{q}{\gamma B} = 1$	$\frac{q}{\gamma B} = 2$
0	1126.48	1131.79	1129.5
1	1274.92	1266.26	1275.39
2	1397.84	1421.07	1440.15
3	1527.44	1545.23	1582.18
4	1669.77	1660.73	1721.51
5	1789.53	1775.19	1776.67
10	2294.75	2296.07	2317.97
15	2640.1	2688.02	2717.07
20	2662.28	2700.32	2740.31
25	2647.73	2684.37	2747.32

Table 8-29. Values corresponding to figure 5-8 for the effect of surcharge with various slope height ratios

$$\frac{D}{B} = 1,\ \beta = 30^{\circ},\ \frac{c}{\gamma B} = 30$$

$\frac{P}{\gamma B}$	$\frac{H}{B}$	$\frac{q}{\gamma B} = 0$	$\frac{q}{\gamma B} = 1$	$\frac{q}{\gamma B} = 2$
	1.00	1879.42	1890.18	1906.43
	3.00	1310.95	1323.46	1337.69
	6.00	1274.92	1266.26	1275.39
	10.00	1280.14	1277.58	1260.48
	16.00	1272.98	1268.09	1275.13

Table 8-30. Values corresponding to figure 5-9 for the effect of surcharge with various slope angles

$$\frac{H}{B} = 6,\ \frac{D}{B} = 1,\ \frac{c}{\gamma B} = 30$$

$\frac{P}{\gamma B}$	β	$\frac{q}{\gamma B} = 0$	$\frac{q}{\gamma B} = 1$	$\frac{q}{\gamma B} = 2$
	30	1274.92	1266.26	1275.39
	60	529.9	533.48	535.6
	90	246.48	239.8	237.53

Table 8-31. Values corresponding to figure 5-17 for the effect of dimensionless strength ratio with dilation angle for 30 degree friction angle

$$\frac{H}{B} = 3\ \ \beta = 45^{\circ}\ \ \frac{D}{B} = 1\ \ \phi = 30^{\circ}$$

$\frac{P}{\gamma B}$	$\frac{c}{\gamma B}$	$\psi = 0^{\circ}$	$\psi = 15^{\circ}$	$\psi = 30^{\circ}$
	1	11.71	14.19	18.04
	10	94.29	103.68	108.91
	20	178.39	189.14	208.84
	30	260.81	299.03	315.08

Table 8-32. Values corresponding to figure 5-18 for the effect of dilation angle with dimensionless strength ratio for 30 degree friction angle

$\frac{H}{B} = 3 \quad \beta = 45^\circ \quad \frac{D}{B} = 1 \quad \phi = 30^\circ$

$\frac{P}{\gamma B}$ \ ψ	$\frac{c}{\gamma B} = 1$	$\frac{c}{\gamma B} = 10$	$\frac{c}{\gamma B} = 20$	$\frac{c}{\gamma B} = 30$
0	11.71	94.29	178.39	260.81
15	14.19	103.68	189.14	299.03
30	18.04	108.91	208.84	315.08

Table 8-33. Values corresponding to figure 5-19 for the effect of dimensionless strength ratio with dilation angle for 40 degree friction angle

$\frac{H}{B} = 3 \quad \beta = 45^\circ \quad \frac{D}{B} = 1 \quad \phi = 40^\circ$

$\frac{P}{\gamma B}$ \ $\frac{c}{\gamma B}$	$\psi = 0^\circ$	$\psi = 20^\circ$	$\psi = 40^\circ$
1	22.32	29.2	56.9
10	141.58	180.88	210.69
20	246.6	369.62	388.84
30	347.9	473.4	552

Table 8-34. Values corresponding to figure 5-20 for the effect of dilation angle with dimensionless strength ratio for 40 degree friction angle

$\frac{H}{B} = 3 \quad \beta = 45^\circ \quad \frac{D}{B} = 1 \quad \phi = 40^\circ$

$\frac{P}{\gamma B}$ \ ψ	$\frac{c}{\gamma B} = 1$	$\frac{c}{\gamma B} = 10$	$\frac{c}{\gamma B} = 20$	$\frac{c}{\gamma B} = 30$
0	22.32	141.58	246.6	347.9
20	29.2	180.88	369.62	473.4
40	56.9	210.69	388.84	552